176(1), 2019

COMBUSTION ENGINES

GAS ON

HORIZON 2020

Gas-Only Internal Combustion Engines

www.gason.eu

PTNSS Supporting Members
Członkowie wspierający PTNSS

BOSMAL Automotive Research and Development Institute Ltd
Instytut Badań i Rozwoju Motoryzacji BOSMAL Sp. z o.o

Motor Transport Institute
Instytut Transportu Samochodowego

The Institute for Sustainable Technologies
Instytut Technologii Eksploatacji

Institute of Aviation
Instytut Lotnictwa

Automotive Industry Institute
Przemysłowy Instytut Motoryzacji

The Rail Vehicles Institute TABOR
Instytut Pojazdów Szynowych TABOR

Institute of Mechanised Construction and Rock Mining
Instytut Mechanizacji Budownictwa i Górnictwa Skalnego

Industrial Institute of Agricultural Engineering
Przemysłowy Instytut Maszyn Rolniczych

AVL List GmbH

Solaris Bus & Coach S.A.

Air Force Institute of Technology
Instytut Techniczny Wojsk Lotniczych

COMBUSTION ENGINES

A Scientific Magazine

2019, 176(1)

Year LVIII

PL ISSN 2300-9896

Editor:

Polskie Towarzystwo Naukowe Silników Spalinowych
43-300 Bielsko-Biała, Sarni Stok 93 Street, Poland
tel.: +48 33 8130402, fax: +48 33 8125038
E-mail: sekretariat@ptnss.pl
WebSite: http://www.ptnss.pl
Papers available on-line: http://combustion-engines.eu

Editorial:
Institute of Combustion Engines and Transport
Poznan University of Technology
60-965 Poznan, Piotrowo 3 Street
tel.: +48 61 2244505, +48 61 2244502
E-mail: papers@ptnss.pl

Prof. Jerzy Merkisz, DSc., DEng. (Editor-in-chief)
Miłosław Kozak, DSc., DEng. (Editorial Secretary for Science) – papers@ptnss.pl
Prof. Ireneusz Pielecha, DSc., DEng.,
Wojciech Cieślik, DEng. (Technical Editors)
Joseph Woodburn, MSci (Proofreading Editor)
Wojciech Serdecki, DSc., DEng. (Statistical Editor)
and Associate Editors

Contents

Declaration of the original version
The original version of the Combustion Engines journal is the printed version.

Papers published in the
Combustion Engines
quarterly receive 13 points as stated by the Notification of the Minister of Science and Higher Education dated 26 January 2017.

Editor
Polish Scientific Society of Combustion Engines
43-300 Bielsko-Biała, Sarni Stok 93 Street, Poland
tel.: +48 33 8130402, fax: +48 33 8125038
E-mail: sekretariat@ptnss.pl
WebSite: http://www.ptnss.pl

Subscriptions
Send subscription requests to the Publisher's address.
Cost of a single issue PLZ30 + VAT.

Preparation for print
ARS NOVA Publishing House
60-782 Poznań, ul. Grunwaldzka 17/10A

Circulation: 700 copies

Printing and binding
Zakład Poligraficzny Moś i Łuczak, sp. j., Poznań, ul. Piwna 1

The journal is registered in the Polish technical journals content database – **BAZTECH** www.baztech.icm.edu.pl

The journal is listed in the international database **IC Journal Master List** – **Index Copernicus** www.indexcopernicus.com

Cover
I – Lean-burn combustion engine with ignition chamber
(*fot. www.vw.com*); background (Sun in the horizon of the road © Whatwolf – Freepik.com)
IV – Engine head with ignition chamber
(*fot. www.vw.com*)

Article citation info:
WEIßNER, M., BEGER, F., SCHÜTTENHELM, M., TALLU, G. Lean-burn CNG engine with ignition chamber: from the idea to a running engine. *Combustion Engines*. 2019, **176(1)**, 3-9. DOI: 10.19206/CE-2019-101

Michael WEIßNER
Frank BEGER
Martin SCHÜTTENHELM
Gunesh TALLU

CE-2019-101

Lean-burn CNG engine with ignition chamber: from the idea to a running engine

Current and further developing CO_2- and emission regulations worldwide and the competition to full electric mobility deliver a challenge for internal combustion engines in general. A state of the art solution is the use of natural gas mainly contending methane to reduce CO_2 significantly and to offer lowest emission levels. The EU-funded project GasOn developed engine concepts to fully exploit the advantages of CNG. This article describes the development of an innovative, monovalent engine dedicated to Compressed Natural Gas (CNG) and characterised by the lean burn concept and the innovative pre-chamber combustion.

Key words: *CNG, scavenged prechamber, lean combustion, ignition system, efficiency*

1. Introduction

CNG engines offer a CO_2 reduction level of above 20% compared to diesel and gasoline engines due to the chemical properties. Methane, the main content of natural gas, offers a higher H/C-ratio than the hydrocarbon molecules of Diesel and gasoline. An additional potential for CO_2-reduction is the possibility of producing renewable methane so a CNG powertrain can become CO_2-neutral.

Current CNG-engines are derived from gasoline engines and are limited by boundaries determined by the bivalent concept. Such a compromise is a low compression ratio, that is usually chosen for the use of gasoline and does not fully exploit the potential of the highly knock resistant CNG. Additionally a stoichiometric combustion is state of the art due to exhaust gas aftertreatment technology. A lean combustion offers further potential to increase efficiency and to reduce CO_2 emissions.

The objective of the described engine concept of GasOn is to fully exploit the efficiency potential of CNG in a dedicated engine, including a high compression ratio ($\varepsilon > 14$) and lean burn ($\lambda = 2$). An enabling technology for lean combustion is the use of a prechamber, which is known from large bore engines, used for example by MAN Energy Solutions. The prechamber can be interpreted as a highly powerful ignition system like a Diesel pilot injection but running on the same fuel like the main combustion. It offers high energy ignition for the lean combustion without adding a second type of fuel.

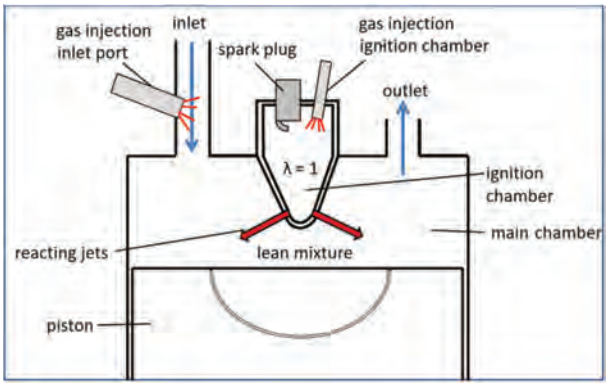

Fig. 1. CNG combustion system of lean burn with prechamber

As shown in Fig. 1 the combustion is divided into two chambers. The main chamber is supplied with the lean mix of CNG and air. After the compression stroke parts of this mixture are pressed into the prechamber. The lean mix cannot be safely ignited under the high pressure of compression. Therefore, a small quantity of pure CNG is dosed into the prechamber via a separate dosing system and creates an approximately stoichiometric mixture inside the prechamber. This mixture can be ignited by the spark plug and the combustion process in the prechamber creates highly energetic flame jets exiting into the main combustion chamber. These flame jets are able to capture the content of the main combustion chamber fast and nearly completely which results in a stable combustion process.

The introduction of this combustion system into a 2L class engine size creates several challenges, which need to be addressed. As a general figure the prechamber system needs to be only 1/3 up to 1/5 of the size of the known components from the large bore engines. These challenges and the related technical solutions are described in the following chapters.

2. Base engine

One of the most important aspects of the new combustion system is the increased compression ratio compared to a gasoline engine. The final value is not fixed at the beginning of the project and a variation of different compression ratios is scheduled. The envisaged range of compression ratios reaches up to eps = 15.5, which leads to expected cylinder peak pressures far beyond the mechanical limit of adequate gasoline engines. Typical peak pressure limits of dual fuel engines are in the range of 100 to 120 bar, while the new combustion system might deliver 150bar or more. To ensure the highest possible mechanical robustness to the project it has been decided to use the Volkswagen EA288 VN diesel-engine as a base engine for the lean burn prechamber combustion system. Diesel engines of the 2.0l class [3] can typically withstand cylinder pressures up to 200 bar and are therefore perfectly suited for the monovalent CNG combustion.

3. Design challenges

The development of the combustion system in the decided Diesel engine offered (amongst others) the following challenges:

– downscaling and package of the prechamber and related components into the cylinder head
– design of the prechamber (shape, nozzles etc.)
– cooling and sealing concept
– piston shape
– dosing system to scavenge the prechamber

The following chapter will describe the mentioned challenges and the chosen technical solutions.

3.1. Package, sealing and cooling

Prechambers are known mainly from gasoline race engines and from large bore Diesel engines. Both concepts offer easier package situations due to an open combustion chamber with angled valves (gasoline engine) or by large bore diameters (industrial engines) which allow for an comparable easy integration of the prechamber and it´s necessary components. The chosen Diesel engine mainly offers the room formerly used by the high pressure Diesel injector in the centre of the cylinder head. In between the vertically oriented valves and the related narrow space between the camshafts it is not possible to integrate components with a diameter much greater than the Diesel injector. In a tubular space of appr. 30 mm all components have to be integrated: the prechamber, the top lid of the prechamber, the check valve, the CNG supply of the dosing system, a pressure sensor, the spark plug and the ignition coil. Being an experimental engine with the plan to test numerous variations of the prechamber it is also important to create a design that offers sufficient serviceability. It is important to be able to change single components without disassembling the cylinder head.

To address these targets all components are made modular and are clamped into the cylinder head by a tubular locking nut as shown in Fig. 2.

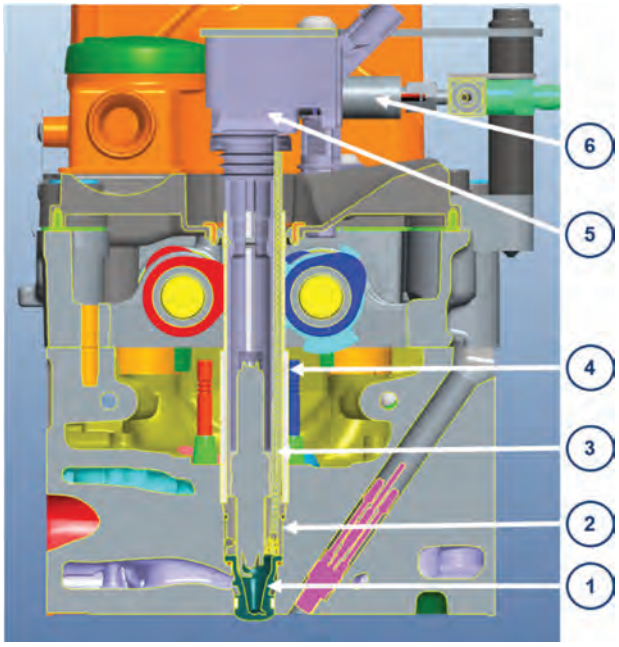

Fig. 2. Section view through cylinder head of GasOn engine with prechamber

The main part of the assembly is the prechamber (1), which is made from a heat resistant steel. The chamber is closed by an aluminium top lid (2), which is carrying the spark plug, a pressure sensor, a check valve and the cannulary tube of the dosing system (3). All parts are clamped onto the cylinder head by a locking nut (4). Outside of the shown tubular space the plug top ignition coil (5) and the dosing system (6) are located.

This layout fits smoothly in between the camshafts and still allows for an comparatively easy access to the named components. The locking nut is a multifunctional part as it also separates the oiled area of the cylinder head from the dry area outside to ensure an oil free operation of the ignition system.

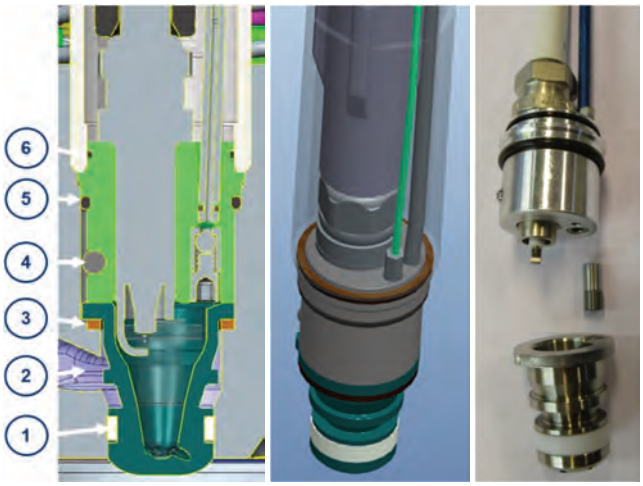

Fig. 3. Section view through prechamber assembly, 3D view and photo of hardware

The sealing concept needs to address all three media coolant, ambient air and oil as well as the hot combustion gases. The prechamber is located in the coolant (2) of the engine to avoid overheating and to allow for a robust engine for the scheduled tests. The sealing between the water area and the main combustion chamber is done by a teflon ring (1). The sealing between the water area and the prechamber area is addressed by a copper ring (3), which is loaded with pressure by the locking nut. With the O-Rings (5) and (6) the sealing towards the oil area and the ambient air area is achieved.

One aim is a good serviceability, which includes an easy change of the spark plug. For the top lid being a rotationally symmetrical part which would turn at the moment when the sparkplug should be screwed in or out, a device is required to avoid a rotation of the lid and also to ensure a defined rotational position. This device is a ball (4) located in the hutch of the lid engaging a groove in the cylinder head.

3.2. Design of the prechamber

The design of the prechamber is determined by various boundaries and parameters. The first boundary is the available space, which is limited by the design of the base engine (valve position) hence defining the maximum diameter. The other aspect is the functional geometry to create an appropriate gas motion for a fast and efficient combustion in both, the prechamber and in the main combustion chamber.

To define suitable geometries numerous CFD simulations have been performed [2] and numerous versions have been built and tested in hardware. The first parameter is the internal shape. Three shapes and accordingly three different chamber volumes between 1.4 and 2.2 cm³ have been designed.

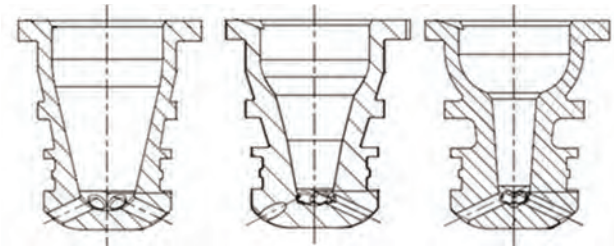

Fig. 4. Three internal shapes with 2.2/1.8/1.4 cm³ volume

The shape of the prechamber is defined by the target to create best possible conditions at the spark plug for a safe and fast ignition. A nearly stoichiometric mixture shall be combined with a certain turbulent kinetic energy (TKE) level [5]. The developed shapes shown in Fig. 4 offer different amounts of a bottle-like section. This shape supports swirl and TKE creation and is a proper solution to adjust the internal volume while allowing for a robust flow structure.

Fig. 5. Orientation of the nozzles: tangential (left) and radial (right)

The internal volume is a parameter that defines the amount of energy, which is supplied by the burned mixture in the prechamber as ignition system for the lean mixture in the main combustion chamber. A bigger volume offers more energy and offers a higher combustion robustness at very lean conditions of above lambda = 1.8. In terms of efficiency a smaller volume is welcome.

A key parameter of the prechamber is the design and orientation of the nozzles. The varied parameters within the project are the nozzle diameter, the quantity and the orientation. The diameter is interesting in terms of creating flame quenching when the flame/reacting gases are moving through the nozzle. Diameters much smaller than 1mm are discussed to result in flame quenching phenomena. In combination with the quantity of nozzles the diameter determines the cross section between prechamber and main combustion chamber. A higher cross section leads to lower pressure gradients, which can influence the complex combustion process. The tested nozzle diameters have been varied between 1.0 and 2.0 mm. The third parameter is the nozzle orientation. An aspect of the orientation is to place them in a radial or tangential orientation as shown in Fig. 5. Using the radial orientation does not add or create any swirl, neither in the prechamber during compression stroke nor in the main combustion chamber during combustion. Swirl can be achieved with tangential nozzles, which can be oriented in the same or in the opposite direction of the swirl flow of the main combustion chamber. A higher significance of the nozzle orientation can be seen inside the prechamber, where the flow structure is totally different when comparing radial with tangential nozzles. While the tangential orientation leads to a controlled swirl structure the radial orientation leads to a straight flow structure. Both can lead to the envisaged conditions at the spark plug.

A CFD comparison in Fig. 6 shows the different character of the flow structure hence the relevance of the nozzle orientation. The velocity distribution of the flow shows a totally different character if changed from tangential to radial nozzles. While the first one creates a clear swirl inside the prechamber with the highest velocities at the outside of the prechamber the radial nozzles create a high velocity field in the core of the prechamber.

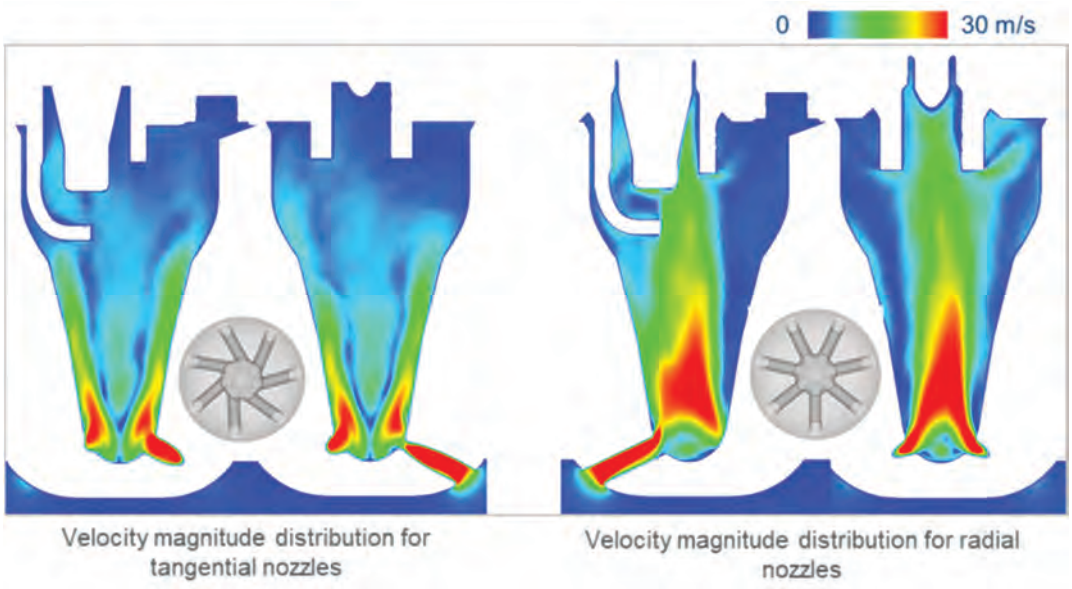

Fig. 6. Flow structure inside the prechamber during compression stroke depending on nozzle orientation

On the basis of the results of further CFD simulations a number of more than 10 different types of prechamber have been designed, produced and tested. This also includes designs with additional nozzles, which are oriented nearly vertically pointing down into the main combustion chamber as shown in Fig. 7. The relevance of this feature is obvious when considering the piston and its bowl as another design parameter for the combustion process.

Fig. 7. Two different samples of prechambers with additional nozzles [4]

3.3. Design of the piston

In Diesel engines typically the Diesel injector and it´s injection coils are matched to the piston bowl to create the best possible combustion in terms of efficiency and emissions. The same approach is necessary for the investigated CNG lean burn prechamber combustion process, which creates flame jets comparable to those of a Diesel injection. Therefore the piston has been designed with different bowls for two purposes: variation of compression ratio between 13.5 and 15.5 as well as matching the bowl with the nozzles of the prechamber. In this article the matching of piston and prechamber is described. All designs of piston and prechamber are created based on CFD simulations [2].

The base design of the piston was a hemispheric bowl as shown in the Fig. 8. It has been tested as a reference in combination with a standard spark plug ignition in the main chamber without any prechamber. This layout delivered the baseline in terms of lean limits in a standard concept. In the next step this hemispheric design has been combined with a set of prechambers containing one array of nozzles pointing nearly horizontally into the main combustion chamber, but varied in terms of orientation, quantity and diameter. It is obvious that the flat array of flame jets does not capture the CNG-air-mixture inside the hemispheric piston bowl completely so the optimisation started in two ways: adding additional nozzles pointing downwards and creating a piston bowl with a omega-shape.

Finally two families of pistons have been designed. The first one are the hemispheric pistons, which adds a version with a rounded edge and a smaller squish area to the shown base design. The second family are the pistons with an omega shape, which are also designed with a sharp and a rounded shape at the squish area. The designs have then been tested in combination with different prechambers. The main concepts are shown in Fig. 9.

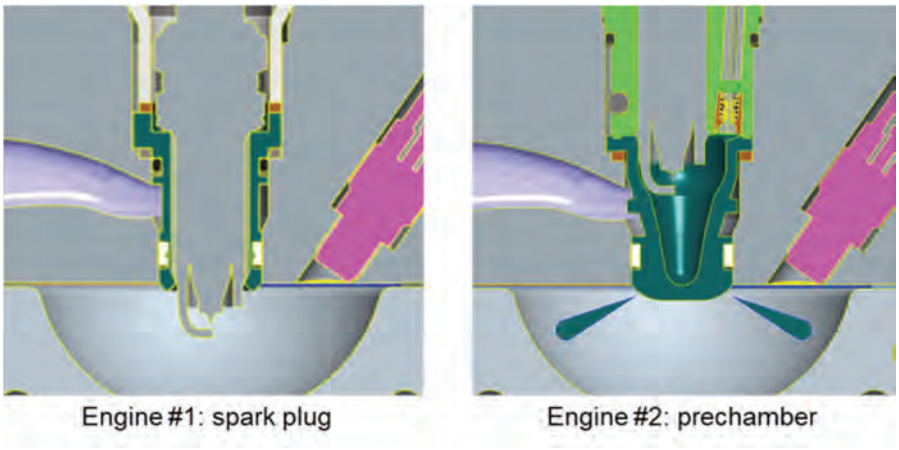

Fig. 8. Hemispheric piston bowl combined with standard spark plug and with prechamber

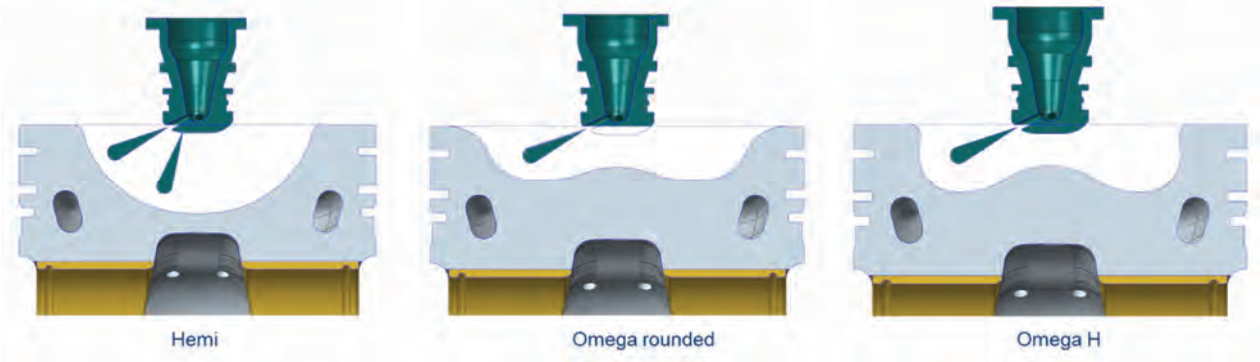

Fig. 9. Hemispheric and omega shaped piston bowls in combination with two different types of nozzle orientation

3.4. Dosing system

Prechambers can work in two different operating modes, a passive and an active one. Passive operation means that no scavenging is actively done within the prechamber so the mixing inside it relies passively on the gas dynamics of fresh and residual components. In GasOn it is scheduled to design an active prechamber, which allows for a dedicated supply of small amounts of CNG directly into the prechamber. This is done to enable the engine for the very lean mix combustion of up to lambda 2.

A general layout of the CNG supply to the engine showing the two different pathways of CNG to the prechamber or the main combustion chamber is shown in the Fig. 10.

To realise a dosing system some technical requirements need to be addressed. The first one is the ability of injecting very small CNG quantities of less than 1mg per stroke. Additionally the system has to be packaged outside of the cylinder head because of the expected size of the injector. After first attempt with an pressure supported electromagnetic valve, which came out to be unreliable and missing the required precision and repeatability from stroke to stroke, a new design had to be created. The dosing system is finally based on Bosch NGI2 injectors, which are integrated in a throttling system and connected to the prechamber via a cannulary tube. All involved components between injector and prechamber are designed to minimise the involved volume to increase controllability and precision. 1D flow simuation and basic testing helped to find the final and reliable solution.

The dosing system is a low pressure system designed for pressures up to 10 bar as known from usual CNG systems feeding the injectors. This is required for the reason of creating very small mass flows per injection and for the simplicity and robustness of the system.

To safe the system from the high pressures inside the combustion chambers the engine needs to be equipped with check valves.

3.5. Check valve

An important element of the dosing system and direct interface to the prechamber is the check valve. It is located directly at the entrance of the dosing system into the prechamber and is important to avoid the high combustion pressures to affect the dosing system.

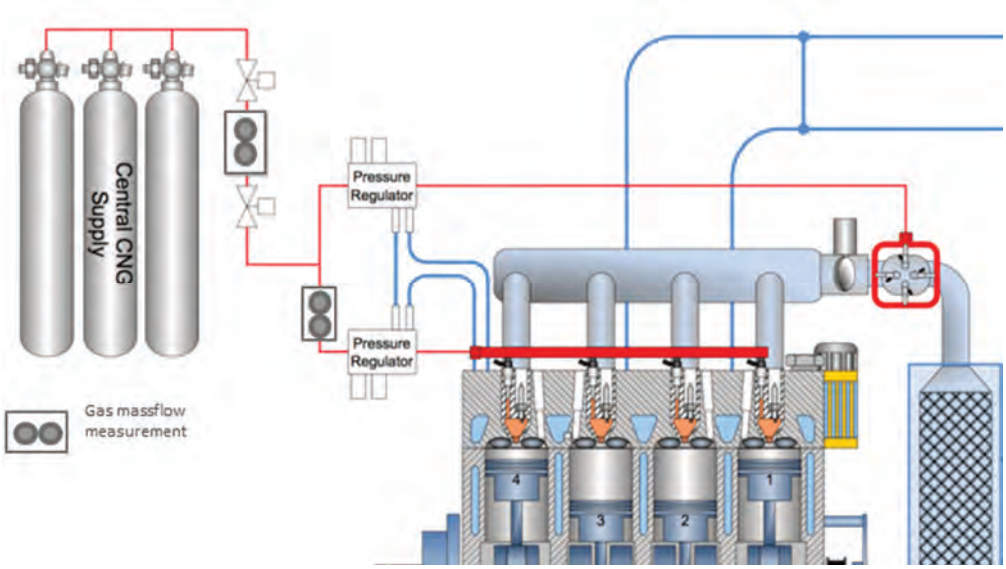

Fig. 10. Schematic overview of the CNG supply of the GasOn engine showing the supply of the main combustion chamber and the separate supply for the prechamber

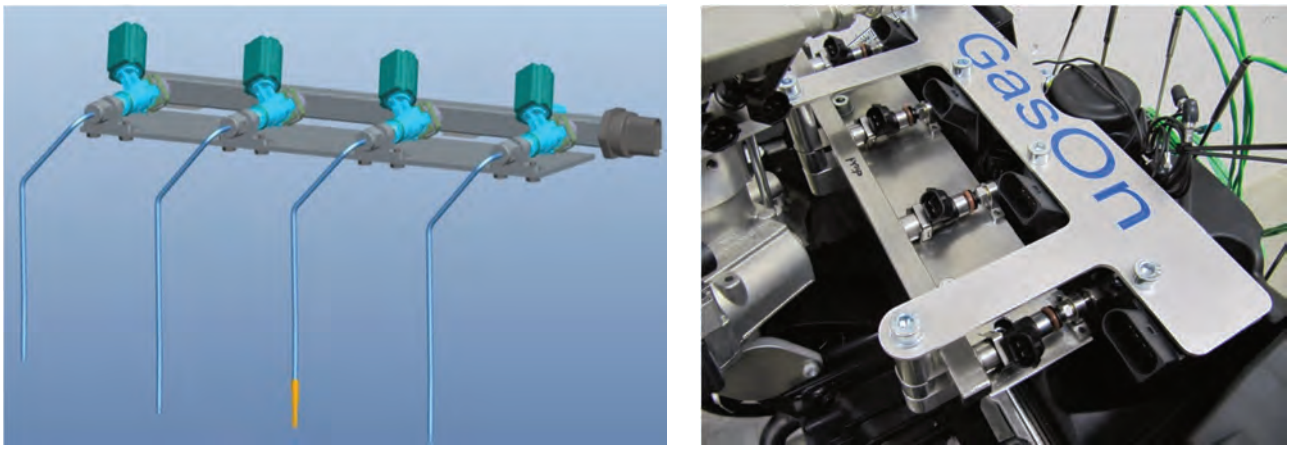

Fig. 11. Dosing system for active (scavenged) prechamber operation

The check valve needs to be designed from scratch because there is no suitable system available in the market. The valve needs to fit into the diameter of 3.5 mm, has to be temperature resistant and should not offer unnecessary dead volume as a HC-trap. A first design has been built, which was perfect in terms of minimum dead volume, but it turned out to be too complex to be manufactured inside suitable tolerances. As a consequence the variation between the built samples was too big.

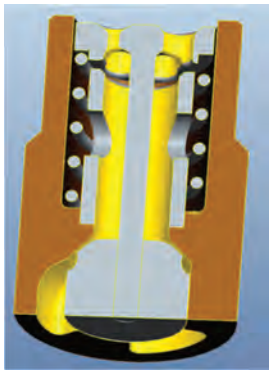

Fig. 12. Check valve, first version with minimised dead volume

To optimise this component, several design steps have been performed as shown below. A key to success was to separate the internals of the valve to avoid risky and hardly controllable welding steps and to create simple, producible parts that are assembled to a valve system in the top lid of the prechamber.

The integration of the check valve in the prechamber top lid is shown in Fig. 14.

Fig. 14. Assembly of check valve (design 1) into prechamber top lid

4. Results

The described components including some more unmentioned design work assembled to a new engine, dedicated to run on CNG only and offering a lean prechamber combustion process. Not touched in this article are the changes to the piston rings to address the different pressure situation of the throttled operation (the Diesel engine is made for unthrottled operation), the modified exhaust manifold and turbocharger, the gasmixer for the CNG-supply to the main combustion chamber and of course the use of special components in the valve train able to run on CNG.

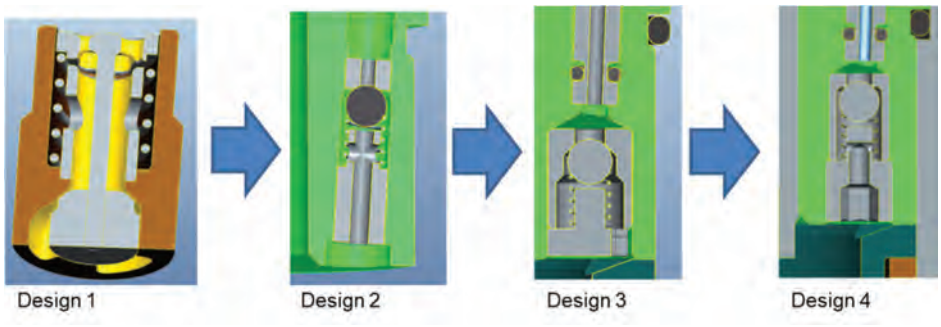

Fig. 13. Evolution of the check valve to the final version

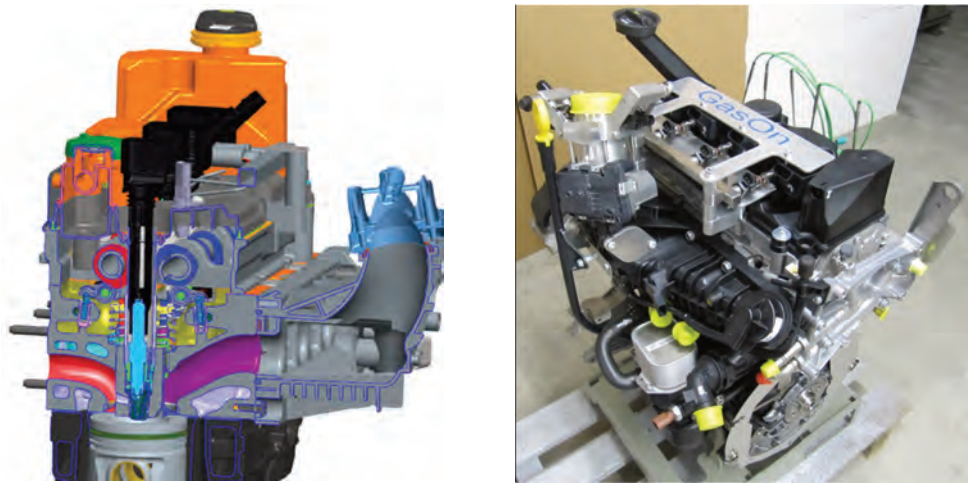

Fig. 15. Section view and photo of GasOn engine

The engines could be driven as planned from the beginning without major problems which was a success for the design and engineering effort creating this engine. The prechamber system is working, the lambda limit for the scavenged operation is above 2, the dosing system is working precisely with very low quantities and all efforts lead to a very promising number: the engine reached a best tested efficiency at lambda 1.7 of more than 44%.

5. Conclusions

In this article, the main challenges for designing a prechamber system for the selected 2.0L Diesel engine have been described and appropriate solutions have been realised. The focus is to find a package and a functional geometry (shape of prechamber, nozzle, piston) at the same time. To achieve the project objective, extensive use of CFD work was required.

An initial question of the project was, if the prechamber combustion system from large bore engines can be applied to much smaller engines as well due to different sizes, diameters, speeds and other parameters. GasOn made a first step of research work in this direction and showed, that the lean prechamber combustion can be applied with a very promising result of working hardware, high combustion efficiency, good combustion robustness and high process controllability.

Acknowledgements

The work presented is part of the Horzon2020 project "GasOn". This project has received funding from the European Union's Horizon 2020 research and innovation programme under grant agreement No 652816.

Bibliography

[1] BOLLA, M. et al. Numerical study of turbulence and fuel-air mixing within a scavenged pre-chamber using RANS and LES. Submitted to *SAE World Congress and Exhibition.* Manuscript no: 19PFL-0664.

[2] LUCAS, G., TALLU, G., WEIßNER, M. CFD-based development of an ignition chamber for a lean and high efficient CNG combustion. *THIESEL 2018 Conf. Thermo- Fluid Dyn. Process*. Direct Inject. Engines High-Pressure. 2018.

[3] NEUSSER, H.J. et al. Volkswagen´s new modular TDI generation. *33rd Vienna Motor Symposium.* 2012.

[4] SOLTIC, P., HILFIKER, T., HUTTER, R., HÄNGGI, S. Experimental comparison of efficiency and emission levels of four-cylinder lean-burn passenger car-sized CNG engines with different ignition concepts. *Combustion Engines*. 2018, **176**(1), 29-37. DOI: 10.19206/CE-2019-104.

[5] TALLU, G. et al. 3D CFD modelling and simulation of spark ignition inclusive turbulence effects and detailed chemical kinetics. *3rd Ignition Conference Berlin.* IAV. 2016, 6-25.

[6] WEIßNER, M. et al. GasOn: a lean CNG combustion for highest engine efficiencies above 43% utilising an ignition chamber. *CO_2 Reduction for Transportation Systems Conference.* 2018, SAE International, Torino.

Michael Weißner, Dipl.-Ing., Volkswagen AG.
e-mail: *Michael.Weissner@volkswagen.de*

Frank Beger, Dipl.-Ing., Volkswagen AG.
e-mail: *Frank.Beger@volkswagen.de*

Martin Schüttenhelm, Dipl.-Ing., Volkswagen AG.
e-mail: *Martin.Schuettenhelm@volkswagen.de*

Gunesh Tallu, M.Sc., Volkswagen AG.
e-mail: *Gunesh.Tallu@volkswagen.de*

Article citation info:
KOTZAGIANNI, M., KYRTATOS, P., BOULOUCHOS, K. Optical investigation of prechamber combustion in an RCEM. *Combustion Engines*. 2018, **176**(1), 10-15. DOI: 10.19206/CE-2019-102

Maria KOTZAGIANNI
Panagiotis KYRTATOS
Konstantinos BOULOUCHOS

CE-2019-102

Optical investigation of prechamber combustion in an RCEM

In this study, detailed investigations of scavenged prechamber engine combustion are performed experimentally in a Rapid Compression Expansion Machine (RCEM), which allows optical access into the main chamber. OH chemiluminescence measurements combined with pressure measurements are used to study the effect of varying ignition timing on combustion and cycle-to-cycle variations. The variation of ignition timing (pressure at ignition) showed an optimum ignition point for a given injection duration. Earlier ignition resulted in weaker but more reactive jets, coupled to increased cyclic variations. Later ignition did not significantly affect heat release rate, but increased cyclic variation.*

Keywords: *scavenged prechamber, optical measurements, ignition timing*

1. Introduction

Efforts to reduce CO_2 emissions from internal combustion engines have led to the use of natural gas as a fuel in lean-burn spark ignition engines [2]. Lean-burn, or alternatively high-dilution combustion concepts, are employed in order to keep engine efficiency high by minimizing thermal losses, while also keeping NO_x emissions below legislated limits. Under high-dilution conditions, operation is limited by high cyclic variability as well as increased unburned hydrocarbon emissions [3, 17]. In order to address these limitations, external ignition engines require high ignition energy and distributed ignition sources in order to ignite and consume the lean/diluted premixed main charge [10, 17].

A widely used technology in these engines is prechamber ignition systems, in which the external ignition source is located in a separate small volume, connected to the main chamber via orifices [3, 17]. This setup allows the design for favorable ignition conditions near the ignition source, which result in fast and repeatable early flame propagation. The pressure difference resulting from combustion taking place inside the prechamber pushes jets containing active radicals and/or hot combustion products into the main chamber, which ignite the lean or diluted mixture. The use of prechamber ignition systems in engines allows the combustion of very lean/diluted mixtures, resulting in higher efficiencies and lower NO_x emissions [17].

Research in the field of prechamber combustion has been extensive in the past years, aiming to increase our understanding and allow the practical application of such systems. Mamar et al. [1] worked on an optically accessible prechamber engine. They reported that a faster combustion was observed using a prechamber in comparison to open chamber ignition. Additionally, faster flame jets induced by higher pressure difference were claimed to reduce the main chamber combustion duration. Moreira et al. [9] analysed an unscavenged prechamber in a four cylinder engine. The unscavenged prechamber system was reported to lead to increased engine efficiency, as well as reduced NO_x emissions and IMEP covariance.

More recently, Kotzagianni et al. [8] compared the scavenged and unscavenged operation modes of a prechamber and investigated the effect of injected fuel amount into the prechamber. The unscavenged operation resulted in slower and longer combustion in the main chamber. Concerning the fuel amount injected into the prechamber, when exceeding a certain amount, additional fuel had no significant impact on the combustion in the main chamber. Some numerical studies [4–7, 11, 16] have studied the effect of turbulence generation in the prechamber. These report that the turbulence inside the prechamber dissipates very quickly between the end of the compression and the ignition; this results in slower jets when ignition timing is late in the cycle. In addition, accurate modelling of the turbulent quantities is important in order to correctly predict prechamber combustion and resulting jet presentation.

In this work, we aim to study the effect of spark timing on the combustion in the prechamber and the main chamber using optical diagnostics and pressure measurements. The purpose is to determine the effect of ignition timing on scavenged prechamber combustion and cycle-to-cycle variation. To this end, an optically accessible Rapid Compression Expansion Machine is used, where information concerning prechamber and main chamber combustion can be obtained through optical measurements. The paper starts with a description of the experimental setup and the measurement conditions chosen. This is followed by the results section, where the prechamber and main chamber combustion are studied, before a brief discussion about the findings and their relevance to scavenged prechamber engine operation. The paper closes with the conclusions of the work.

2. Experimental setup and measurement conditions

The current study was performed in a Rapid Compression Expansion Machine (RCEM). The RCEM operates in a single cycle mode (compression-expansion) and combines excellent optical access with high flexibility in independently changing parameters, such as mixture composition, start of ignition, initial chamber conditions, etc. The RCEM uses a free-floating piston, which is driven by a pneumatic-hydraulic system towards the cylinder head. This motion creates the compression stroke, while the increasing pressure due to compression and combustion eventually drive the piston back. The piston contains a quartz window, which allows optical access towards the cylinder head, where the different pre-chambers are mounted cen-

trally. A UV-enhanced mirror is placed behind the quartz piston in order to allow the detection of the area where the reacting jets were exiting and the combustion inside the main chamber. A schematic of the RCEM, showing the most important components, is shown in Fig. 1. The most important technical characteristics are summarized in Table 1, while further details about the driving part and the principle of operation of the RCEM can be found in [8, 12–14].

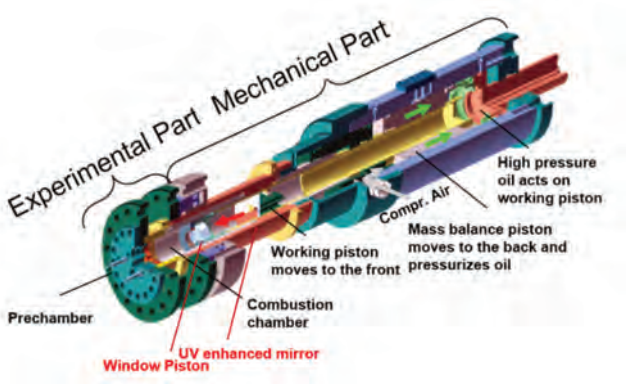

Fig. 1. Schematic of the RCEM, adapted from [15]

Table 1. Technical characteristics of the Rapid Compression Expansion Machine

Parameter	Description
Bore (B)	84mm
Stroke length (s)	Adjustable from 120–249 mm (here 249 mm)
Compression stroke (ε)	5–30
Loading pressure (P_{load})	1–3 bar (here 1.2 bar)
Max. cylinder pressure (P_{max})	Up to 200 bar
Piston bowl	d_b = 52 mm, 2.2 mm depth (top hat)
Piston optical access	d_w = 52 mm, quartz window
Heating system	Cylinder head and cylinder liner heating
Ignition	Spark plug mounted inside the pre-chamber

The RCEM bore diameter is B = 84 mm and the quartz piston has a top hat bowl shape with diameter of 52 mm and depth of 2.2 mm. The piston stroke is adjustable (s = = 120–250 mm), and for this study was set at maximum. The temperature of the cylinder head and liner was set to 383 K using different heating elements and measured by 6 K-type thermocouples. Differently than in an engine, the filling process of the RCEM cylinder is occurring well before the compression and thus no turbulence exists in the main chamber at the beginning of the stroke.

The pre-chamber used is a prototype, and was positioned centrally and in a plane normal to the cylinder axis, similarly to its placement in an engine cylinder. The prechamber has 7 nozzles of 1.5 mm in diameter, which are placed at an angle to the cylinder axis in order to induce a swirling flow within the prechamber during compression.

The pressure measurements inside the main chamber were performed using a cooled piezoelectric pressure sensor (Kistler no. 7061B, 0–250 bar), which was coupled to a Kistler 5011 charge amplifier. An absolute piezoresistive pressure sensor (Kistler no. 4053, 0.0–5.0 bar) was employed for the pressure correction (pegging) of the piezoelectric pressure sensor. The absolute pressure sensor was connected to the cylinder through an automatic switching adaptor (Kistler 741A), which allowed the piezoelectric sensor pegging during the early stages of compression. The initial pressure inside the combustion chamber was set at 1.2 bar for all operating points. Additional piezo-resistive pressure sensors were mounted on the driving piston and the fuel supply line of the PC and MC to control the filling of the driving gas, which was set at 27 bar, and the fuel pressure for the PC and the MC, which were set to 10 and at 60 bar respectively. The synchronisation of all triggering signals, i.e. for the start of injection in the pre- and main chamber, the ignition timing and the image acquisition using the high speed camera, was achieved using a cylinder pressure-based system, which allows triggering at certain cylinder pressures.

The fuel for the filling of the main chamber was administered by a Siemens hollow cone piezo actuated injector, which was located 35 mm off-axis in the cylinder head. The piezo injector has an umbrella angle of 90 degrees and was operated with a nominal needle lift of 25 µm. The injection pressure was 60 bar. For safety reasons and in order to achieve a homogeneous background methane-air mixture, the gaseous methane was injected into the chamber filled with pure air (P_{load} = 1.2 bar) about 3 seconds bTDC and prior to the start of compression. The composition of the main chamber was set to λ = 2.0 for all measurement points. The methane injection for filling the pre-chamber was performed using a prototype injector (EFF-Dunken KSV 017). The injector was supplied with fuel through a pre-chamber injector rail, and the rail pressure was kept constant at 10 bar throughout the experiments. The start of injection was performed during the compression, when the pressure of the main chamber reached 2.0 bar. The injection duration for the pre-chamber fuel filling was kept constant at 2.5 ms for this investigation. The fuel for the PC and MC was supplied from high purity methane bottles (99.995% CH_4). The ignition was initiated by an ignition coil (VW AG 06.J.905.110.G, BEO S3) with a G-type spark plug (NGK R – M10) which has a 0.5 mm gap. The pressure at ignition was varied between 15 and 30 bar. A description of the main parameters for the current measurements is shown in Table 2, which includes the main chamber air/fuel ratio, the prechamber injection duration, the set and measured average pressure at ignition and the average resulting ignition timing referenced to the top dead centre (TDC) point. All measurement points were repeated 12 times; the pressure results reported are the averages of the 12 repetitions.

Table 2. Operating conditions

Main chamber λ	PC injection duration (ms)	Set pressure at Ignition (bar)	Meas. av. pres. at ignition (bar)	Av. ignition time bTDC (ms)
2.0	2.5	15	14.9	–5.12
2.0	2.5	18	18.2	–4.53
2.0	2.5	23	23.1	–3.31
2.0	2.5	26	25.6	–3.10
2.0	2.5	30	29.6	–2.59

Information about the combustion characteristics of the flame/radical jets and the flame propagation inside the main chamber were acquired using high speed 2D OH* chemiluminescence imaging. The spatial distribution of OH* chemiluminescence was recorded with an intensified high speed camera at 32 kHz repetition rate (LaVision HSSX and image intensifier, 10/12 bits dynamic range) equipped with a 50 mm UV lens (f/20) and a bandpass filter for a wavelength of 306 nm and 12.1 nm FWHM. The acquired 2D OH* chemiluminescence images have been analysed using a purpose-built Matlab routine in order to obtain information about the jet exiting time.

3. Results

The study undertaken involves the variation of the spark timing with respect to TDC, which was achieved by varying the value of cylinder pressure when the ignition is triggered. The ignition was triggered at cylinder pressures from 15 to 30 bar, with steps of around 4 bar (15, 18, 23, 26, 30 bar). This variation is expected to have multiple effects on the prechamber combustion. The variation of pressure directly affects the thermodynamic conditions at ignition, since the pressure and temperature are correlated if we assume a near-adiabatic, closed system. The exact temperature at the ignition location is very difficult to be estimated since the heat losses, particularly within the prechamber, are unknown; nevertheless, the gas temperature is expected to be increasing with increasing pressure, resulting in a faster laminar flame speed (the increase of laminar flame speed with temperature is higher than the corresponding decrease with increasing pressure). In addition to this, during the compression stroke, as the main chamber pressure increases, more of the leaner main charge is pushed into the prechamber, increasing the average air to fuel ratio. This, along with the degree of homogenization of the prechamber which increases with time, is expected to have a significant effect on the flame speed in the prechamber. At earlier ignition timings the fuel-air mixture near the spark location is expected to be rich, while at later spark timings it is expected to be leaner. Finally, the turbulence intensity in the prechamber, which varies significantly with time due to the variable turbulence production from the incoming flow and the turbulence dissipation over time, is expected to mostly decrease with later ignition timings (i.e. with higher pressures at ignition).

In the present investigation three diagnostics are used to investigate the prechamber and main chamber combustion with different ignition timings. For the prechamber combustion, the jet emergence timing after ignition into the main chamber as the primary diagnostic. The earlier timing after ignition indicates faster combustion in the prechamber. For the main chamber combustion we use the main chamber optical images which give an indication of jet and flame reactivity, as well as the calculated main chamber heat release rate (HRR). The prechamber and main chamber combustion are presented separately in the subsections which follow. The results section closes with a discussion of the findings and an attempt to connect these results to engine operation.

3.1. Prechamber combustion

In this study we use the jet emergence timing after ignition into the main chamber as the primary diagnostic of the prechamber combustion. The jet exit timing is determined when a certain level of OH* is visible in the main chamber. The level of OH* was arbitrarily chosen to avoid measurement noise affecting the study. Figure 2 shows the jet exit timing in ms after the ignition timing, for the different ignition pressures and for each of the 12 repetitions at each pressure point.

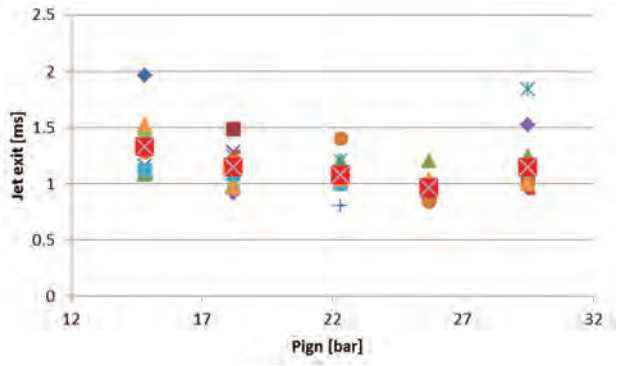

Fig. 2. Time of burning jet emergence into the main chamber for all 12 repetitions per operating point, plotted versus P_{ign}

The average trend indicates the combustion in the prechamber to be faster with increasing pressure at ignition up to P_{ign} = 26 bar. This is expected to be the result of the combination of increasing reactivity due to the charge temperature and in particular better mixing of prechamber fuel with incoming main chamber charge later in the cycle. A further increase in pressure at ignition to P_{ign} = 30 bar results in a longer time for the jets to emerge, despite the expected increasing temperature of the charge. This can be explained by two possible effects: on the one hand, the reactivity of the mixture near the spark location and during the flame propagation might reduced due to over-leaning of the mixture from the incoming main chamber charge. Alternatively, or in addition, the turbulence intensity caused by the high-velocity incoming flow from the prechamber nozzles during the compression stroke has dissipated significantly at this point, leading to reduced turbulent flame speed and thus delayed jet exit.

What can also be observed from Figure 2 is that the cyclic variation also decreases when approaching the P_{ign} = 26 bar point. The cyclic variation is expected to arise mainly during the early flame development, since the following turbulence-driven flame propagation is expected to be repeatable due to the turbulence being generated by the piston stroke. Thus, the cyclic variation is expected to be connected to small changes in local reactivity around the spark plug; this is supported by the observation that the highest cyclic variation is at the extreme points: P_{ign} = 15 bar and P_{ign} = 30 bar. In the former the mixture near the spark plug is rich, while in the latter the mixture is lean. Further analysis of these effects will require the contribution of CFD calculations for these cases, in order to obtain spatial and temporal information concerning the thermochemical conditions in the prechamber.

3.2. Main chamber combustion

Figure 3 shows the time-resolved OH* chemiluminescence images for representative cycles with P_{ign} = 15, 23 and 30 bar. The representative cycles were chosen to be the single realisations of the experiment which have a pressure trace closest to the average pressure trace of all 12 repetitions at these conditions. What is interesting to observe is that the case of P_{ign} = 15 bar shows the highest OH* signal from the early jets (time instant 1.6ms after ignition). This is understood to be due to reactions which occur on the jet surface, from the mixing of the rich jets with the surrounding lean mixture. The intensity then is significantly reduced, before a premixed flame is formed. At this point of main chamber flame propagation higher OH* intensity

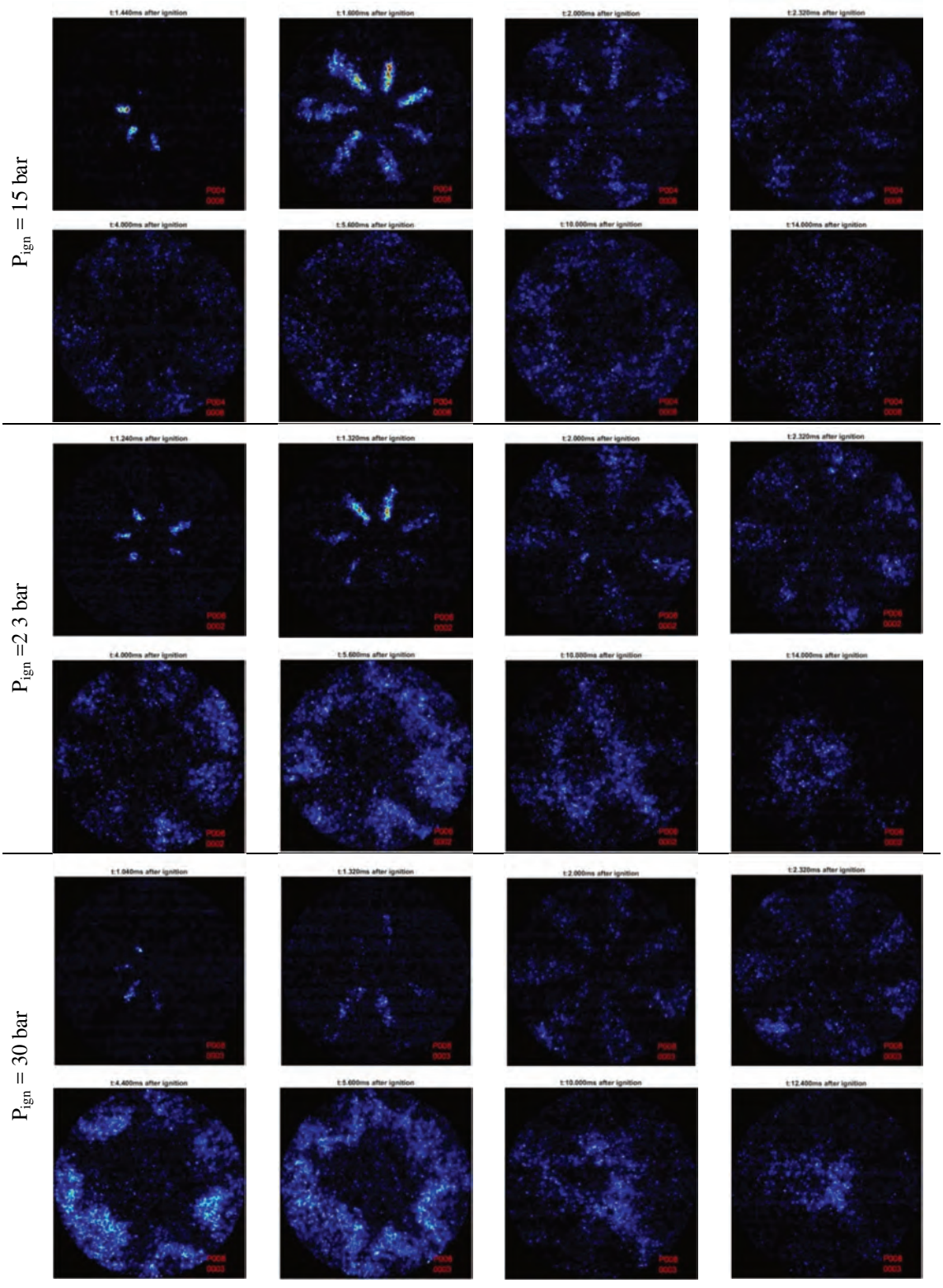

Fig. 3. OH* chemiluminescence images, showing the prechamber jets and the combustion evolution in the main chamber in cases when ignition occurred at 15 bar (first two lines), 23 bar (middle two lines) and 30 bar (last two lines)

observed in the cases with later ignition. This indicates that the ignition and subsequent combustion in the main chamber is slower for the early ignition case, possibly due to the reduced reactivity of the main chamber mixture at jet exit (the pressure and as a consequence the charge temperature is lower) and the reduced turbulence intensity induced by the weaker jet.

The observations presented above are supported by the HRR traces of the representative cycles for the same three measurement points, shown in Fig. 4. In the figure the HRRs are plotted against time with the reference at ignition (left plot), as well as with time = 0 ms at TDC (right plot). These plots allow the comparison of the HRRs in cycle time as well as with respect to ignition timing. The main chamber HRR induced by the jets in the earlier ignited case (P_{ign} = 15 bar) shows a slower increase and a significantly reduced peak. What is also noticeable is the delay in the establishment of the premixed flame after the jet exit, which is indicative of the lower reactivity of the main chamber mixture at this jet exit timing. In addition, the possibly lower The two cases with later ignition show very similar HRRs, despite a small delay of the jet exit in the P_{ign} = 30 bar case.

The automotive industry has been intensively modernized in recent years in the aspect of exhaust emissions reduction. Modern passenger vehicles must comply with emission norms in real driving conditions and extended environmental conditions relative to the pre-existing dynamometer tests (variable ambient temperature, pressure, congestion, driving style etc.) [16]. RDE road tests should therefore take into account all possible road situations while maintaining a set specific driving style, so that the obtained emission results are indicative of the vehicle technical characteristics [2]. Thus, there is a number of conditions that must be met in order to perform these test [3].

Vehicle manufacturers continuously introduce modern drive systems in order to meet the stringent emission norms. Despite the increase in the electric vehicles market share, the internal combustion engine continues to be the main propulsion mechanism used in vehicle drive systems (Fig. 1). Their presence will be noticeable in all kinds of hybrid drives [4, 11].

3.3. Discussion

In all, the variation of ignition timing (pressure at ignition) showed to significantly affect the prechamber combustion and subsequent main chamber HRR. Early ignition resulted in slower prechamber combustion and the emergence of possibly rich jets early in the cycle, which then lead to a delayed and slower main chamber combustion due to the reduced main chamber reactivity at that time, and possibly low turbulence generation from the jets. Progressively later ignition seemed to produce more stable conditions for prechamber ignition and faster prechamber combustion, up to the point where the trend was reversed possibly due to over-leaning of the prechamber charge through mixing with the incoming main chamber charge and reduced turbulence intensity in the prechamber. Nevertheless the slightly delayed jet emergence timing for the case with late ignition did not seem to affect the main chamber HRR appreciably.

In terms of the relevance to engine operation, it seems clear that the ignition timing in scavenged prechamber engines will need to be coupled to the prechamber injection amount. For early timings, smaller amounts will need to be injected, while in later timings larger amounts are appropriate; this is in order to ensure high-reactivity mixture near the spark plug at ignition, in order to achieve repeatable combustion in the prechamber and low cyclic variation in the main chamber. In addition, high early flame reactivity coupled to high turbulence levels should be sought in order to enhance the main chamber combustion rate and thus engine cycle efficiency.

4. Conclusions

In this study the combustion in the prechamber and main chamber for a scavenged prechamber system was investigated experimentally at engine relevant conditions with varying ignition timing in a Rapid Compression Expansion Machine (RCEM). The RCEM allows single parameter variation in addition to optical access into the main chamber for optical diagnostics of the prechamber jets and subsequent flame development. The optical information was obtained using OH* chemiluminescence measurements,

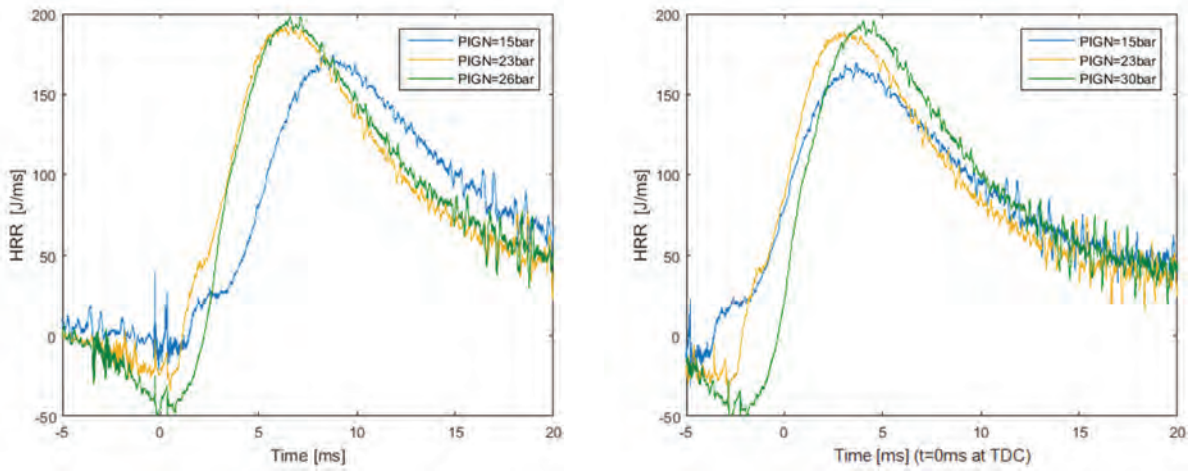

Fig. 4. Heat release rate for the representative cycles of the P_{ign} variation plotted against time after ignition (left) and time after TDC (right)

in order to gain useful insights on the jets exiting the prechamber and combustion propagation in the main chamber. Besides the optical data, pressure measurements were recorded during all the experiments, which allowed the identification of cycle-to-cycle variability and the calculation of heat release rate in the main chamber.

In the present investigation the fuel concentration inside the main chamber (λ_{main}) and in the prechamber (i.e. the prechamber injection duration) were kept constant, while the pressure at which the ignition was triggered was varied, resulting in an effective change in ignition timing.

The variation of ignition timing (pressure at ignition) showed to significantly affect the prechamber combustion and subsequent main chamber HRR. Early ignition resulted in slower prechamber combustion and the emergence of possibly rich jets early in the cycle, which then result in a delayed and slower main chamber combustion. Progressively later ignition seemed to produce more stable conditions for prechamber ignition and faster prechamber combustion, up to the point where the trend was reversed. This reversal in trend was attributed to over-leaning of the prechamber charge through mixing with the incoming main chamber charge and reduced turbulence intensity in the prechamber with increasingly late ignition timings.

The results indicate that adapted prechamber injection strategies should be followed when varying spark timing in prechamber engines; early ignition should be coupled with low injection amounts, whereas late ignition should be coupled with higher injection amounts. This is expected to lead to faster main chamber combustion and reduced cycle-to-cycle variation.

Bibliography

[1] AL-MAMAR, F.N.A.A., HYNES, J., SHEPPARD, C.G.W. Combustion rate in a dual chamber S.I. engine. *Combustion Science and Technology*. 1986, **45**(1-2), 85-100.

[2] BHANDARI, K. et al. Performance and emissions of natural gas fueled internal combustion engine: A review. 2005.

[3] DALE, J.D., CHECKEL, M.D., SMY, P.R. Application of high energy ignition systems to engines. *Progress in Energy and Combustion Science*. 1997, **23**(5-6), 379-398.

[4] GENTZ, G. et al. A study of the influence of orifice diameter on a turbulent jet ignition system through combustion visualization and performance characterization in a Rapid Compression Machine. *Applied Thermal Engineering*. 2015, **81** (Supplement C), 399-411.

[5] GHOLAMISHEERI, M. et al. CFD modeling of an auxiliary fueled turbulent jet ignition system in a Rapid Compression Machine. *SAE Technical Paper* 2016-01-0599, 2016.

[6] GHOLAMISHEERI, M. et al. Rapid Compression Machine study of a premixed, variable inlet density and flow rate, confined turbulent jet. *Combustion and Flame*. 2016, **169**, 321-332.

[7] GHOLAMISHEERI, M., WICHMAN, I.S., TOULSON, E. A study of the turbulent jet flow field in a methane fueled turbulent jet ignition (TJI) system. *Combustion and Flame*. 2017, **183**(Supplement C), 194-206.

[8] KOTZAGIANNI, M. et al. Experimental and computational investigations of prechamber jet ignition in a Rapid Compression Expansion Machine. *10th Mediterranean Combustion Symposium*. 2017. Naples, Italy.

[9] MOREIRA, T.A.A. et al. Characterization of a multi-cylinder torch ignition system operating with homogenous charge and lean mixture. *SAE Technical Paper* 2014-36-0333. 2014.

[10] MORSY, M.H. Review and recent developments of laser ignition for internal combustion engines applications. *Renewable and Sustainable Energy Reviews*. 2012, **16**(7), 4849-4875.

[11] THELEN, B.C.,TOULSON, E. A computational study of the effects of spark location on the performance of a turbulent jet ignition system. *SAE Technical Paper* 2016-01-0608, 2016.

[12] SCHLATTER, S. et al. Experimental study of ignition and combustion characteristics of a diesel pilot spray in a lean premixed methane/air charge using a Rapid Compression Expansion Machine. *SAE Technical Paper* 2012-01-0825, 2012.

[13] SCHLATTER, S. et al. N-heptane micro pilot assisted methane combustion in a Rapid Compression Expansion Machine. *Fuel*. 2016, 179, 339-352.

[14] SCHLATTER, S. et al. Comparative study of ignition systems for lean burn gas engines in an optically accessible Rapid Compression Expansion Machine. *SAE Technical Paper* 2013-24-0112, 2013.

[15] Testem, Technical Manual TeRCM-K48: Rapid Compression Machine for in-cylinder spray development and combustion processes analysis. 2004, Testem – Gesellschaft für Mess- und Datentechnik GmbH.

[16] THELEN, B.C.,TOULSON, E. A computational study on the effect of the orifice size on the performance of a turbulent jet ignition system. *Proceedings of the Institution of Mechanical Engineers, Part D: Journal of Automobile Engineering*. 2016.

[17] TOULSON, E., SCHOCK, H.J., ATTARD, W.P. A review of pre-chamber initiated jet ignition combustion systems. *SAE Technical Paper* 2010-01-2263. 2010.

Maria Kotzagianni, MEng. – Institute of Energy Technology, ETH Zurich.

e-mail: *M.Kotzagianni@lav.mavt.ethz.ch*

Panagiotis Kyrtatos, DEng. – Institute of Energy Technology, ETH Zurich & Vir2sense GmbH.

e-mail: *Kyrtatos@lav.mavt.ethz.ch*

Prof. Konstantinos Boulouchos, DEng. – Institute of Energy Technology, ETH Zurich.

e-mail: *Boulouchos@lav.mavt.ethz.ch*

Article citation info:
PIELECHA, I., BUESCHKE, W., SKOWRON, M. et al. Prechamber optimal selection for a two stage turbulent jet ignition type combustion system in CNG-fuelled engine. *Combustion Engines*. 2019, **176**(1), 16-26. DOI: 10.19206/CE-2019-103

Ireneusz PIELECHA
Wojciech BUESCHKE
Maciej SKOWRON
Łukasz FIEDKIEWICZ
Filip SZWAJCA
Wojciech CIEŚLIK
Krzysztof WISŁOCKI

CE-2019-103

Prechamber optimal selection for a two stage turbulent jet ignition type combustion system in CNG-fuelled engine

Searching for further reduction of fuel consumption simultaneously with the reduction of toxic compounds emission new systems for lean-mixture combustion for SI engines are being discussed by many manufacturers. Within the European GasOn-Project (Gas Only Internal Combustion Engines) the two-stage combustion and Turbulent Jet Ignition concept for CNG-fuelled high speed engine has been proposed and thoroughly investigated where the reduction of gas consumption and increasing of engine efficiency together with the reduction of emission, especially CO_2 was expected. In the investigated cases the lean-burn combustion process was conducted with selection of the most effective pre-combustion chamber. The experimental investigations have been performed on single-cylinder AVL5804 research engine, which has been modified to SI and CNG fuelling. For the analysis of the thermodynamic, operational and emission indexes very advanced equipment has been applied. Based on the measuring results achieved for different pre-chamber configurations the extended methodology of polioptimization by pre-chamber selection and the shape of main chamber in the piston crown for proposed combustion system has been described and discussed. The results of the three versions of the optimization methods have been comparatively summarized in conclusions.

Key words: *gas engine, prechamber, thermodynamic analysis, combustion, exhaust emission, optimisation*

1. Introduction

The global production of automotive vehicles continues to increase every year, reaching the level of over 97 million units produced in 2017 [28]. Currently, the majority of these vehicles (estimated in 2012 at 96%) are powered by combustion engines running on liquid petroleum fuels [8]. However, the availability of such fuels is increasingly limited due to the depletion of oil resources. At the same time, the content of heavier hydrocarbon fractions creates numerous problems with the emission of harmful compounds and particulate matter.

In this context, increasingly attention is paid to gaseous fuels. Among them, the most popular is natural gas, whose global production in 2017 reached over 3700 billion m^3 [2]. The share of this fuel in the global energy consumption by the transport sector is forecast to increase from 3% in 2012 to 11% in 2040 [22, 26]. This is supported, inter alia, by the intensive development of CNG refueling infrastructure [5, 10] and the lower impact of pollutant emissions from gas engines on the natural environment.

Due to the relatively low density of natural gas (0.7–0.9 kg/m^3) [11], the lower flame propagation rate (0.37 m/s at $\lambda = 0.9$) [18] and high A/F value (17.2) [11], changing the fuel supplied to a high-speed SI engine with indirect injection from liquid to CNG results in a reduction of power and torque [29]. A positive aspect of using CNG in these types of constructions is the reduction of some exhaust components emission [7, 19], in particular CO_2 emissions.

The parameters of natural gas listed above require the use of a dedicated system for the charge preparation and combustion. Currently, in addition to the aforementioned conventional combustion system with SI and indirect injection, two alternative system types that effectively burn natural gas can be distinguished. First is the direct injection of natural gas into the combustion chamber, which allows limiting the volumetric losses in the low engine speed range. The use of direct injection results in increased power and torque, as well as an increase in thermal efficiency [6].

An alternative solution is a two-stage combustion system (TJI – *Turbulent Jet Ignition*) [22, 25] that uses an ignition chamber directly powered with gas and the main chamber with external mixture preparation. There is a spark plug located in the prechamber (ignition chamber) and a gas supply channel through a one-way valve as well. This enables obtaining a rich, easily flammable gas/air mixture. The streams of burning fuel flowing through the inter-chamber channels lead to surface ignition of a lean fuel mixture located in the main combustion chamber, while the lean fuel mixture itself is prepared in a mixer or by means of gas injection into the intake manifold.

2. Literature study

The combustion with excess oxygen, called lean combustion, is being used due to the increase in engine thermal efficiency and to exploit the potential to reduce some engine emissions [25], with special focus put on the NO_x-emissions, which decreases with the increase in air-fuel equivalence ratio – in parallel with the decrease in combustion temperature – one of main factors influencing emission of these compounds. However, the biggest benefits in the reduction of thermal NO_x emissions happen for the $\lambda > 1.4$. This value is the lean combustion limit for conventional spark ignition systems, but can be further extended with the implementation of turbulent jet ignition (TJI), which can deliver much higher activation energy to start the combustion process of a lean mixture. Such a system can be used either without injection to the ignition chamber (passive or unscavenged configuration) or with

prechamber injection (active or scavenged configuration) [2, 3, 12]. Hence the active TJI has been introduced to the engine, stable operation has been achieved for $\lambda \sim 2.2$, in parallel with better indicated net thermal efficiency values from $\lambda > 1.2$ and also 2% greater η_{t_max} (at $\lambda \sim 1.6$).

The prechamber system has been widely investigated in heavy duty engines [14, 17, 24] and the positive impact of TJI implementation has been confirmed regarding the combustion indicators. However, the high level of its complexity results in reduced scalability and confirms the necessity of functional analysis in case of small reciprocating engines [21].

TJI indicates the potential in knock characteristic improvement at high load engine operation [1]. In the scope of the mentioned study several fuel blends with reduced octane number in the range of 93–60 have been supplied during WOT operation to the dual stage combustion system in unscavenged configuration. At the constant engine speed of 1500 rpm, the knock limit extension that was sourced in improved burn rate, allowed using fuel with octane number 10 points lower. Further, with optimized ignition timing and due to the reduced ignition delay and faster combustion, the benefit of 15 octane number fuel has been proven, which enables increasing the CR by approximately 3 points and also thermal efficiency benefits [30].

The prechamber-initiated combustion system has been investigated by the authors of this study [15] with focus on determination of possible and beneficial fuel supply strategies for both chambers. The main chamber has been fed indirectly with CNG doses in the range $q_{0\_MC} = (14.8–19.0)$ mg/inj, while the prechamber injection has been set at $q_{0\_PC} = (0.63–2.76)$ mg/inj. Considering the ignitability limit for the prechamber system supplied with the main CNG dose greater than 17.7 mg/inj, the top end limitation in prechamber fuel supply is clearly marked with rapid increase in CoV(IMEP) – for $q_{0\_PC} > 1.7$ mg/inj and a reduced HRR. As indicated, this is caused by the conditions in the pre-combustion chamber being too rich. In case of the low dose value ($q_{0\_MC} = 14.8$ mg/inj), the combustion stability penalty has been observed for a much greater prechamber dose ($q_{0\_PC} > 2.2$ mg/inj), however the prechamber supplied with fuel quantity reduced below $q_{0\_PC} < 1.1$ mg/inj resulted in significant increase in the combustion non-uniformity. This confirms the lower ignitability limit, which is marked by too lean prechamber conditions.

Geometrical configuration of the prechamber system has a significant impact on the main combustion process. The literature-indicated prechamber cavity V_{pc} share in total combustion chamber volume is given by [27]:

$$r_v = \frac{V_{pc}}{V_{pc}+V_{mc}} \tag{1}$$

where V_{mc} is the volume of main chamber, and varies in range of $r_v = (1.1–37)\%$.

Oversizing the pre-combustion cavity causes excessive energy to be transferred to the main combustion chamber (assuming a constant prechamber stoichiometry). In studies of lean mixtures combustion in the main chamber a significant increase in r_v, at a constant lambda value, results in an increase of NO_x emission [13]. Other studies confirm the 5% volume limit regarding the heat losses level in various cited works of Attard, compare with [1–3].

Bunce et al. conducted research into the number of nozzles and their diameter using an optically accessible engine with a displacement of 0.601 dm^3 [4]. As an obvious result of increasing the number of nozzles from 4 and 8 (both with a diameter of 1.36 mm) was the lower peak PC/MC pressure difference – from 6 bars at $\lambda = 1.55$ to 4 bars at $\lambda = 1.99$ respectively. However, the prechamber light-off accelerates with the increase in nozzle flow area. The reasons for this outcome are the better scavenging of residuals from the previous combustion cycle and more favourable air-fuel stoichiometry in the area of the spark plug. The faster prechamber light-off has its reflection in the earlier ignition of the main charge – up to 2.5 deg CA at $\lambda = 1.8$ – and faster MFB10–90 promoting better control of the main combustion process. Another numerical study focused on the diameter of a single nozzle (diameters of 3, 4, 6 and 9 mm have been compared) and the mentioned relation has been confirmed with indication of bigger heated volume of the main chamber at the defined time instance after prechamber ignition [9].

The common impact of both the prechamber volume and the nozzles diameter on combustion stability and emission of NO_x has been investigated by Shah et al. [20]. The $r_v = (1.4–3.7)\%$ and nozzle area to volume ratio $A_{PC}/V_{PC} = (0.025–0.045)$ cm^{-1} have been investigated. Increasing the prechamber volume increases combustion stability, however also results in higher NO_x emission. The opposite result has been noted with the increase in nozzles diameter, so both these relations need to be considered regarding the criteria, which have to be met when TJI is being applied.

As described, the impacts of system constructional features on the engine operation have been individually investigated, but there are no studies considering the prechambers multiparametrically (volume of prechamber in combination with nozzles diameter and their angularity) and providing their comparison under selected criteria. Thus, the comparative investigations have been undertaken and a new optimization method has been created, described and implemented.

3. The objective of the research

The decision to perform this research was to select the combustion system parameters, allowing for improvement of the engine operating indicators. The focus was on the issue of increasing the engine work cycle efficiency while minimizing the toxic exhaust emissions. For the assumptions made as stated, variables were defined as the geometrical parameters of: the prechamber and chambers in the piston, as well as the fuel supply system. The final result of the research was to find the best possible solution for the defined criterion function including indicated efficiency, CO, THC and NO_x emission intensities and the mean effective pressure value.

4. Research methodology

4.1. Research objects: prechambers

The research involved using six ignition chambers of different geometry, with parameters as shown in Table 1. Each of them has six to seventeen outflow channels with diameters ranging from 0.9 to 2.0 mm, located in the lower part of the chamber (Fig. 1).

Table 1. Prechambers parameters

No.	V_{chr}	No. of nozzles	Ø nozzle	Type of nozzles
–	cm^3	–	mm	–
P1	1.826	7	1.5	radial (R)
P2	1.826	6	1.5	radial (R)
P3	2.287	6	2.0	radial (R)
P4	2.287	6	1.5	radial (R)
H1	1.826	7R+3A	1.5R+1.4A	radial (R)/axial (A)
H2	1.826	12R+5A	0.9	radial (R)/axial (A)

The volume of the ignition chambers was 1.8 and 2.2 cm^3, constituting from 5% to 6.2% of the total volume of the combustion chamber.

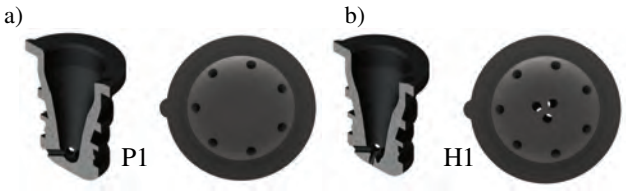

Fig. 1. Prechambers cross-section and a bottom-side image: a) P1, b) H1

Due to the location of the outflow channels and the resulting need to use different shapes of the piston crown, the chambers were divided into two groups marked with the symbols "P" and "H". The "P" chambers have radial outflow channels (R-radial), in which a piston with an "omega" combustion chamber was used (Fig. 2a). The "H" chambers were characterized by radial and axial outflow channels (H-horizontal). Placing the outflow channels in the central part of the bottom of the chamber required the use of a piston with a semicircular, open, hemi-spherical combustion chamber (Fig. 2b).

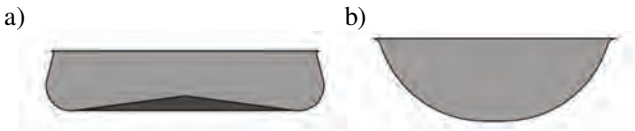

Fig. 2. Cross-section of combustion chambers used in the piston: a) omega, b) hemi-spherical

4.2. Test-bench

The investigations of new combustion systems have been conducted on single cylinder research engine AVL 5804, originally CI, modified to use CNG fuel and with a two-stage SI combustion system (Fig. 3). Selected measuring equipment has been installed on the test rig (compare with chapter 4.3), as well as a dedicated control system.

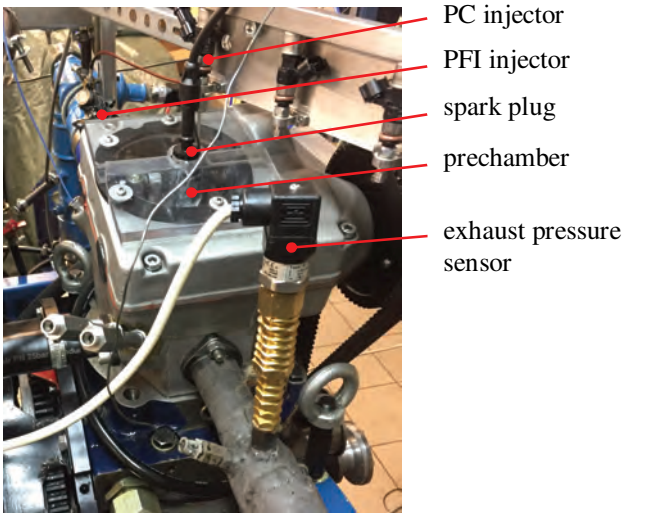

Fig. 3. AVL 5804 test bench

Fuel supply system in the first version consists of electromagnetic Bosch CNG nozzle injecting the fuel to the helical intake port – chosen based on the results of other investigations with spray ignition [16] – and the second nozzle directed into the prechamber (Fig. 4a), scavenged prechamber system has been investigated. Second version, used to achieve a better homogenization of the main mixture, consisted of a CNG mixing device, which has been installed at a greater distance from the cylinder head (Fig. 4b). This change in the fuel supply system has been implemented in parallel with the introduction of a Hemi-like main combustion chamber and the use of prechambers with axial nozzles – designated as "H".

The parameters of AVL 5804-engine are listed in Table 2. Auxiliary supercharging system with intake throttle has been used to achieve the required air mass flow. The exhaust system throttle body has been installed to implement the flow restriction resulting from the turbocharging system, with assumption of characteristic intake pressure p_1 and exhaust pressure p_2 ratio as in the full engine investigations [23]:

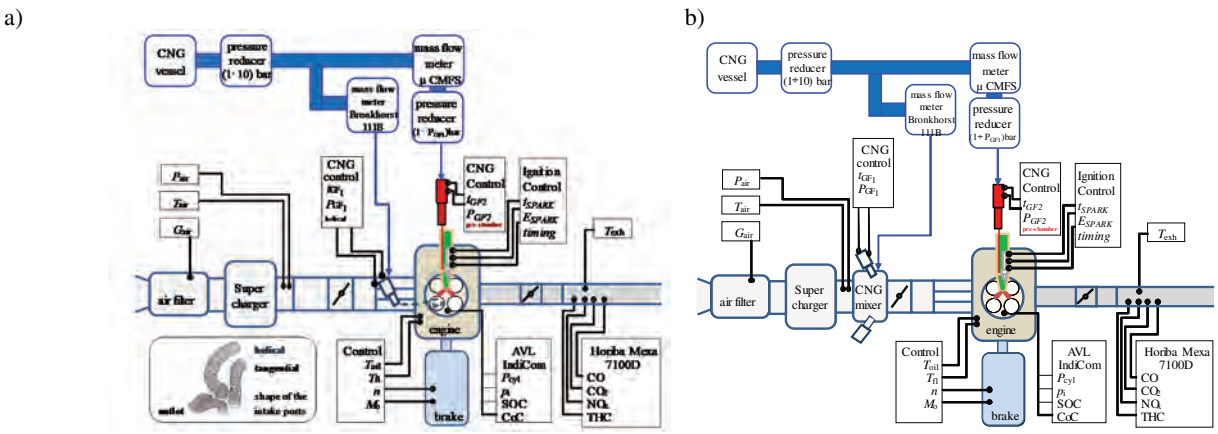

Fig. 4. Functional schematic of the test bench with AVL 5804 engine: a) prechamber injection and port fuel injection, b) prechamber injection and CNG mixer in the intake port

$$x_p = \frac{p_2}{p_1} \quad (2)$$

The emissions measurements have been performed using Horiba Mexa 7100D system.

Table 2. Technical parameters of AVL 5804-engine

Parameter	Unit	Value/Type
Engine	–	1-cylinder, prechamber
Swept volume	dm^3	0.5107
Bore × Stroke	mm	85 x 90
Compression ratio	–	15.2
Fuel supply	–	1. PFI (helical port), prechamber injection 2. Heinzmann-mixer, prechamber injection
Intake system	–	Throttled, with auxiliary supercharging system
Exhaust system	–	Throttled

4.3. Measuring equipment

In order to precisely determine the basic parameters of the engine's operation, including the mass consumption of air and fuel, a number of indicators, engine load, as well as harmful exhaust emissions, measuring apparatus described in Table 3 was used. A fuel supply double system (indirect to the main chamber and direct to the prechamber) necessitated the use of two natural gas flowmeters with different measurement ranges. Pressure sensors installed independently in the main combustion chamber and in the prechamber allowed to determine differences in the thermodynamic processes characteristic.

Table 3. Measuring equipment of the researched engine AVL 5804

Parameter	Description	Range
Engine brake	AVL AMK DW13-170	–50–300 Nm
Air consumption	Sensycon Sensyflow	0–720 kg/h
Charging system	Eaton M62	0–2 bar
Fuel consumption (prechamber)	Bronkhorst 111B	0.1–100 g/h
Fuel consumption (main chamber)	Emerson µCMFS	0.1–2 kg/h
Air pressure, fuel pressure	Wika A-10	0–10 bar
Air temperature, fuel temperature	Linuatherm Pt100	–50 – 500 deg. C
Lubrication system	AVL 577	0–150 °C
Cooling system	AVL 577	0–150 °C
Data acquisition	AVL IndiSmart	8-kanałowy system
	AVL Concerto	Post-processing
Emission measurement	Horiba Mexa 7100D	10–50000 ppmHC 50–5000 ppm CO(L) 0,5–10 % CO(H) 0,5–20 % CO_2 10–10000 ppm NO_x

4.4. Research plan

After selecting the variables of the studied processes and their value ranges, the appropriate test apparatus was chosen and the scope of the experiment was defined. The engine operating points were selected and described using parameters:

– Engine speed n = 1500 rpm,
– Engine load IMEP = 0.7 MPa,
– Presence of a combustion center at 8 deg ATDC,
– Ignition coil charging current 6.5 A.

For a point so defined, the fuel dose size was determined and variables defining the comparison points were selected.

In order to obtain different values of the excess air coefficient (λ = 1.32; 1.50; 1.65), the boost was controlled accordingly. To simulate the throttling of the air caused by the turbocharger (in a four-cylinder engine) a Venturi with adjustable setting was used and the ratio of inlet-to-outlet pressures corresponding to the values of the turbocharged engine was maintained.

The division of the fuel dose between the pre-chamber and the main chamber was an important variable parameter; needed to assign a map of points and verify the best possible power combination for each of the tested systems.

The data point set was shown in Table 4.

Table 4. Pre-selection of test points

No.	Lambda	Fuel dose q_{0_PC}
1.	1.65	ca. 1.9 mg/inj→ 6 research points → ca 0.35 mg/inj (18 research points) (change of the excess air coefficient by changing the amount of air)
2.	1.5	
3.	1.32	
Constant value		n = 1500 rpm CoC = 8 deg ATDC I_{coil} = 6.5 A Full fuel dose (q_{0_MC} + q_{0_PC}) ≈ 21.7 mg/inj
Resultant values		IMEP, emission

5. Normalizing of the measurements results

Analysis of the measurement results revealed a discrepancy between the excess air coefficient λ and the qo_PC fuel dose in individual measurement cycles (Fig. 5). Therefore, it became necessary to normalize these values to enable results comparison.

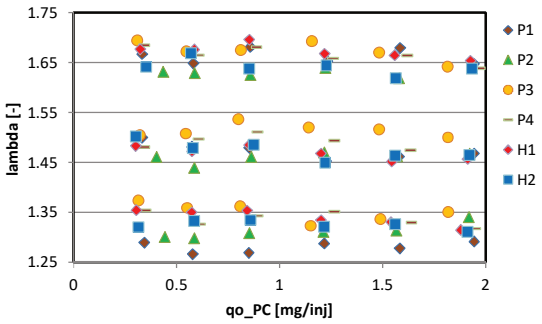

Fig. 5. Values of excess air coefficient and fuel dose before normalization

Based on the raw data three lambda values (1.65; 1.5; 1.32) were selected as representative for three loads of engine operation. An exhaust gas analysis was performed

based on the real resulting lambda value – meaning not exactly for values selected as representative ones (Fig. 6). To get the emission, efficiency and IMEP values for the preselected level of lambda an interpolation procedure has been applied.

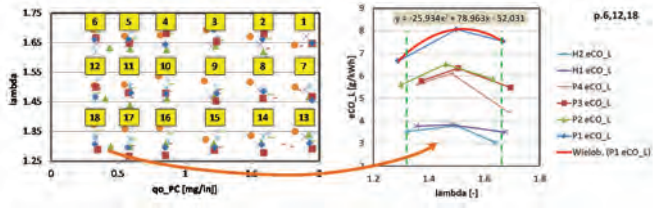

Fig. 6. The method of determining constant values of the excess air coefficient

Using the interpolation of the $ax^2 + bx + c$ quadratic function for each CO_L emission curve based on measured values, the resulting emissions for selected lambda values (1.65, 1.5, 1.32) were determined. Values of lambda were determined using the Van der Mond matrix (a, b, c-values). Emission (CO, THC, NO_x), efficiency (eta_o) and others (IMEP, CoV_IMEP) were determined for lambda = 1.65; 1.5; 1.32 as well (Fig. 7).

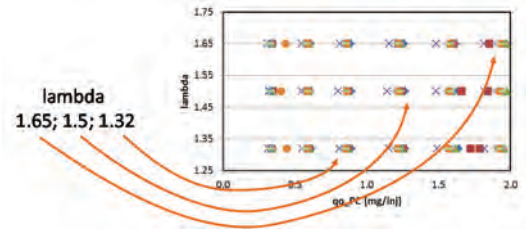

Fig. 7. Predefined constant values of excess air coefficient

By averaging of the qo_PC values, the representative points qo_PC were selected. These were: 0.35; 0.6; 0.9; 1.2; 1.6; 1.9 mg/inj (Fig. 8).

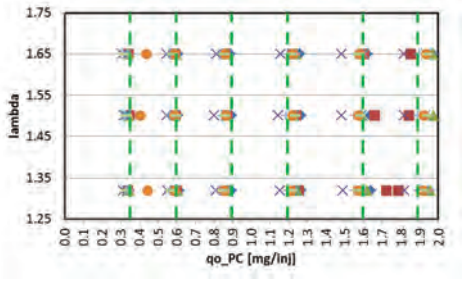

Fig. 8. Adoption of fixed fuel dose values qo_PC

Due to the lack of monotonous function for designation of qo_PC (Fig. 9) the following steps were performed:

a) for lambda values: min (1.35) and max (1.9) an extrapolation based on three curve extreme points using the Van der Mond matrix were accepted (Fig. 10);

b) for internal value points the calculation was based on interpolation (Fig. 11a) between determined measuring points (as illustrated in Fig. 11b).

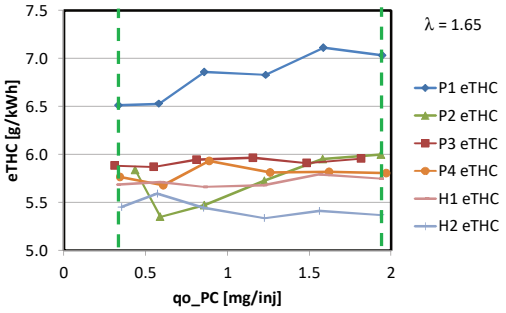

Fig. 9. Determination of the interpolated values of emission intensity (e.g. for THC)

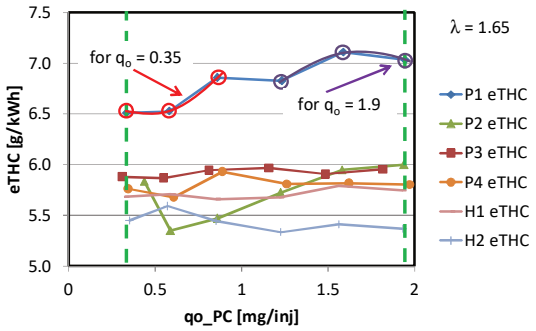

Fig. 10. Selection of points for emission intensity determination by extreme fuel doses qo_PC

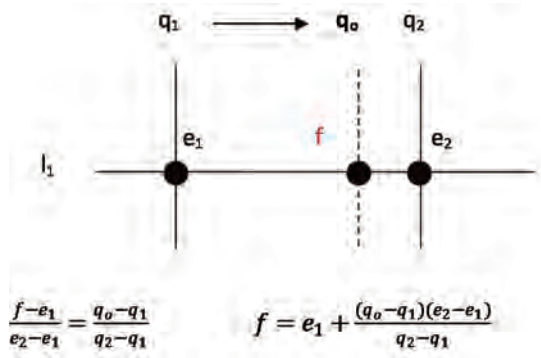

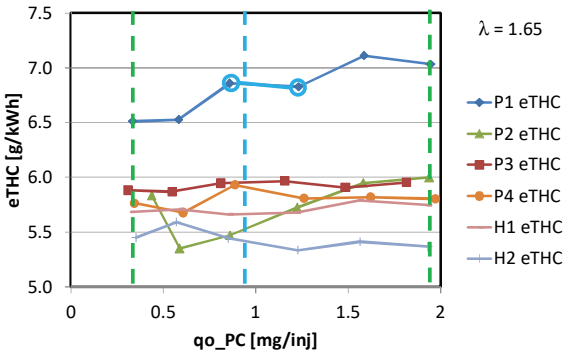

Fig. 11. Determination of emission values for internal fuel dose points qo_PC intervals: a) example of linear interpolation, b) example analysis points

For the extrapolated and interpolated data the optimization procedure described in chapter 8 was performed (Fig. 12).

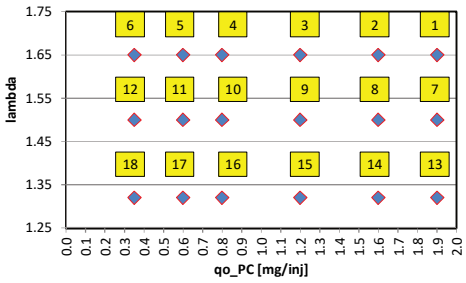

Fig. 12. The research points table after measured value normalization

6. Analysis of thermodynamical results

The results of the thermodynamic analysis of the engine's operating cycles indicated that the best results, mainly the highest values of the indicated mean effective pressure (IMEP), were achieved for the engine operation using the H-type prechamber (PC with a double row of outflow channels). The maps shown in Fig. 13 indicate higher IMEP values for such a combustion system in the whole range compared to the values achieved using the P-type system (with a single row of outflow channels). The combustion system using prechambers with a single row of outflow channels is characterized by reaching the maximum values of IMEP in the range of smaller doses of fuel supplied to the PC. The combustion system with H-prechambers is characterized by an even increase of IMEP with the increase of the excess air coefficient. The largest recorded IMEP values were obtained for the H2 prechamber.

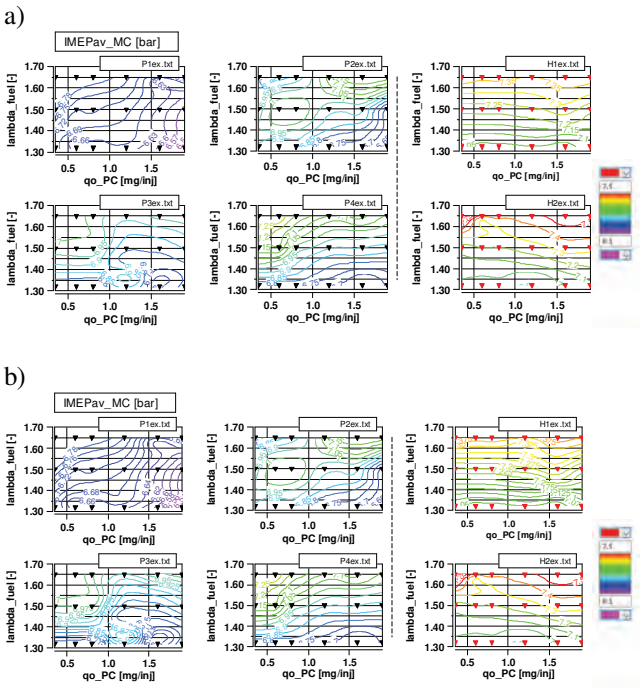

Fig. 13. The maps of IMEP-values measured for prechambers of type P (a) and type H (b)

The maps of overall engine efficiency (Fig. 14) have been determined similarly to those shown above. The lowest efficiency was found for the P1 prechamber, using which the test engine achieves a maximum efficiency of 0.33. The use of the H1 prechamber allowed to achieve an increase in the general engine efficiency of over 7%. Similarly to the value of IMEP, the efficiency analysis also indicates an even increase of the eta_o value based on the increasing lambda value in the case of using the H-type prechamber. PCs with single outflow channels are characterized by greater sensitivity to variable prechamber fuel dosing conditions.

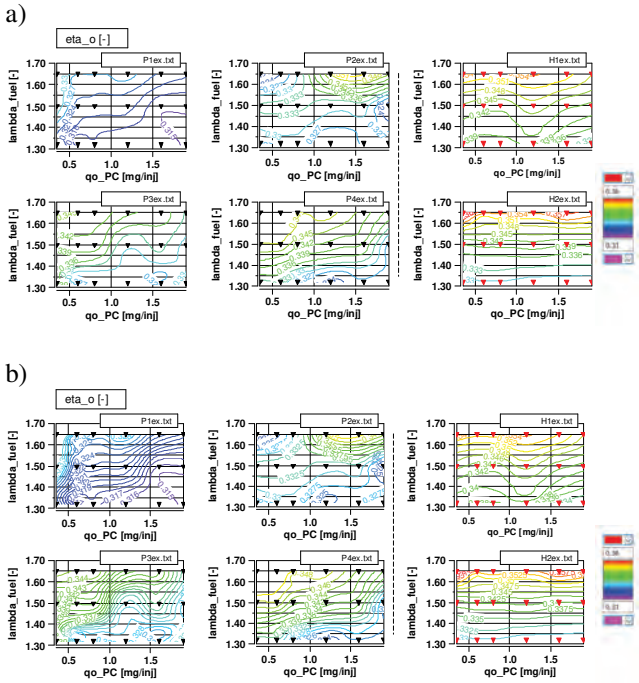

Fig. 14. The maps of overall efficiency achieved for prechamber type P (a) and type H (b)

Additionally a differential analysis of the efficiency achieved for the prechamber H1 and H2 showed that:

- in the range of average excess air coefficient values, the values for both H type prechambers are similar,
- with small values of excess air coefficient and lower fuel doses to the prechamber, the H1 prechamber (smaller number of outflow channels) achieves higher efficiency,
- for the limit values of $\lambda > 1.6$ greater efficiency is obtained using the H2 prechamber.

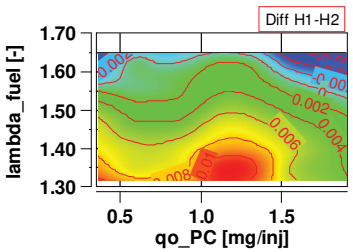

Fig. 15. The differential map of overall efficiency between prechambers of type H (H1–H2)

7. Emission measurement results evaluation

The measured concentrations of toxic exhaust compounds are presented in the form of specific emission maps for comparison purposes.

Figure 16 shows a map of nitrogen oxides emissions. The prechamber type H combustion system shows lower NO_x emission over the whole emission map range compared to the type P prechamber. The most favorable result was obtained for the H2 prechamber, where there was the least discrepancy between the min and max values. The result depends mainly on global conditions (air excess coefficient λ) and a change in the trend is visible only for very small doses to the prechamber.

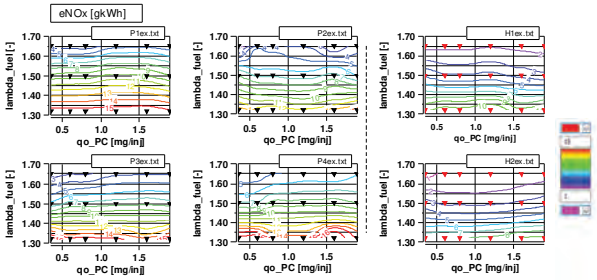

Fig. 16. The NO_x emission maps obtained for prechamber type P (a) and type H (b)

Hydrocarbon emission is shown in Fig. 17. As with NO_x, the best results were obtained for the H-prechamber, but the P3 and P4 prechambers have produced similar results, especially for the minimum doses of fuel for the PC. The global condition (lambda) has the most impact on the trend, but in relation to NO_x, the effect of dosing to the PC can be observed (especially for P-type prechambers).

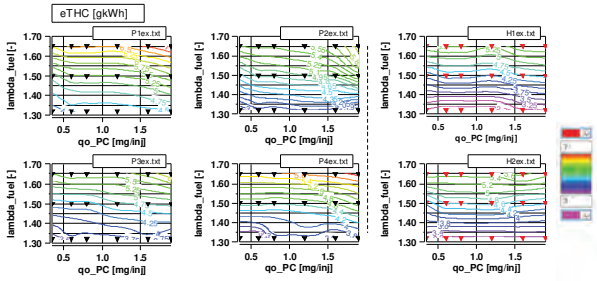

Fig. 17. The THC emission maps obtained for P- and H-type prechambers

As in the case of other emission factors, in the case of the carbon monoxide emission (Fig. 18) the H-type prechamber systems provided better emission results. In this case, however, the local conditions had more impact on the obtained values – such as the prechamber fuel dose. Global conditions affected the results distribution to a lesser degree. This tendency is opposite in relation to the other emission factors.

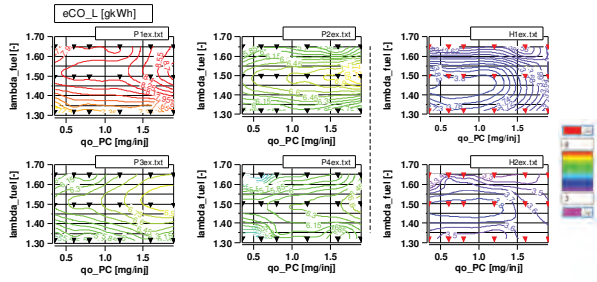

Fig. 18. The CO_L emission maps achieved for prechamber type P and type H

8. Polioptimization procedure

8.1. Methodology for determination of the best solution

Due to the varied trends of changes in thermodynamic and emission factors, the polioptimization methodology involving three calculation variants was used:

– 1st approach: modified selection of the „best PC":
  - all prechambers have been taken into account,
  - all λ-values were included in the procedure,
  - values of fuel quantities and of λ were normalized based on interpolation and extrapolation of the nearest values (for every indicator exist only one min- and only one max-value),
– 2nd approach: individualized selection of the „best PC":
  - all λ-values were included in the procedure,
  - values of fuel quantities and of λ were normalized based on interpolation and extrapolation of the nearest values (for every indicator exists only one min. and only one max-value) – as in the 1st approach,
  - every PC was analyzed separately – for every PC the „best point" (1 out of 18) has been determined based on the values of CO, HC, NO_x, eta-o, IMEP, and CoV(IMEP),
  - indication of advantages of individual engine operating points (1 out of 18) for every PC separately; such procedure makes it possible to define operating points with better engine indicators (could be used- for setting the engine control unit),
– 3rd approach: individualized and normalized selection of the „best PC":
  - all values of λ and fuel injection quantity have been normalized,
  - every PC was analyzed separately – for every PC the „best point" (1 out of 18) was selected,
  - advantages for every engine operating point (1 out of 18) have been selected for every PC separately,
  - each lambdavalue was analyzed separately: for every PC and each lambda the „best PC" has been chosen.

8.2. 1st approach: modified selection of the „best PC"

The optimization procedure was performed in the following manner:

– the emission results of CO, THC, NO_x and for overall efficiency were interpolated or extrapolated respectively,
– the following methodology was adopted (for each prechamber):
  - selection of the global (for all 9 cases) min and max values for every component,
  - normalizing all absolute measured values to the relative values in the range <0;1>:
    - max of emission – value 0
    - min of emission – value 1
    - max of efficiency – value 1
    - min of efficiency – value 0
– determining the quantities totals for all 18 operating points,
– varying selection of the impact factors (IF) for every emission component and efficiency (Σ = 1); IMEP-values were not taken into account (IF = 0),

– determining the products of sums and impact factors,
– the designation of the resulting sums.

Results of these analyzes have been summed up in Table 5 and Fig. 19.

Table 5. Selection of the best combustion system configuration for different impact factor values (1st approach): a) all 0.25; b) eta_o = 0.4, c) eta_o = 0.55

a)

Factor	Chamber	P1	P2	P3	P4	H1	H2
0.25	eCO_L	2.47	7.93	7.47	8.83	15.04	15.73
0.25	eta_o	2.72	7.83	7.68	8.92	10.87	9.98
0.25	eTHC	6.58	8.69	9.64	9.93	11.40	10.64
0.25	eNOx	7.66	9.91	8.84	7.89	12.56	13.75
0	IMEP_av	2.25	6.54	5.10	5.84	9.38	9.91
0	CoV_IMEP	7.06	9.34	7.76	10.07	11.76	12.22
	Best	4.86	8.59	8.41	8.89	12.47	12.53

b)

Factor	Chamber	P1	P2	P3	P4	H1	H2
0.2	eCO_L	2.47	7.93	7.47	8.83	15.04	15.73
0.4	eta_o	2.72	7.83	7.68	8.92	10.87	9.98
0.2	eTHC	6.58	8.69	9.64	9.93	11.40	10.64
0.2	eNOx	7.66	9.91	8.84	7.89	12.56	13.75
0	IMEP_av	2.25	6.54	5.10	5.84	9.38	9.91
0	CoV_IMEP	7.06	9.34	7.76	10.07	11.76	12.22
	Best	4.43	8.44	8.26	8.90	12.15	12.02

c)

Factor	Chamber	P1	P2	P3	P4	H1	H2
0.15	eCO_L	2.47	7.93	7.47	8.83	15.04	15.73
0.55	eta_o	2.72	7.83	7.68	8.92	10.87	9.98
0.15	eTHC	6.58	8.69	9.64	9.93	11.40	10.64
0.15	eNOx	7.66	9.91	8.84	7.89	12.56	13.75
0	IMEP_av	2.25	6.54	5.10	5.84	9.38	9.91
0	CoV_IMEP	7.06	9.34	7.76	10.07	11.76	12.22
	Best	4.00	8.29	8.12	8.90	11.83	11.51

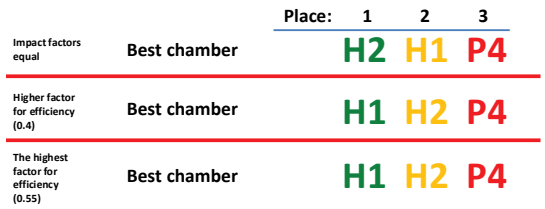

Fig. 19. Results of the search for the best configuration of the combustion system for different impact factors assigned to different coefficients (1st approach)

8.4. 2nd approach: individualized selection of the „best PC"

In this case the following procedure has been performed:

– all lambda values were included in the procedure;
– values of fuel quantities and of lambda were normalized based on interpolation and extrapolation of the nearest values (for every indicator exists only one min and only one max-value) – as in the 1st approach,
– every PC was analyzed separately – for every PC the „best point" (1 out of 18) according values of CO, HC, NO_x, eta_o, IMEP has been selected,
indication of advantages of individual engine operating points (1 out of 18) for every PC separately; such procedure makes it possible to define points with more favorable engine indicators (could be used for setting the engine control unit).

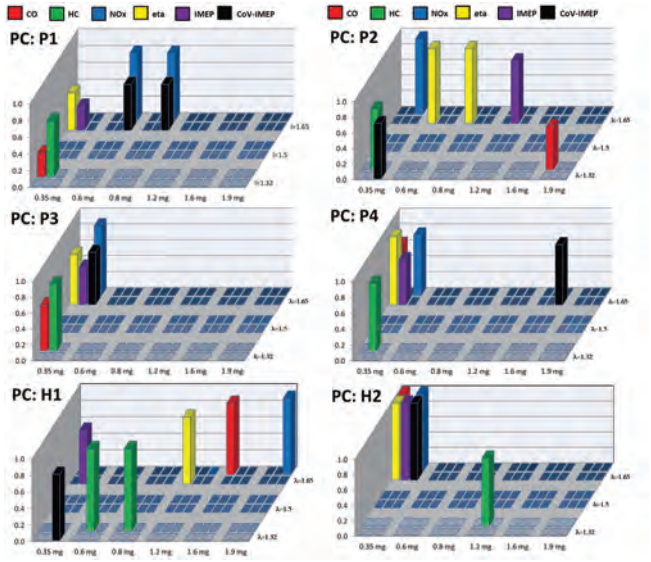

Fig. 20. Selection of the best combustion system configuration for different impact factors assigned to different coefficients (2nd approach)

Conclusions from the2nd approach were following:

– „Lowest emissions" for min. of qo_PC,
– „Highest efficiency" for min. of qo_PC,
– „Best points": 6 (min. qo_PC & $\lambda = 1.65$),
– PC P4: all engine indicators for min. of qo_PC,
– PC H2: best emission indicators.

8.5. 3rd approach: individualized and normalized selection of the „best PC"

Methodology described in chapter 8.4 was modified as follows:

– all values of lambda and fuel injection quantity have been normalized,
– every PC was analyzed separately – for every PC the „best point" (1 out of 18) was selected,
– advantages for every engine operating point (1 out of 18) have been selected for every PC separately,
– each lambda value was analyzed separately: for every PC and for each lambda the „best PC" has been chosen.

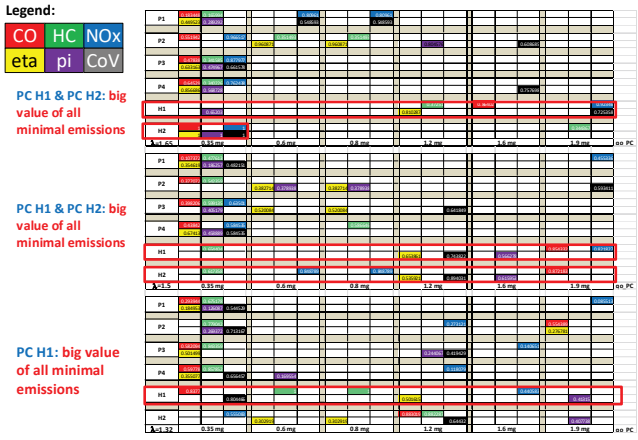

Fig. 21. Selection of the best combustion system configuration for different impact factors assigned to different coefficients (3rd approach)

Following conclusions were reached from the 3rd approach:

- Best prechamber: PC H2
- Lambda = 1.65
  - the best indicators for higher lambda values,
  - all indicators found for one operating point;
- Lambda = 1.5
  - many maximum indicator values at one engine operating point,
  - only the maximum efficiency found for the operating point close to selected one,
- Lambda = 1.3
  - min. CO and min. HC emission for the same operating point as above (qo_PC → min)
  - high efficiency for this point.

9. Summary and conclusions

The polioptimization method has been applied to the selective research on the prechambers construction. The aim of the study was to create a comparison procedure for prechamber systems having multiple variable parameters based on the characteristic measurement points and providing the configuration assessment result based on the selected criteria (emissions, efficiency or combustion stability) and highlighting the operating points that score high on these criteria. Two combustion system configurations have been tested:

- ω-type piston cavity with PFI and 4 prechamberswithout bottom orientated nozzles,
- hemispherical piston cavity with Heinzmann-mixer, two prechambers with nozzles orientated radially and axially.

Three different selection procedures have been analyzed and compared:

- 1st modified approach,
- 2nd individualized approach,
- 3rd individualized and normalized approach.

In all investigated cases the 18 real operating points (variable λ and q_{0_PC}) have been normalized using the interpolation and extrapolation procedures, therefore ensuring their comparability.

Based on the measured emissions (CO, THC, NO_x) and efficiency, the approach-dependent matrix of beneficial configurations has been drawn (Table 6).

Independently from the approach described (Table 4), better results were achieved for the combustion system in its second configuration – with hemispherical main chamber, Heinzmann-mixer fuel supply system and prechambers providing the axial development of igniting jets – to the chamber's bottom. This is the result of the better main mixture homogenization and better distribution of igniting jets in the main combustion chamber volume.

Table 6. Approach-dependent matrix of best PC configurations

1st approach (extrapolated data – one „best" PC)	Best: PC H2 (overall) & PC H1 (efficiency)
2st approach (individual „best" PC – all researach point)	Best: PC H2 (overall) & PC H1 (emission)
3st approach (individual „best" PC & for each lambda value)	Best: PC H1 (best for all lambda-value)

Using the first approach, and assuming similar importance of emissions and efficiency, prechamber H2 indicated the best results. When considering the engine overall efficiency as more important, the prechamber H1 achieved better results. This PC had a greater nozzle flow area, which leads to a smaller velocity of igniting jet, therefore smaller jet-wall effect (reducing the heat flux to the piston) and better distribution of the jets in the direction perpendicular to the flow. Both contribute to better overall engine efficiency.

Second approach indicates the best operating points individually for each prechamber and separately for each criteria. When taking into account all assessment criteria combined – emissions, efficiency, achieved IMEP and combustion stability– the best results distribution has been achieved for the prechamber H2 (second combustion system configuration). However, with focus on emissions, more beneficial operating points have been found for prechamber H1.

Based on the results from the third approach, it is stated, that measurements done with prechamber H1 resulted in the biggest spread of minimal values (in combination with their beneficial values) over the investigated range of λ and q_{0_PC}.

The investigation results from all proposed approaches suggest that the total best results have been achieved for the second configuration of combustion system with prechamber H1.

Acknowledgements

This work was supported by the EU – Horizon 2020 [grant number 652816].

Nomenclature

A	area
AI	heat release angle (10% – SOC or 90% – EOC)
CoV	coefficient of variation
CR	compression ratio
q_o	fuel dose
CI	compression ignition
CNG	compressed natural gas
CoC	centre of combustion (AI50)
CO_L	carbon monoxide (low value)
EOC	end of combustion
HRR	heat release rate
IF	impact factor
IMEP	indicated mean effective pressure
n	engine speed
NO_x	nitrogen oxides
p	pressure
r_v	total combustion chamber volume
SOC	start of combustion
TDC	top dead centre
THC	total hydrocarbons (HC)

TJI	turbulent jet ignition	λ	lambda value
V	volume	η	efficiency
WOT	wide open throttle	Ø	diameter

Indexes

air	air	o	overall
ch	chamber	PC	prechamber
exh	exhaust	t	thermal
MC	main chamber	V	volume

Bibliography

[1] ATTARD, W.P., BLAXILL, H., ANDERSON, E., LITKE, P., Knock limit extension with a gasoline fueled prechamber jet igniter in a modern vehicle powertrain. *SAE Technical Paper* 2012-01-1143. 2012. DOI:10.4271/2012-01-1143.

[2] ATTARD, W.P., FRASER, N., PARSONS, P., TOULSON, E. A turbulent jet ignition pre-chamber combustion system for large fuel economy improvements in a modern vehicle powertrain. *SAE Technical Paper* 2010-01-1457. 2010. DOI: 10.4271/2010-01-1457.

[3] ATTARD, W.P., PARSONS, P. A normally aspirated spark initiated combustion system capable of high load, high efficiency and near zero NO_x emissions in a modern vehicle powertrain. *SAE International Journal of Engines*. 2010, **3**(2), 269-287.

[4] BUNCE, M., BLAXILL, H., KULATILAKA, W., JIANG, N. The effects of turbulent jet characteristics on engine performance using a pre-chamber combustor. *SAE Technical Paper* 2014-01-1195. 2014. DOI:10.4271/2014-01-1195.

[5] FARZANEH-GORDA, M., SAADAT-TARGHI, M., KHADEM, J. Selecting optimal volume ratio of reservoir tanks in CNG refueling station with multi-line storage system. *International Journal of Hydrogen Energy*. 2016, **41** (48), 23109-23119, DOI:10.1016/j.ijhydene.2016.10.050.

[6] FERRERA, M. Highly efficient natural gas engines. *SAE Technical Paper* 2017-24-0059, 2017, DOI:10.4271/2017-24-0059.

[7] GEOK, H., MOHAMAD, T., ABDULLAH, S., et al. Experimental investigation of performance and emissions of a sequential port injection compressed natural gas converted engine. *SAE Technical Paper* 2009-32-0026. 2009.

[8] Global energy statistical yearbook 2018. https://yearbook.enerdata.net/oil-products/world-refined-production-statistics.html (accessed 20.12.2018).

[9] JAMROZIK, A., TUTAK, W., KOCISZEWSKI, A., SOSNOWSKI, M. Numerical simulation of two-stage combustion in SI engine with prechamber. *Applied Mathematical Modelling*. 2013, **37**, 2961-2982.

[10] KAGIRI, C., ZHANG, L., XIA, X. Optimal energy cost management of a CNG fuelling station. *IFAC Papers-OnLine*. 2017, **50**-2, 94-97. DOI:10.1016/j.ifacol.2017.12.017.

[11] KHAN, M.I., YASMEEN, T., M.I. KHAN, M. et al. Research progress in the development of natural gas as fuel for road vehicles: A bibliographic review (1991-2016). *Renewable and Sustainable Energy Reviews*. 2016, **66**, 702-741, DOI: 10.1016/j.rser.2016.08.041.

[12] KOTZAGIANNI, M., KYRTATOS, P., BOULOUCHOS, K., Optical investigation of prechamber combustion in RCEM. *Combustion Engines*. 2019, **176**(1), 12-17. DOI: 10.19206/CE-2019-102.

[13] NAKAZANO, T., NATSUME, Y. Effect of dimensions of prechamber on lean burn gas engine. *Japan Society of Mechanical Engineers International Journal*. 1994, **37**-B(4), 951-956.

[14] OLSEN, D.B., KIRKPATRICK, A. Experimental examination of prechamber heat release in a large bore natural gas engine. *Journal of Engineering for Gas Turbines and Power*. 2008, **130**(5). DOI:10.1115/1.2906182.

[15] PIELECHA, I., BUESCHKE, W., CIEŚLIK, W., SKOWRON, M. Turbulent spark-jet ignition in SI gas fuelled engine. *MATEC Web of Conferences*. 2017, 118, 00010. DOI: 10.1051/matecconf/201711800010.

[16] PIELECHA, I., WISŁOCKI, K., BUESCHKE, W. et al. Influence of gas injector position on the engine performance of a dual-fuel diesel engine. *FISITA World Automotive Congress*. 2016.

[17] PIRKER, G., WIMMER, A. Sustainable power generation with large gas engines. *Energy Conversion and Management*. 2017, **149,** 1048-1065. DOI:10.1016/j.enconman. 2017.06.023.

[18] PIZZUTI, L., MARTINS, A.M., dos SANTOS, L.R. et al. Laminar burning velocity of methane/ air mixtures and flame propagation speed close to the chamber wall. *Energy Procedia*. 2017, **120**, 126-133. DOI:10.1016/j.egypro. 2017.07.145.

[19] ROULEAU, L., SERRANO, D., LECOINTE, B. CNG direct injection spark-ignition engine with high turbulence and high compression ratio: numerical and experimental investigations. *12th Conference Gaseous-Fuel Powered Vehicles A Sustainable Alternative*. Stuttgart 2017.

[20] SHAH, A., TUNESTAL, P., JOHANSSON, B. Effect of prechamber volume and nozzle diameter on pre-chamber ignition in heavy duty natural gas engines. *SAE Technical Paper* 2015-01-0867. 2015. DOI:10.4271/2015-01-0867.

[21] SHAH, A., TUNESTAL, P., JOHANSSON, B. Scalability aspects on pre-chamber ignition in heavy duty natural gas engines. *SAE Technical Paper* 2016-01-0796. 2016. DOI: 10.4271/2016-01-0796.

[22] SOLTIC, P., HILFIKER, T., HÄNGGI, S. et al. Ignition- and combustion concepts for lean operated passenger car natural gas engines. *12th Conference Gaseous-Fuel Powered Vehicles a Sustainable Alternative*. Stuttgart 2017.

[23] SOLTIC, P., HILFIKER, T., HUTTER, R., HÄNGGI, S. Experimental comparison of efficiency and emission levels of four-cylinder lean-burn passenger car-sized CNG engines with different ignition concepts. *Combustion Engines*. 2019, **176**(1), 29-37. DOI:10.19206/CE-2019-104.

[24] ŚLEFARSKI, R., GOŁĘBIOWSKI, M., CZYŻEWSKI, P. et al. Analysis of combustion process in industrial gas engine with prechamber-based ignition system. *Energies*. 2018, **336**(11). DOI:10.3390/en11020336.

[25] TOULSON, E., SCHOCK, H.J., ATTARD, W.P. A review of pre-chamber initiated jet ignition combustion systems. *SAE Technical Paper* 2010-01-2263. 2010. DOI: 10.4271/2010-01-2263.

[26] U.S. Energy Information Administration, International Energy Outlook 2016, Chapter 8, 127-131. https://www.eia.gov/outlooks/ieo/pdf/transportation.pdf.
[27] VALLE, R.M., CANDIDO de SA, D.C., RAMALHO FILHO, F.A. Constructive parameters analysis of combustion pre-chamber adopted in torch-ignition system of Otto cycle engine. *SAE Technical Paper* 2003-01-3713. 2003. DOI: 10.4271/2003-01-3713.
[28] Worldwide car production through 2017. www.statista.com (accessed 10.12.2018).
[29] YANG, C., LI, W., YIN, J., SHEN, Y. Port fuel injection of CNG for downsized 1-liter 3-cylinder turbocharged engine with high efficiency. *SAE Technical Paper* 2017-01-2275. 2017. DOI:10.4271/2017-01-2275.
[30] ZHENG, J.-J., WANG, J.-H., WANG, B., HUANG, Z.-H. Effect of the compression ratio on the performance and combustion of a natural-gas direct-injection engine. *Proceedings of the Institution of Mechanical Engineers, Part D: Journal of Automobile Engineering*. 2009, **223**(1), 85-98. DOI:10.1243/09544070JAUTO976.

Prof. Ireneusz Pielecha, DSc., DEng. – Faculty of Transport Engineering, Poznan University of Technology.
e-mail: *Ireneusz.Pielecha@put.poznan.pl*

Wojciech Bueschke, DEng. – Faculty of Transport Engineering, Poznan University of Technology.
e-mail: *Wojciech.Bueschke@put.poznan.pl*

Maciej Skowron, MEng. – Faculty of Transport Engineering, Poznan University of Technology.
e-mail: *Maciej.Skowron@put.poznan.pl*

Łukasz Fiedkiewicz, MEng. – Faculty of Transport Engineering, Poznan University of Technology.
e-mail: *Lukasz.Fiedkiewicz@put.poznan.pl*

Filip Szwajca, MEng. – Faculty of Transport Engineering, Poznan University of Technology.
e-mail: *Filip.Szwajca@put.poznan.pl*

Wojciech Cieślik, DEng. – Faculty of Transport Engineering, Poznan University of Technology.
e-mail: *Wojciech.Cieslik@put.poznan.pl*

Prof. Krzysztof Wisłocki, DSc., DEng. – Faculty of Transport Engineering, Poznan University of Technology.
e-mail: *Krzysztof. Wislocki@put.poznan.pl*

Article citation info:
SOLTIC, P., HILFIKER, T., HUTTER, R., HÄNGGI, S. Experimental comparison of efficiency and emission levels of four-cylinder lean-burn passenger car-sized CNG engines with different ignition concepts. *Combustion Engines*. 2018, **176**(1), 27-35.
DOI: 10.19206/CE-2019-104

Patrik SOLTIC
Thomas HILFIKER
Richard HUTTER
Severin HÄNGGI

CE-2019-104

Experimental comparison of efficiency and emission levels of four-cylinder lean-burn passenger car-sized CNG engines with different ignition concepts

Today's passenger car CNG engines are based on petrol engines which typically have restrictions preventing the exploitation of the full potential of methane based fuels, especially if they have to be operated also on petrol as a second fuel. Additionally, the use of three-way-catalysis limits the engine operation to λ = 1. Here, we present the efficiency potential and the raw emission characteristics for a dedicated four cylinder passenger car CNG engine without sticking to the usual combustion peak pressure and λ limitations. Lean combustion reduces the knocking tendency but, because of the higher pressure levels, increases the ignition energy demand. Therefore, different ignition systems (spark plug, prechamber, Diesel pilot) have been used.

Keywords: *dual-fuel, diesel pilot, spark ignition, prechamber*

1. Introduction

Natural gas offers distinct CO_2 advantages over classical liquid fuels and it is therefore of interest in the mobility sector [12, 14]. Additionally, renewable methane is chemically identical with the natural gas' main component methane and can be therefore blended in any ratio without need to change engine hardware or calibration. Hydrogen can also be added to Methane which leads to additional advantages, especially if engine control parameters are adapted [16]. All this gives compressed natural gas (CNG) an ecologic and economic long-term perspective in the mobility sector. Consequently, natural gas is one of the attractive fuel options for the automotive industry which is facing worldwide continuously tightening CO_2 emission regulations [17].

Today's mass-produced natural gas engines for passenger cars are typically based on petrol engines, mostly with some adaptations such as increased compression ratio, increased boost pressure, adapted valves and valve seats, or high-temperature-capable turbine materials. Such adaptations do not fully take the advantageous properties of natural gas into account as for example the peak combustion pressure limitation of typically around 100 bar remains from the basic petrol engine. Passenger car natural gas engines are nowadays operated stoichiometrically which leads, in combination with three-way-catalysis, to very low emissions not only in legislative cycled but also in real-world operation [1]. Also, natural gas engines have the potential for practically zero emissions [2]. However, it is well-known that stoichiometric operation leads to reduced efficiencies compared to lean operation, especially due to higher pumping losses and heat transfer [5].

In the project described here, limitation regarding combustion peak pressure levels and stoichiometric operation are omitted to find the potentials and constraints for natural gas combustion in passenger-car-sized engines. A Diesel engine is used as an experimental basis as modern Diesel engines can cope with considerably higher peak pressures than gasoline engines. High combustion pressures, especially at lean conditions, need high ignition energies and a special focus is therefore put on the ignition systems. Three distinctly different ignition systems are used: An inductive ignition system using a well-insulated spark plug (engine 1), an inductive ignition system in prechambers of different geometries which could be used with or without prechamber gas injection (engine 2), and a Diesel pilot injection system (engine 3).

2. Engines

The engines for the spark ignited versions had gone through the following modifications:

- inserts for spark plugs (engine 1) or prechambers (engine 2) instead of the Diesel injectors,
- modified valve seats (engines 1 and 2),
- reduced swirl level (engines 1 and 2),
- modified pistons / modified piston rings (engines 1 and 2),
- wastegate instead of VTG turbocharger (engines 1 and 2).

The Diesel pilot engine is only slightly modified by implementing a PFI CNG supply system; all other details are identical from the serial production Diesel engine. The engines are operated with rapid prototyping ECUs and in all engines, closed-loop center of combustion (COC) control is implemented. The main characteristics of the engines discussed here are listed in Table 1 and additional information is given in the following subsections.

Table 1. Main characteristics of the used engines

	Engine 1 Spark Plug Engine	**Engine 2 Prechamber Engine**	**Engine 3 Diesel Pilot Engine**
Base engine	Volkswagen EA 288	Volkswagen EA 288	Volkswagen EA189
# of cylinders / valves per cylinder	4 / 4	4 / 4	4 / 4
Displacement [cm^3]	1968	1968	1968
Bore/stroke [mm]	81 / 95.5	81 / 95.5	81 / 95.5
Compression ratio	14.5	14.5	16.5
Ignition system	Inductive	Inductive	–
Spark plugs	NGK M12 in open chamber	NGK M10 in prechamber	–

Table 1 cont.

Diesel injection system	–	–	Common Rail with Piezo Injectors
Gas port fuel injectors	Bosch NGI2	Bosch NGI2	Bosch NGI2
Prechamber injectors	–	Bosch NGI2	–
Turbocharger	Wastegate	Wastegate	VTG
EGR	Not installed	Not installed	Present, not used
ECU	Rapid prototyping unit (dSPACE)	Rapid prototyping unit (dSPACE)	Rapid prototyping unit (dSPACE)
Cylinder pressure indication	All 4 cylinders using Kistler sensors	All 4 cylinders using Kistler sensors	All 4 cylinders using Kistler sensors
Prechamber pressure indication	–	One prechamber using Kistler sensor	–

2.1. Spark plug engine (Engine 1)

The cylinder head is redesigned to hold an insert with a spark plug instead of a Diesel injector. To achieve good combustion chamber geometry for premixed combustion, pistons with hemispherical bowls with a distinct squich-area are used. Figure 1 shows a cross-cut where the combustion chamber geometry can be seen. It shows also the flush-mounted water-cooled cylinder pressure sensor.

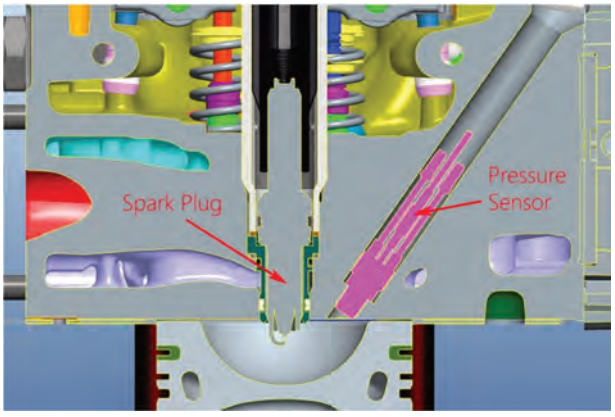

Fig. 1. CAD visualisation of the combustion chamber of the spark plug engine

Figure 2 depicts the intake manifold with the upstream throttle and gas mixer. A gas mixer enables a nearly perfect

Fig. 2. CAD visualisation of gas mixer, throttle and intake manifold

mixing of methane and air. The injection timing was synchronized to the crankshaft signal and the injectors were activated alternatively over 720 °CA with the lowest possible rail pressure in order to enable injection durations as close as possible to 180 °CA. In comparison to a setup with the gas injectors mounted closer to the cylinder intake valves, the present setup is suited for transient operation only to a limited extent. However, this is not an issue since the focus of the work presented here lies on steady-state operation only.

2.2. Prechamber engine (Engine 2)

The prechamber engine is built on the same basis as the spark plug engine with the difference, that the cylinder head is equipped with specifically designed prechambers, see Fig. 3. Prechamber parts are shown in Fig. 4. Prechamber operation can be passive (i.e. without gas injection to the prechamber) or scavenged (i.e. with gas supply to the prechamber). A higly insulated M10 spark plug is used for ignition. A check valve at the prechamber entrance enables the use of a recessed dosing valve. Additionally, a small uncooled piezoelectric pressure sensor is implemented in the upper part of the prechamber. The prechamber insert are placed in cooling water channels and sealed with gasket rings.

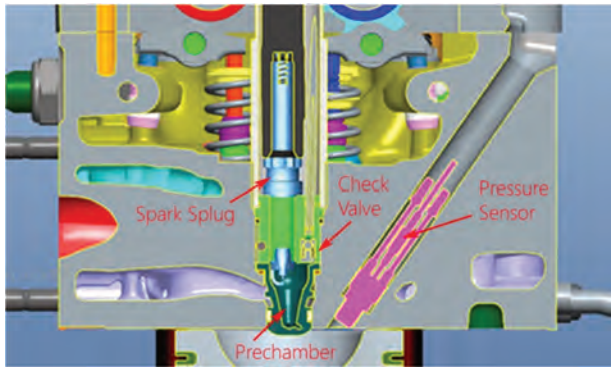

Fig. 3. CAD visualisation of the combustion chamber of the prechamber engine

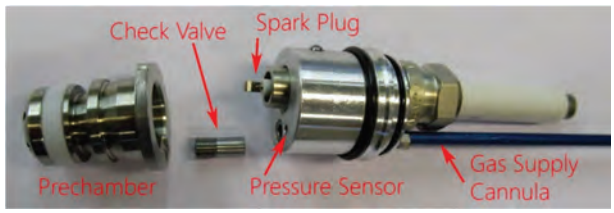

Fig. 4. Prechamber assembly, including the prechamber pressure sensor and the gas supply cannula

The air/fuel equivalence ratio (λ) of the mixture inside the prechamber at time of ignition is crucial for the operation of the scavenged prechamber. The goal is to achieve a mixture inside the prechamber when ignition is applied which is close to stoichiometric condition. This is not a trivial task as during compression a lean mixture with a certain λ is pushed back into the prechamber if the engine is run lean. Therefore, the resulting λ at spark timing depends on the λ in the main chamber, on the amount of gas injected to the prechamber and on the spark timing itself. A dedicat-

ed prechamber controller adapts the injection and ignition timing based on the estimated prechamber λ accordingly [6]. Finally, we optimized for best efficiency and lowest THC emissions which turned out to occur at early injection with the start of prechamber injection around 300 °CA before TDC.

Prechamber geometries are designed and optimized using CFD tools by Volkswagen Konzernforschung, Ricardo Software and ETH Zürich [3, 4, 10, 11, 15]. The performance of different prechamber designs was tested on a rapid compression and expansion machine at ETH Zürich and on a single cylinder engine at Poznan University of Technology with focus on prechamber performance [9, 13]. A selection of prechambers was then implemented on the full engine described here where the behavior of the overall combustion system is addressed and engine efficiency and emission levels are assessed. In this article, we focus on two prechamber geometries which show a distinct different performance, both with identical volume but with a different channel configuration. Figure 5 shows a picture of the two prechambers and Table 2 lists the main characteristics.

Fig. 5. Used prechambers (jet exit sides)

Table 2. Main characteristics of the prechambers compared in this study

	Prechamber 1	**Prechamber 2**
Prechamber volume	1.826 cm^3	1.826 cm^3
Number x diameter of horizontal nozzles	7 x 1.5 mm	12 x 0.9 mm
Number x diameter of vertical nozzles	3 x 1.4 mm	5 x 0.9 mm

2.3. Diesel pilot engine (Engine 3)

The Diesel pilot engine is only slightly modified for Diesel pilot operation: Four gas injectors are added to the swirl flap adapter just before the engine's intake channels (Fig. 6). The Diesel fuel is directly injected into the cylinders using the standard Diesel injection system. Once compression ignited, the Diesel provides ignition centres for the premixed natural gas. The amount of Diesel defines the level of energy that is available for the ignition of the gas/air mixture. The point in time at which the Diesel is injected, influences the type of combustion significantly. Very early injections allow for much better mixing of the Diesel with the gas/air mixture than it is the case with late injections. According to this, different injection strategies can result in combustions with the same combustion phasing but different CO_2 emission, thermal efficiency and pollutant emissions. In this study, the Diesel injection parameters, i.e. the start and duration of injection, are chosen such that the desired combustion phasing is achieved using the least amount of Diesel possible [18]. In general, this "Minimal Diesel Control" minimizes the CO_2 emissions of the engine as the substitution rate is maximized. In addition, when operated with a fixed total fuel/air mixture, fewer Diesel leads to less excess oxygen in the air/gas mixture. This favors flame propagation since laminar flame speed is increased. At high loads, the mechanical limitation on the maximum cylinder pressure prohibited the air/fuel ratios to exceed a λ of about 1.4.

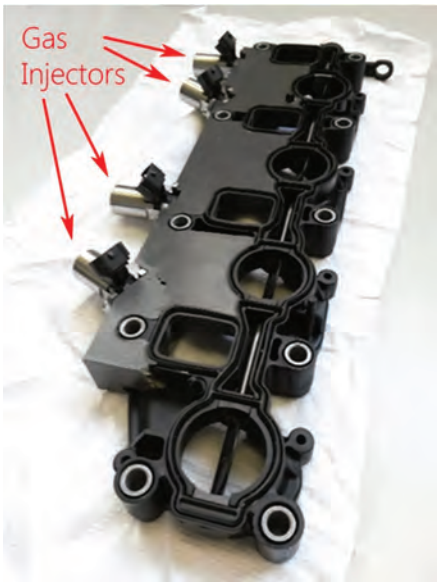

Fig. 6. Four PFI gas injectors mounted on the swirl flap adapter of the original Diesel engine

3. Fuel

For all experiments, natural gas from the local grid is compressed in bottles and fed to the engine's pressure regulators. The gas composition is analyzed from time to time using a process gas chromatograph. A stable gas composition was observed. Table 3 shows the main components. The resulting lower heating value is 48.6 MJ/kg (standard deviation 0.2 MJ/kg) and the methane number is 87 (standard deviation 0.7).

Table 3: Composition of the used gas (values of 7 gas analyses)

	Methane	Ethane	CO_2	Nitrogen	Propane
Mean	94.5 Mole%	3.5 Mole%	0.8 Mole%	0.5 Mole%	0.4 Mole%
Standard deviation	0.4 Mole%	0.2 Mole%	0.1 Mole%	0.1 Mole%	0.1 Mole%

4. Results

For the discussion of efficiency, emissions and temperature levels, we concentrate here on the following two operating points:

- Operating point 1 (low load): Engine speed 1400 min^{-1}, brake torque 50 Nm (bmep = 3.2 bar),
- Operating point 2 (higher load): Engine speed 2000 min^{-1}, brake torque 220 Nm (bmep = 14.0 bar).

Those two operating points cover all the dominant effects seen across the engine map. It has to be noted that the turbochargers are not able to cover all possible operating conditions from λ = 1 until the lean limits at all engine speed/torque combinations. Especially at very lean condi-

tions and in combination with high load operation and comparably low engine speed, boost pressure limitations occur which lead to a power loss since the desired λ cannot be met. Such operating conditions are marked in the following Figures with a grey background.

4.1. Brake engine efficiencies

The base Diesel engine for the Diesel pilot experiments is not the same as the base engine for the spark ignited versions, also the turbocharges are different (VTG versus wastegate). Therefore, the direct comparison of absolute numbers can be misleading as the gas exchange losses and friction can be different. However, the main objective in engine design is generally to maximize the efficiency while meeting pollutant emission limits and keeping the engine in safe operation for all setups. In this section, we discuss the influence of different parameters on efficiency. Brake engine efficiencies depend on:

- The properties of the working fluid, which are influenced by the air-to-fuel ratio.
- The combustion duration, which is influenced by the air-to-fuel ratio, the in-cylinder charge motion and the ignition characteristics.
- The combustion phasing, whereas it was experimentally confirmed that the center of combustion at 8 °CA gives best efficiency for all cases so that this phasing was fixed for all experiments presented here (with exception of retarded combustion phasing for cases where knock occurred at COC = 8 °CA).
- The completeness of combustion, which is influenced by the global air-to-fuel ratio, by the in-cylinder charge motion and by crevice volumes.

Figure 7 shows the measured brake engine efficiencies versus λ for the lower load operating point. Best efficiencies occur in the λ range of 1.5 … 1.7 for all concepts. The spark plug engine shows efficiencies very similar to the engine equipped with prechamber 2, but prechamber 2 allowed keeping a high efficiency up to leaner mixtures.

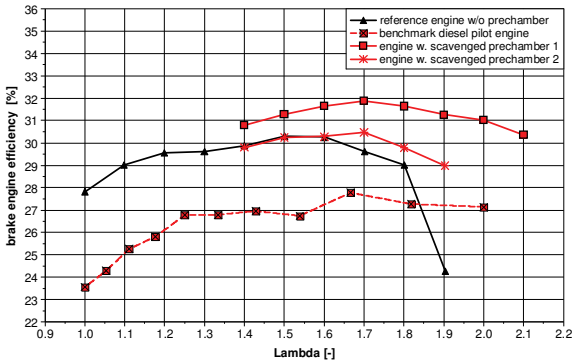

Fig. 7. Brake engine efficiencies for the operating point 1 (1400 rpm/ 50 Nm/bmep 3.2 bar)

The Diesel pilot engine shows a clear disadvantage in terms of efficiency which results from an impaired Diesel ignition. Since the fresh air is throttled under such load conditions, the pressure after compression diminishes and, in turn, the ignition delay is prolonged. Consequently, the Diesel mass for proper ignition has to be strongly increased, see section 3.3 and [7]. Prechamber 1 shows the best efficiency of all combustion concepts; it performs clearly better than prechamber 2, which points out the importance of the prechamber channel configuration.

Figure 8 shows the measured brake engine efficiencies versus λ for the higher load operating point. Here, the spark plug option shows clearly the lowest efficiencies across the whole λ range. The Diesel pilot setup peaks its efficiency at λ = 1.43 where the allowed cylinder peak pressure is met. Prechamber 2 shows similar efficiency levels as the Diesel pilot setup, but was able to run leaner without hitting the peak pressure limit; this is mainly due to the lower compression ratio of 14.5 versus 16.5 of the Diesel pilot version. Also at this higher load point, prechamber 1 shows the best brake thermal efficiency level with nearly 44% at λ levels around 1.6 … 1.7. The gray area in the plot shows the λ region where the turbochrger was not able to deliver enough air, the resulting reducions in bmep are indicated.

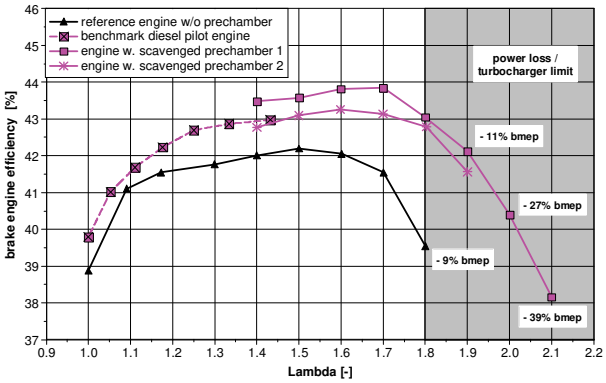

Fig. 8. Brake engine efficiencies for the operating point 2 (2000 rpm/ 220 Nm/bmep 14.0 bar)

4.2. Peak cylinder pressure and center of combustion settings

Figure 9 shows the peak cylinder pressures for the low load operating point. In all variants, the center of combustion (i.e. the crank angle where 50% of the fuel is burned) is set to 8 °CA after TDC. For the spark ignited versions, especially for the spark plug version, a clear increase in peak pressure with increasing charge dilution can be seen. In the region of best efficiency, the prechambers show higher peak pressures than the pure spark plug ignition. The

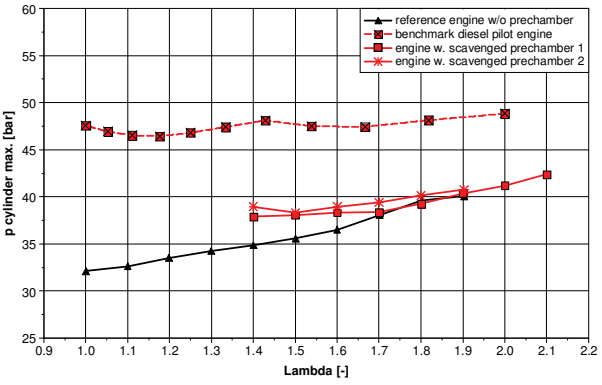

Fig. 9. Peak cylinder pressures for the operating point 1 (1400 rpm/50 Nm/ bmep 3.2 bar)

Diesel pilot engine shows the highest peak pressures levels in general, which is attributed to it's higher compression ratio. In this operating point with unfavorable conditions for the Diesel pilot and thus high Diesel pilot quantities, the peak pressure is fairly unaffected by increasing air dilution.

Figure 10 shows the cylinder peak pressure levels for the higher load point and Fig. 11 shows the corresponding settings of the center of combustion. For λ values below about 1.4 ... 1.5, the combustion phasing had to be delayed to prevent knock. At λ = 1, the spark plug engine had the most delayed center of combustion setting which is attributed to the comparably slow combustion and therefore to an increased knock tendency. The Diesel pilot engine, even it has an considerably higher compression ratio than the spark ignited versions, could keep the center of combustion at a near-optimum level. This is most likely attributed to the fact that the Diesel pilot catches a large volume fraction of the cylinder filling which reduces the time for the end-gas to pass through pre-reactions. In terms of peak cylinder pressure levels, the Diesel pilot engines shows, due to its higher compression ratio, the highest levels. The spark plug engine shows the lowest levels. However, prechamber ignition increases the peak pressure levels which is attributed to considerably faster combustion compared to the spark plug version, see section 3.5.

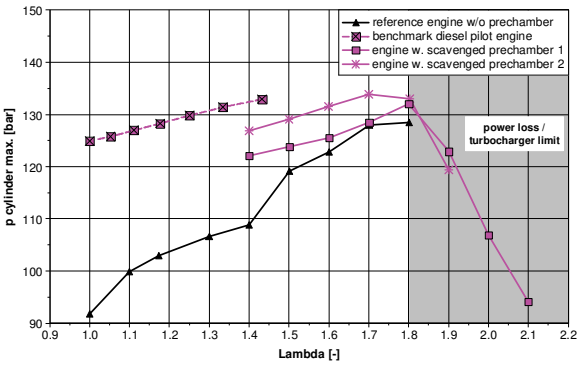

Fig. 10. Peak cylinder pressures for the operating point 2 (2000 rpm/ 220 Nm/bmep 14.0 bar)

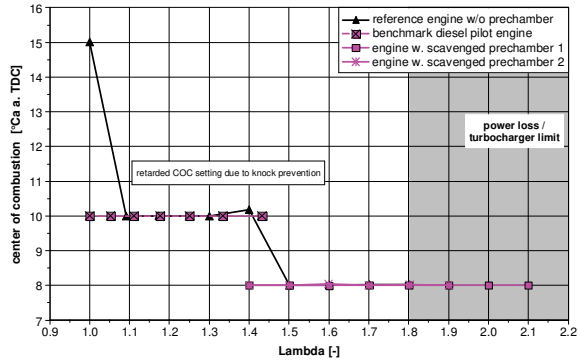

Fig. 11. Center of combustion settings for operating point 2 (2000 rpm/ 220 Nm/bmep 14.0 bar)

4.3. Energy fraction for ignition

In addition to the air/fuel mixture the engine aspirates, the Diesel pilot and the prechamber versions use additional fuel for the ignition process. For the Diesel pilot engine, the amount of pilot fuel is minimized to minimize soot formation and to use as little Diesel of this more carbon-intensive fuel as possible [18]. In case of the prechaber variants, the amount of gas supplied to the prechamber is set in such a way, that the efficiency is maximised [6]. The resulting energetic amounts of fuel provided to the prechambers and the Diesel pilot respectively are shown in Fig. 12 and Fig. 13 for the two discussed operating points. For the prechambers, the necessary amount of fuel provided to the prechamber increases with increasing charge dilution for both operating points whereas prechamber 2 needs more fuel than prechamber 1, in spite of the same prechamber volume. This points out the strong coupling of the flow and composition structure in the prechamber with its performance. For the Diesel pilot engine, the energetic share for the Diesel pilot strongly increases at decreasing load, especially with decreasing air excess. This is because of the unfavourable conditions for compression ignition when pressure levels are decreased with intake flow throttling. At higher load conditions, the minimum amount of Diesel fuel is used which the injectors can provide. With the injectors used, this is the case with injection durations of around 120 µs.

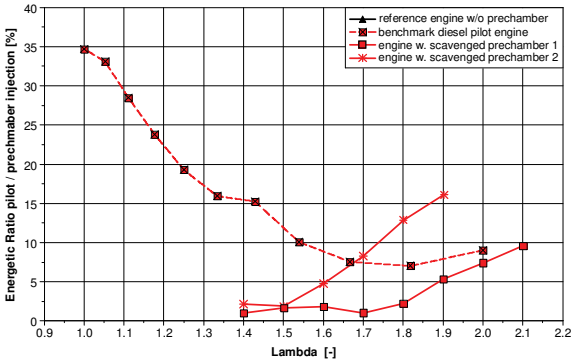

Fig. 12. Energy fraction for Diesel pilot or prechamber fueling for operating point 1 (1400 rpm/50 Nm/bmep 3.2 bar)

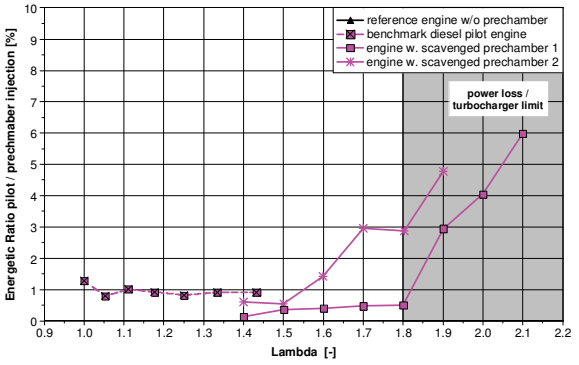

Fig. 13. Energy fraction for Diesel pilot or prechamber fueling for operating point 2 (2000 rpm/220 Nm/bmep 14.0 bar)

4.4. Combustion stability

To assess combustion stability, the coefficient of variation of the indicated mean effective pressure (CoV(IMEP), which is standard deviation divided by mean value) is usually taken as a measure. Here, we calculated the CoV(IMEP) based on 300 consecutively recorded in-cylinder pressure traces of cylinder #1. CoV(IMEP) values below about 5% are typically regarded as desirable as these levels of cyclic variations guarantee a smooth engine operation.

Figure 14 shows the cyclic variation levels for the lower load operating point. The spark plug and prechamber 2 overshoot the desired CoV(IMEP) levels above a λ value of 1.8 and reach there their lean burn limits. Prechamber 2 does not show this behaviour at all; it enables stable combustion to well above λ values of 2. The same can be observed for Diesel pilot operation.

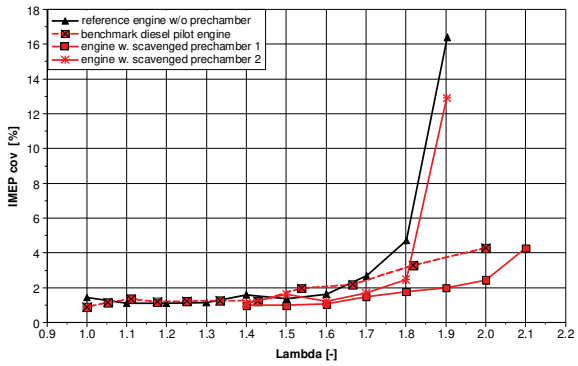

Fig. 14. Cyclic variations for the operating point 1 (1400 rpm/50 Nm)

Figure 15 shows the cyclic variation levels for the higher load operating point. Here, a similar behaviour can be observed for the spark ignited variants: the spark plug versions has its lean burn limit at a λ value of 1.8, the prechamber 2 at a slightly higher λ value, prechamber 1 runs stable even at λ values above 2. The Diesel pilot engine shows a completely different behaviour than for the lower load operating point: CoV(IMEP) increases already at comparably low air dilution levels. The reason for this behaviour is most likely the cyclic variability of the Diesel pilot quantity. At high load, the Diesel quantity is very small and at the operating border of the Diesel injectors, see section 4.3.

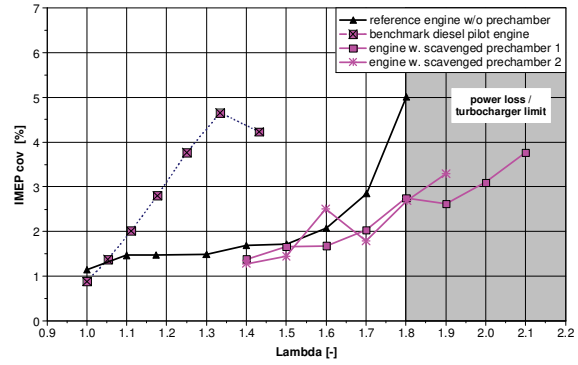

Fig. 15. Cyclic variations for the operating point 2 (2000 rpm/220 Nm)

4.5. Combustion duration

Ignition systems affect the subsequent combustion considerably. The ignition systems discussed in this paper are very different. A spark plug driven by a capacitive ignition system creates a thermal plasma which initializes flame propagation directly in the combustion chamber [8]. The flame development in case of a prechamber is protected from the combustion chamber and hot radicals are ejected [10], ignite the mixture and create turbulence. In case of a Diesel pilot ignition, a diffusion-controlled self-ignition of Diesel jets ignites the mixture. Because of these differences in the underlying physico-chemical processes it is clear, that the combustion characteristics have to be very different.

Figure 16 shows the combustion duration, defined as the crank angle from 5…90% mass fraction burned, for the low load point. The spark plug version shows the slowest combustion, whereas the prechambers lead to a much faster combustion. The Diesel pilot, which is energetically a large amount in this operating point (see section 3.3) leads to extremely fast combustion.

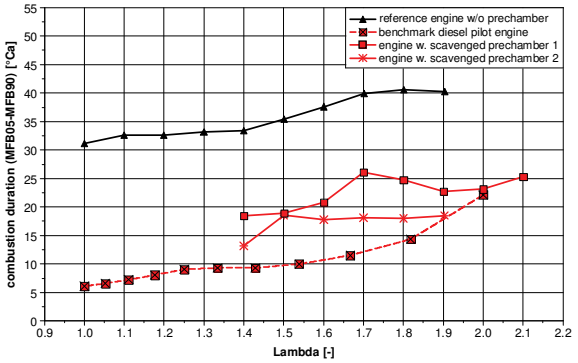

Fig. 16. Combustion durations for the operating point 1 (1400 rpm/50 Nm)

Figure 17 shows the combustion durations for the higher load point. In this point, the Diesel pilot engine shows similar combustion durations as the spark plug version. This is because at higher loads, the Diesel pilot quantities are much lower than at lower loads which transfers in a slower combustion. The prechambers show fast combustion, whereas prechamber 2 leads to even faster combustion than prechamber 1. However, the faster combustion of prechamber 2 does not increase the thermal efficiency of the engine compared to prechamber 1, neither in the high- nor in the low-load operating point. This is most likely attributed to increased wall heat losses due to very intense flame/wall interactions.

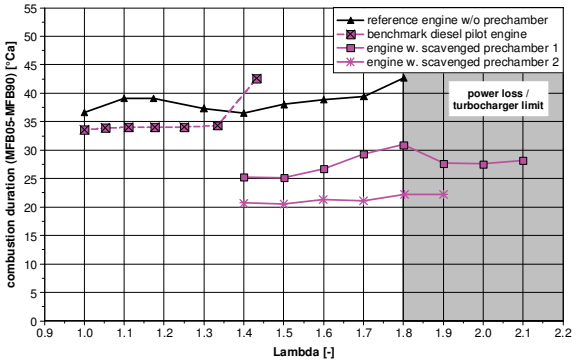

Fig. 17. Combustion durations for the operating point 2 (2000 rpm/220 Nm)

4.6. NO_x emissions

The NO_x emissions shown in Figure 18 and 19 indicate slight benefits for the prechamber engine concepts versus a simple spark plug for operation at a given λ. However, since the prechambers versions show best efficiencies at higher λ values than the spark plug versions, the prechambers proved to be a very good approach to maximise effi-

ciency and minimize NO_x raw emissions. At $\lambda = 1$, the Diesel pilot and the spark plug versions show very similar NO_x levels for low- and high-load operation. At low load operation, the Diesel pilot version shows the highest NO_x level at lean conditions. This is caused by the high amount of Diesel fuel used at these conditions.

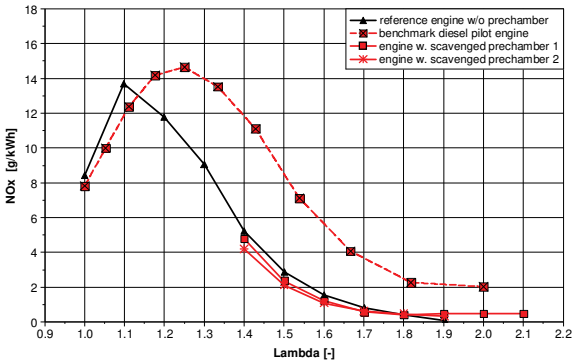

Fig. 18. Raw NO_x emissions for the operating point 1 (1400 rpm/50 Nm)

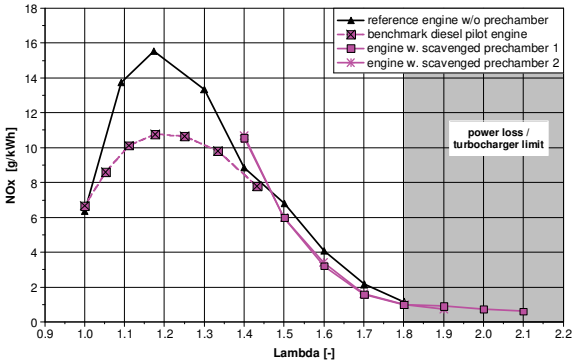

Fig. 19. Raw NO_x emissions for the operating point 2 (2000 rpm/220 Nm)

4.7. THC emissions

The measured raw THC emissions, shown in Figs 20 and 21, indicate clear benefits for the prechambers. At low load, the Diesel pilot version with its high percentage of Diesel used shows the highest THC levels. The THC analyzer used for the Diesel pilot experiments was not able to distinguish between methane- and non-methane hydrocarbons so it is unknown, which portion of the THC emissions come from the Diesel pilot. However, as the Diesel share decreases with increasing air excess but the THC level increases monotonically it is very likely that the source of the THC emissions is not the Diesel pilot. As this engine has Diesel pistons without any optimization for low-HC crevices a large portion of the HC emissions may be caused by crevice volumes. For the prechamber engines, the methane- as well as the non-methane hydrocarbons were analyzed which revealed a stable methane share of 92 mole% This corresponds well with the methane share in the fuel. The THC levels at lean conditions, especially at best efficiency setting at λ above 1.5, are generally high and ask for an efficient methane reduction technology under lean conditions, which is not yet available.

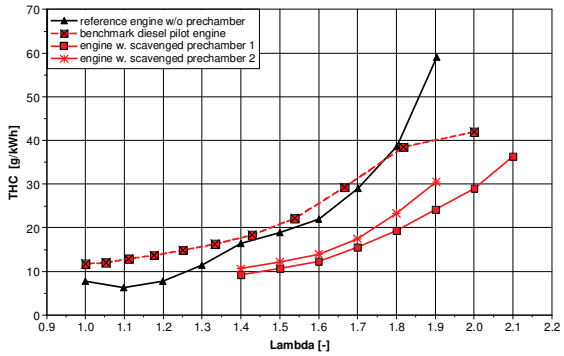

Fig. 20. Raw THC emissions for the operating point 1 (1400 rpm/50 Nm)

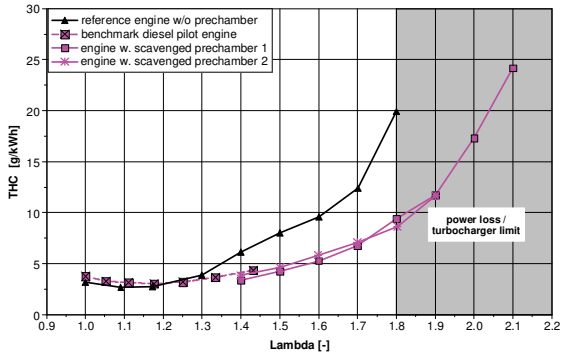

Fig. 21. Raw THC emissions for the operating point 2 (2000 rpm/220 Nm)

4.8. Exhaust temperature levels

Figure 22 and 23 show the temperature levels of the exhaust gases at turbine exit. This represents a location upstream of a potential exhaust aftertreatment system and indicates the thermal range of operation which could be expected for such a device. Due to the increasing air excess at lean burn operation, temperatures drop significantly and the temperature levels can become challenging for catalytic conversion, especially for methane oxidation.

Generally, the lowest exhaust gas temperature levels can be observed for the prechamber versions. This comes from on the one hand from the high efficiency level leading to less waste heat but, on the other hand, also to potentially increased heat losses to the cylinder walls.

The lower temperature level for lean combustion leads to challenges for exhaust gas aftertreatment but it reduces the thermal requirements for the turbocharger so that for example variable turbine geometries could be used.

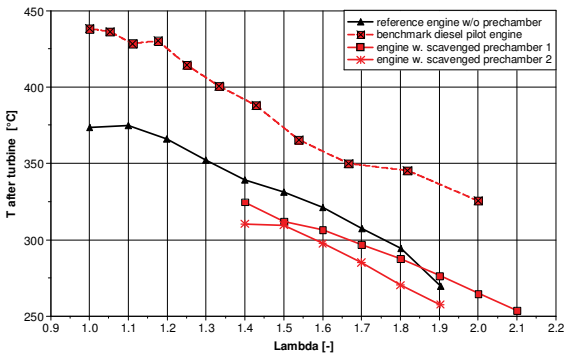

Fig. 22. Temperature after turbine for the operating point 1 (1400 rpm/50 Nm)

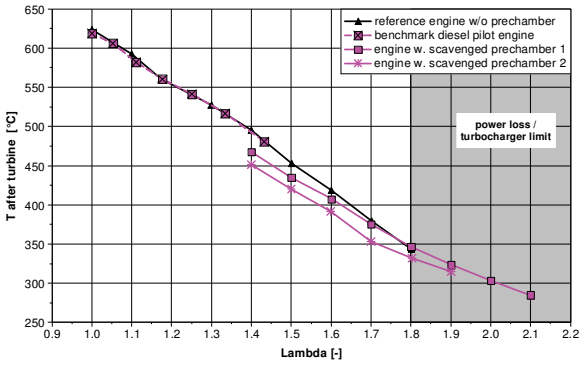

Fig. 23. Temperature after turbine for the operating point 2 (2000 rpm/220 Nm)

4.9. Examples of cylinder pressure traces

In order to directly compare cylinder pressure traces for the different configuration, an operating point is chosen which allows stable premixed combustion in all cases. At low load, the Diesel pilot engine needs a high Diesel share and at higher loads, the Diesel pilot engine is peak-pressure limited. Therefore, the comparison is done on a medium-load point at 1500 1/min and a brake torque of 100 Nm (bmep = 6.4 bar) and at λ = 1.7, center of combustion was set to 8 °CA after TDC for all configurations. Figure 24 shows the corresponding p(V) diagrams in double-logarithmic (left) and normal representation (right). The Diesel pilot version shows in this operating point the highest intake- and peak pressure levels. In this operating point, the Diesel pilot version shows also the lowest efficiency of all configurations (not shown here) which demands higher boost pressure. The very fast combustion of the prechamber versions, especially for prechamber 2, can nicely be seen in the p(V) diagrams.

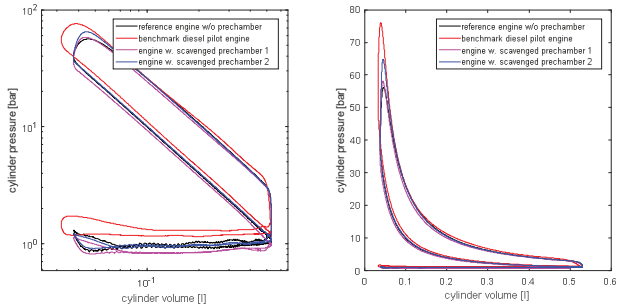

Fig. 24. Cylinder pressure versus cylinder volume for the operating point (1500 rpm/100 Nm), λ = 1.7 and COC = 8 °CA after TDC

4.10. Examples of net heat release rates

Figure 25 shows the net heat release rates for the same medium load operating point as discussed for the cylinder pressure traces. Figure 25 also shows the ignition timings and the start of injection (SOI) timing for the Diesel pilot, respectively. The spark plug version needs the earliest ignition timing, the flame develops slowly and the peak heat release rate is comparably low. In contrast, the prechambers need much later ignition timing, the onset of combustion is very fast and the peak heat release rates are high. This is especially the case for prechamber 2 where the ignition timing is set to 7 °CA before TDC to achieve COC at 8 °CA after TDC, i.e. only 15 °CA later. Diesel-pilot ignition shows in this operating point a very similar heat release shape as the prechamber variants. The combustion noise characteristics for the prechamber-equipped and for the Diesel-pilot engines are therefore very Diesel-like; a hard combustion noise is clearly audible.

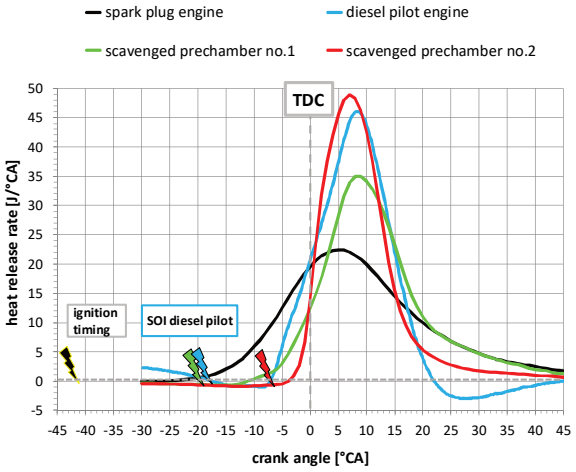

Fig. 25. Net heat release rates for operating point 1500 rpm/100 Nm and λ = 1.5

5. Conclusions

Among the engines considered here, the prechamber-equipped engine showed the highest peak brake efficiency of nearly 44% at λ around 1.7 and higher load levels. This is a Diesel-like efficiency level, even if the compression ratio is considerably lower than for typical Diesel engines. At such lean combustion, the prechamber enables moderate NO_x levels in the order of 1 g/kWh which would need a de-NO_x system such as SCR. The THC levels can be considerably lowered with a prechamber and lean combustion but levels in the order of 5…10 g/kWh need a very efficient methane oxidation technology, which is currently not available. The prechamber-equipped engines showed good performance and stable combustion across the whole engine map.

The Diesel pilot engine showed similar efficiency levels as the prechamber versions but at lower λ values of around 1.4. Stable combustion could be achieved with only small Diesel pilot energies of about 1% at high load conditions. With decreasing load, especially at throttled operation, the Diesel pilot quantity has to be considerably increased to enable stable ignition and combustion. At extremely low loads, which are not discussed in this article, Diesel pilot operation is impossible and the engine has to be operated in pure Diesel mode. Therefore, lean Diesel pilot combustion proved to be a fuel-efficient concept for mainly high load operation.

The purely spark-plug equipped engine showed the poorest performance of all concepts. Combustion is comparably slow, the lean burn limit is comparably low and THC emissions are high. For efficient and low raw-emission lean-burn gas engines, prechamber or Diesel-pilot injection proved to be the best solutions. However, to limit greenhouse gas emissions and to meet strict on-road THC limits, efficient methane oxidation catalysts have to be found.

Funding

The work presented is part of the Horzon2020 project "GasOn". This project has received funding from the European Union's Horizon 2020 research and innovation programme under grant agreement No 652816.

The Swiss partners have been supported by the Swiss State Secretariat for Education, Research and Innovation (SERI) under contract number 15.0145-1. The opinions expressed and arguments employed herein do not necessarily reflect the official views of the Swiss Government.

Acronyms

bmep	brake mean effective pressure
CA	crank angle
CFD	computational fluid dynamics
COC	center of combustion (i.e. crank angle, where 50% of the fuel is burned)
IMEP	indicated mean effective pressure
SCR	selective catalytic reduction
SOI	start of injection
TDC	top dead center
THC	total hydrocarbons
λ	stoichiometric air-fuel-ratio

Bibliography

[1] BACH, C., BÜTLER. T., HUBER, M. Abgasemissionen von Gasfahrzeugen. *Aqua&Gas*. 2017, **7/8**, 40-43.

[2] BACH, C., LÄMMLE, C., BILL, R. et al. Clean engine vehicle a natural gas driven Euro-4/SULEV with 30% reduced CO2-emissions. *SAE Technical Paper* 2004-01-0645. 2004. DOI:10.4271/2004-01-0645.

[3] BARDIS, K., XU, G., KYRTATOS, P. et al. A zero dimensional turbulence and heat transfer phenomenological model for pre-chamber gas engines. *SAE Technical Paper* 2018-01-1453, 2018. DOI:10.4271/2018-01-1453.

[4] BOLLA, M., SHAPIRO, E., KOTZAGIANNI, M. et al. Numerical study of fuel and turbulence distributions in an automotive-sized scavenged pre-chamber. *Combustion Engines*. 2019, 176(1), 63-68. DOI: 10.19206/CE-2019-108.

[5] CATON, J.A. A comparison of lean operation and exhaust gas recirculation: thermodynamic reasons for the increases of efficiency. *SAE Technical Paper* 2013-01-0266, 2013. DOI:10.4271/2013-01-0266.

[6] HÄNGGI, S., HILFIKER, T., SOLTIC, P. et al. Control-oriented analysis of a lean-burn light-duty natural gas research engine with scavenged pre-chamber ignition. *Combustion Engines*. 2019, **176**(1), 44-55. DOI: 10.19206/CE-2019-106.

[7] HUTTER, R., RITZMANN, J., ELBERT, P., ONDER, C. Low-load limit in a diesel-ignited gas engine. *Energies*. 2017, **10**, 1-27. DOI:10.3390/en10101450.

[8] KAMMERMANN, T., KREUTNER, W., TROTTMANN, M. et al. Spark-induced breakdown spectroscopy of methane/air and hydrogen-enriched methane/air mixtures at engine relevant conditions. *Spectrochim Acta – Part B At Spectrosc.* 2018, 148, 152-164. DOI:10.1016/j.sab.2018.06.013.

[9] KOTZAGIANNI, M., KYRTATOS, P., BOULOUCHOS, K. Optical investigation of prechamber combustion in an RCEM. *Combustion Engines*. 2018, **176**(1), 12-17. DOI: 10.19206/CE-2019-102.

[10] KYRTATOS, P., BARDIS, K., BOLLA, M. et al. Transferability of insights from fundamental investigations into practical applications of prechamber combustion systems. *Ignition Syst. Gasol. Engines – 4th Int. Conf.* December 6-7, 2018, Berlin, IAV, 442-459.

[11] LUCAS, G., TALLU, G., WEIßNER, M. CFD-based development of an ignition chamber for a lean and high efficient CNG combustion. *THIESEL 2018 Conf. Thermo- Fluid Dyn. Process*. Direct Inject. Engines High-Pressure. 2018.

[12] N/N. International Energy Agency – World Energy Outlook. 2017.

[13] PIELECHA, I., BUESCHKE, W., SKOWRON, M. et al. Prechamber optimal selection for a two stage turbulent jet ignition type combustion system in CNG-fuelled engine. *Combustion Engines*. 2019, **176**(1), 18-28. DOI: 10.19206/CE-2019-103.

[14] SCHULLER, O., REUTER, B., HENGSTLER, J. et al. Greenhouse gas intensity of natural gas transport. 2017.

[15] SHAPIRO, E., AHMED, I., TINEY, N. Advanced ignition modelling for pre-chamber combustion in lean burn gas engines. *Ignition Syst. Gasol. Engines – 4th Int. Conf.* December 6-7, 2018, Berlin, IAV, 104-121.

[16] THURNHEER, T, SOLTIC, P, DIMOPOULOS EGGENSCHWILER, P. S.I. engine fuelled with gasoline, methane and methane/hydrogen blends: Heat release and loss analysis. *Int J Hydrogen Energy*. 2009, **34**, 2494-2503. DOI:10.1016/j.ijhydene.2008.12.048.

[17] Volkswagen. Volkswagen Konzern treibt gemeinschaftlichen Ausbau der Erdgas- Mobilität voran. Press Release from 02052017 2017.

[18] ZURBRIGGEN, F., HUTTER, R., ONDER, C. Diesel-minimal combustion control of a natural gas-diesel engine. *Energies*. 2016, **9**. DOI:10.3390/en9010058.

Patrik Soltic, DEng. – ETH, Empa, Swiss Federal Laboratories for Materials Science and Technology, Dübendorf (Switzerland).

e-mail: *Patrik.Soltic@empa.ch*

Thomas Hilfiker, Eng. – Empa, Swiss Federal Laboratories for Materials Science and Technology, Dübendorf (Switzerland).

e-mail: *Thomas.Hilfiker@empa.ch*

Richard Hutter, MEng. – ETH, Swiss Federal Institute of Technology, Zürich (Switzerland).

e-mail: *RiHutter@idsc.mavt.ethz.ch*

Severin Hänggi, MEng. – Swiss Federal Institute of Technology, Zürich (Switzerland).

e-mail: *SHaenggi@idsc.mavt.ethz.ch*

Article citation info:
BUESCHKE, W., SKOWRON, M., WISŁOCKI, K., SZWAJCA, F. Comparative study on combustion characteristics of lean premixed CH_4/air mixtures in RCM using spark ignition and turbulent jet ignition in terms of orifices angular position change. *Combustion Engines*. 2019, **176**(**1**), 36-41. DOI: 10.19206/CE-2019-105

Wojciech BUESCHKE
Maciej SKOWRON
Krzysztof WISŁOCKI
Filip SZWAJCA

CE-2019-105

Comparative study on combustion characteristics of lean premixed CH_4/air mixtures in RCM using spark ignition and turbulent jet ignition in terms of orifices angular position change

The increase in ignitability consist a main aim of implementation of the turbulent jet ignition (TJI) in relation to the combustion of diluted charges. Such an ignition system has been introduced to the lean-burn CNG engine in the scope of GasOn-Project (Gas Only Internal Combustion Engines). In this study the impact of TJI application on the main combustion indexes has been investigated using RCM and analyzed on the bases of the indicating and optical observations data. The images have been recorded using LaVision HSS5 camera and post-processed with Davis software. Second part of the study based on indicating measurements consist the analysis of combustion regarding the variation in the geometry of pre-chamber nozzles. It has been noted, that combustion with TJI indicates significantly bigger flame luminescence and simultaneously – faster flame front development, than the combustion initiated with conventional SI. The positive impact of nozzles angular position on engine operational data has been found in the static charge movement conditions, regarding the combustion stability.

Key words: *CNG, turbulent jet ignition, pre-chamber, optical analysis, flame development, heat release rate*

1. Introduction

GasOn project was aimed to develop the monovalent engines fuelled with CNG. Methane-rich CNG, as a low carbon fuel, is alternative and environment-friendly chemical energy source for automotive powertrains. Poznan University of Technology participated in the GasOn work package 5, which was focused on lean burn combustion system indicating potential to increase the efficiency and emission indexes.

The potential in methane-based fuelling of the spark ignition engines (SI) is emphasized among others with its high octane number (up to 120) and therefore high knock resistance [1]. This determines the possibility to significant increase the compression ratio (CR), according to various investigations up to 15.6, what affects positively the combustion thermal efficiency and the engine brake efficiency [9, 10, 13]. Further increase of engine efficiency provides the implementation of lean-mixture combustion by means of excessive oxidizer content in the supplied mixture. With increase in dilution of the combusted mixtures, the thermal efficiency is being increased [22]. Also the combustion of lean charges generates smaller in-cylinder temperature resulting in smaller temperature-dependent emission of NO_x [8]. Both effects correlate positively on increase in air-fuel equivalence ratio, which is however significantly limited due to the inflammation capability of spark ignition [2, 7].For the specific NO_x emission, the introduction of TJI to the gas engine results in reduced THC and CO emission [23].

As mentioned, one of the biggest challenges in lean-mixture combustion is the demand on ignition energy, which is rising along the λ increase. In case of methane combustion in model conditions, the minimal ignition energy (MIE) for stoichiometric process equals 0.35 mJ, while for $\emptyset = \frac{1}{\lambda} = 0.5$ the MIE increases up to approximately 10 mJ [11].

The air-fuel stoichiometry is not the only factor influencing the inflammation capability, what the author of this paper has already studied [4], so the MIE demand in real engine conditions is in fact much bigger. Some studies rate the ignition energy generated from TJI on 10^4–10^5 bigger as this achieved with conventional ignition system [19], what makes it interesting for lean-burn applications. Also another ignition mechanism (multipoint type) makes the TJI beneficial in terms of mixture inflammation capability [3].

As the studies deliver, two main approaches are known: jet ignition and flame ignition. In first approach the flame from pre-combustion is being quenched when passing the orifices. The main combustion process is being started with hot combustion products. When the orifice diameter is being increased, the on-ignition is tending to the second approach – flame ignition.

The studies on combustion of diluted charges applied to the full engine confirmed positive results related to the thermal efficiency [18]. The air dilution of the mixture indicated in another study 2% greater increase in thermal efficiency, than dilution with EGR, combined with 2-times better THC emission, however with some NO_x emission drawback [20]. This can be covered with further mixture dilution, which cannot be achieved with recirculated exhaust gasses.

The challenges of CNG fuelled engines consist both the conversion of unburned methane in the exhaust aftertreatment systems and the low exhaust gas temperature affecting negatively the activity of catalyst. There are known however measures from the side of engine control [12] and aftertreatment systems as alternative catalytic materials [15], reducing this issue significantly, what is the important fact intensifying the research activities on CNG lean combustion.

The TJI initiated combustion is being influenced by system constructional factors and operational parameters. The control strategies indicate top and bottom limitations, which are sourced in boarder parameters and determine ignitabi-

lity and the flame propagation in pre-chamber [6, 21]. Kotzagianni et al. investigated SOI using RCM and found increase in cyclic variation, when ignition is being retarded [17]. Roethlisberger and Farvat conducted research into pre-chamber volume and its internal shape [24], using the 6-cylinder CNG fuelled engine with CR = 12.0 and pre-chamber consisting 2–3% of main chamber volume. In lean conditions (λ = 1.61–1.67) the ignition chamber with smaller volume caused 2 deg CA advance in main chamber heat release, 0.3 bar bigger Δp and reduced concentrations of THC and CO for up to 100 mg/m^3. Another investigations discovered positive correlation between the brake specific emission of NO_x and the pre-chamber volume fraction [26].

Tanoue compared the single orifice prechamber to double-nozzle system, regarding the knock combustion, based on the optical data recorded on RCM [25]. The shift of the knock source position has been noted. Double nozzle system caused the move of knock source to the away from the pre-chamber tip. Kawabata noted that the larger number of pre-chamber orifices impacts positively HRR and promotes therefore faster combustion in the main chamber [16].

The analysis of flame propagation in terms of orifice diameter has been studied by Gholamisheeri et al. [14]. The orifices with diameters of 2.0, 2.5 and 3.0 mm have been introduced to the RCM and investigated at Ø = 1.0, 0.8, 0.67. The strict dependency of jet tip penetration speed on orifice diameter and fuel stoichiometry has been proven. The increase in orifices diameter results in the jets speed reduction. The same tendency is valid also for air-fuel stoichiometry – increased λ causes reduced flame development speed. However, the calculated Reynolds numbers indicate the turbulent character of the flow in all investigated cases, which is affecting positively the mixing in the main chamber, heat exchange between jet and unburned fraction and, in consequence, promoting faster inflammation of main charge.

This study has been conducted to complement insufficient state of knowledge regarding the prechamber nozzles angularity.

2. Investigations methodology

2.1. Test bench

Investigations have been performed using the rapid compression machine (RCM) executing the single combustion cycles, equipped with CNG fuelling system and spark/spark-jet ignition (Fig. 1).

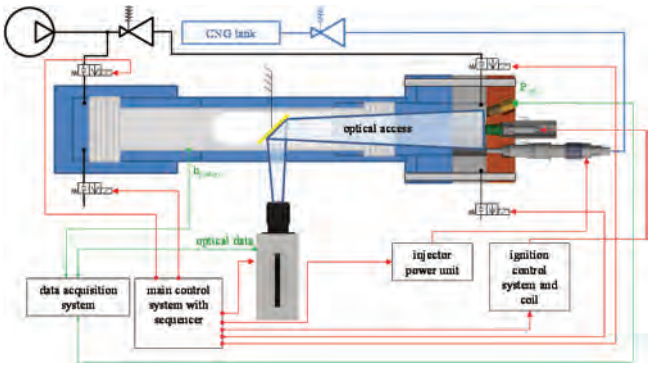

Fig. 1. RCM Test bench

The RCM has pneumatic piston activation (pressure chamber in the bottom of piston connected to fast solenoids) with air pressure delivered from the compressor, which has been designed to driving pressure p_d < 80 bars. However, in this study p_d = 38 bars has been applied and provided requested piston velocity, which has also the connection to the crank mechanism. The crank mechanism makes the piston movement independent from driving parameters. In the middle part of the piston, the flat mirror has been fixed to redirect the optical view from combustion chamber (quartz glass window with g = 50 mm assembled in piston crown) to the camera system – LaVision HSS5. The recorded images have been processed using Davis software.

The ignition energy has been delivered from the dedicated adjustable ignition control module with variable time of coil loading (regulation of ignition energy) and its phase. Both, for SI and for TJI, the e_{DIS} = 34 mJ has been applied.

The dimensional parameters of RCM used in this study have been collected in the Tab. 1. Methane N35 has been used as a fuel to the measurements.

Tab. 1. Main data of the Rapid Compression Machine (RCM)

Parameter	Value	Unit
Cylinder displacement	438	cm^3
Compression ratio	15.0 (SI) / 14.2 (TJI)	–
D_{OA}	Ø48	mm
Driving pressure	< 80	bar
Pressure sensor – main chamber	AVL GM11D	–
Pressure sensor – prechamber	FOS CPS 2000	–

2.2. Investigated combustion systems

The modular construction of used RCM provides the implementation of spark ignition and spark-jet ignition system, which are replaceable in the cylinder head (Fig. 2).

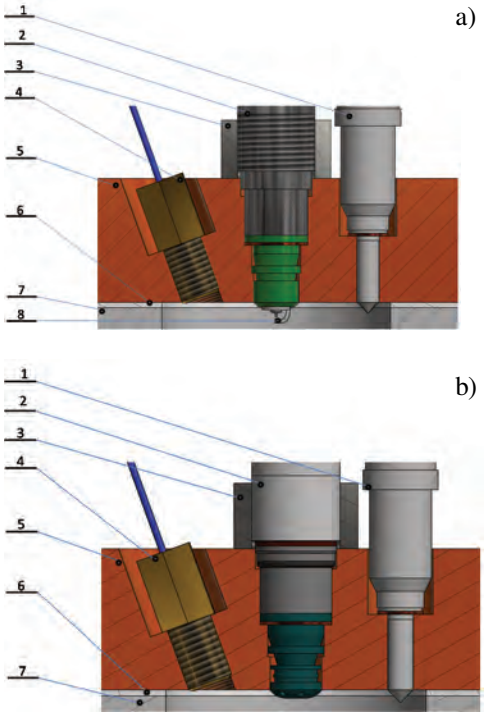

Fig. 2. SI (a) and TJI (b) assembled in the RCM body

The RCM in both configurations (Fig. 2) – with SI and with TJI – has got the Bosch electromagnetic CNG nozzle (1) to direct CNG injection assembled in the cylinder head (5), separated with head gasket (6) from cylinder (7). The cylinder head consists also the pressure transducer (4) and ignition system fixed with adapter (3). In the SI configuration (Fig. 2a) the spark plug (8) has been mounted in the adapter (marked with green) and fixed with sleeve (2). The TJI-setup (Fig. 2b) consist the pre-combustion chamber (marked with blue), which is fixed with adapter (dark gray) consisting fuel supply channel and pressure transducer. Abovementioned components are immobilized with sleeve (light gray).

2.3. Scope of investigations

The measurements have been divided in two campaigns:

– comparison of SI and TJI with tangential nozzles,
– comparison of tangential and tilted nozzles in TJI.

Both SI and TJI systems have been compared (a) at constant $\lambda = 1.5$. The λ value has been calculated according the equation:

$$\lambda = \frac{m_{air}}{m_{fuel} \cdot L_t} = \frac{m_{air}}{(q_{0\_PC} + q_{0\_MC}) \cdot L_t} \tag{1}$$

The air mass has been calculated based on the total volume of combustion chamber. Because of its scavenging with fresh charge, which is preceding the start of sequence, no significant residual content has been assumed. In case of SI application, the m_{fuel} injected directly to the combustion chamber has been considered in the λ calculation, while with TJI it was the sum of $q_{0_PC}$and q_{0_MC}. The comparison of SI and TJI has been performed based on the optical signal from MC. Based on this signal share of flame exposition A_f in the optically accessible part of combustion chamber A_{oa} has been calculated:

$$r = \frac{A_f}{A_{oa}} = \frac{4 \cdot A_f}{\pi \cdot D_{oa}^2} \tag{2}$$

The intensity of the flame at the defined time instances has been assessed relative to the maximal value:

$$c = \frac{I}{I_{max}} \tag{3}$$

The combustion nozzles angularity (b) has been assessed for following conditions:

– $\lambda = 1.5$, $q_{0tot} = 20$ mg/cycle,
– $\lambda = 1.3$, $q_{0tot} = 23$ mg/cycle.

The analysis concerns:

– maximal cylinder pressure $Pmax(t_{pmax})$,
– maximal rate of heat release $HRR(t_{HRRmax})$.

The HRR has been calculated according the formula presented in [27].

3. Comparison of spark ignition and turbulent jet ignition

The combustion process (for TJI: combustion of main charge) indicates changes in its course, when replacing the conventional spark ignition system with TJI. The analysis contains the flame propagation investigation providing qualitative information about intensity distribution based on recorded chemiluminescent combustion signal (Fig. 3). In the further steps, images have been parameterized regarding the flame intensity and area of its exposition at the defined time instances (Fig. 4).

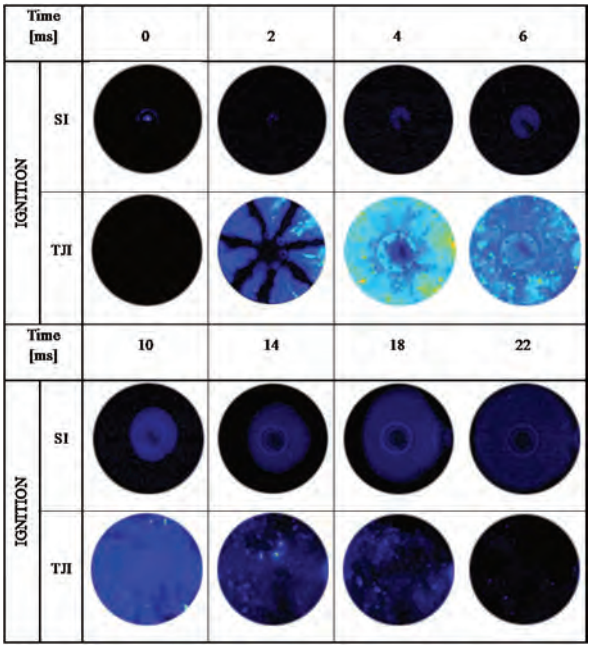

Fig. 3. Flame propagation for $\lambda = 1.5$ for SI and TJI

The images (Fig. 3) represent the flame development over the time for SI (top) and TJI (bottom) in the optically accessible part of combustion chamber ($Ø_{OA}$ = 48 mm) at $\lambda = 1.5$. First pictures, marked as 0, represent the view from combustion chamber at the moment of ignition(SOI) and the spark plug discharge visible in the undivided combustion chamber (Fig. 3, top, 0 ms). Further pictures captured for SI indicate typical premixed flame characteristic for well homogenized mixture with tangential development from the ignition source to the auxiliary regions of combustion chamber. In case of combustion initiated with TJI, 2 ms after SOI the igniting jets already developed throughout the optically accessible part of combustion chamber. This, and also conical shape of captured jets expositions with expanded jets tips (generated from cylindrical nozzles) suggests significant contribution of jets interaction with walls of combustion chamber in the flame development. Next time steps indicate bigger flame luminescence in the auxiliary parts of combustion chamber, while the combustion intensity is getting significantly lower, from the time of 4 ms after SOI. Based on the optical signal it can be stated, that TJI provides significant more intensive and faster combustion.

The parameterized optical data (Fig. 4) indicates significant differences in the character of flame development. For the conventionally initiated combustion, 1.6 ms after SOI flame luminescence achieve approximately 50% of its maximal value, which has been reached 14 ms after SOI, and reduced to 80% during next 8 ms. The maximal value of flames intensity for TJI has been achieved much earlier, 4 ms after SOI, dropped intensively within next 6 ms to 23%, then has been slowly quenched. As the peak flame luminescence intensity has been achieved 4 ms after SOI, also the large increase in the area of flame occurs in first 4 ms, when the flame area covers almost entire (98%) combustion chamber.

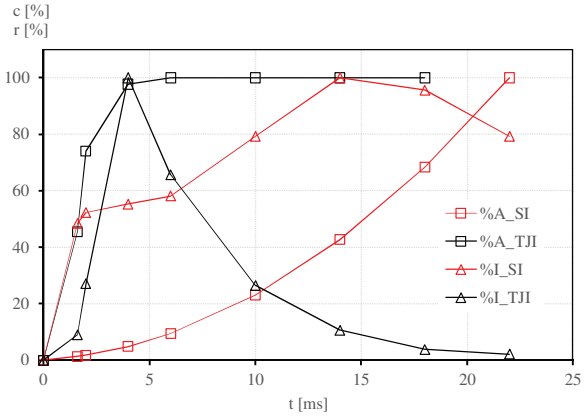

Fig. 4. Share of the flame (square points) and intensity (triangular points) in the optically accessible part of combustion chamber for SI (red line) and TJI (black line)

The impact of ignition type on cylinder pressure has been analyzed using the indicating approach based on the cylinder pressure to investigate more generalized, quantitative effect (Fig. 5).

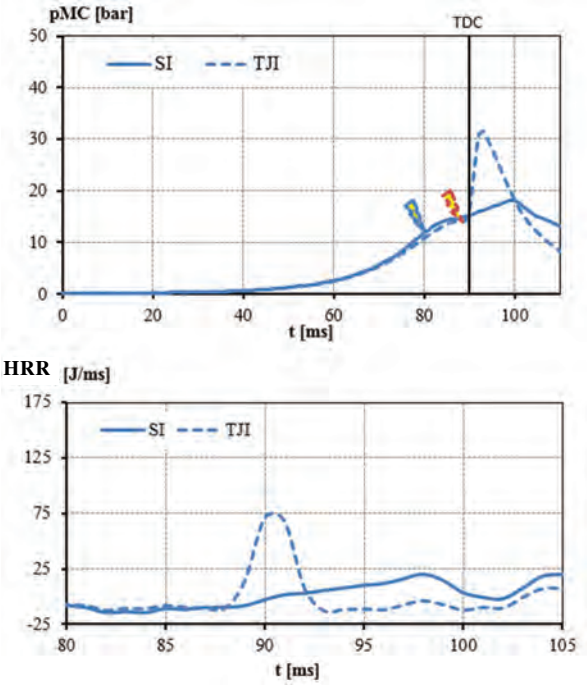

Fig. 5. Cylinder pressure (a) and HRR (b) for SI (solid line) and TJI (dashed line)

The traces of PMC indicate smaller cylinder pressure during the compression stroke for TJI, what is caused with smaller geometrical CR due to additional volume introduced to the combustion chamber. The SOI has been adjusted adequately to the ignition – retarded for 18 ms when TJI used. The pressure and HRR curves have been presented for abovementioned single operation cycle. Using the SI, cylinder pressure has been increased for 6 bars from the SOI to time instance, when maximal value has been achieved (time period of approximately 20 ms), while with use of TJI, the pressure has been increased for 16 bars within 5 ms. The HRR curves show increase in HRR to the maximal values in 18 ms and 4 ms with magnitudes of 25 J/ms and 75 J/ms, respectively for SI and TJI.

Based on the results, it has been noted, that during the combustion of defined fuel quantity heat is being released much more intensive, when TJI introduced, then with use of conventional ignition system. The different on-ignition mechanism is here important. TJI generates hot jets, which are developing both downstream the flow from pre-chambers nozzle and perpendicularly to the flow. This takes place due to the areal mixing the hot gasses with unburned fraction on the jets surface and makes the inflammation source decentralized. The combustion initiated parallel from the multiple hot surfaces indicates faster flame development, which covers bigger volume and provides bigger value of heat release rate.

4. Impact of TJI nozzles angularity on combustion

The angularity of pre-chamber nozzles has been particularly investigated within the scope of another authorship study, using the optical measurement approach [5]. The combustion, at λ = 1.3 with tangential nozzles TJI and without introduced charge motion, indicated bigger intensity then in case of tilted nozzles. In this study, the combustion in bigger λ range and using the pressure based on indicating investigation approach (Fig. 6, Fig. 7).

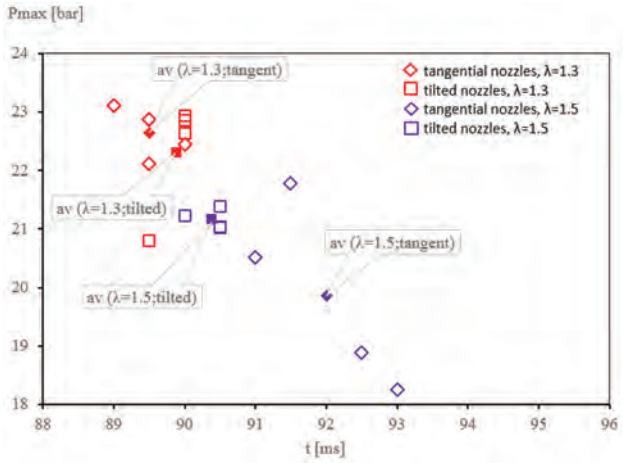

Fig. 6. Pmax for tangential and tilted nozzles

The Pmax values over their occurrence time at λ = 1.3 and λ = 1.5 (red and violet color respectively) for tangential (rotated squares) and tilted (squares) nozzles have been indicated for the single combustion cycles (Fig. 6). All mentioned cycles have been performed for the constant ignition advance. It can be noted, that combustion at λ = 1.5 indicates bigger spread of maximal pressures – an obvious effect of worse combustion stability, which is typically being found when increasing mixture dilution. When the charge with λ = 1.5 has been combusted, the tilted nozzles caused in average 7% increase in Pmax, which has been advanced for 1.6 ms. This increase has been caused by the better mixing the lean charge, what consists an critical factor by such a conditions to the inflammation capability. In contrast to this, at more rich conditions (λ = 1.3) the differences are very small (ca. 0.4 bar and 0.4 ms of advance) and beneficial effect achieved tangential nozzles.

In general, along the increase in maximal cylinder pressure, the occurrence of this value is being advanced. This effect is better visible for more diluted mixtures.

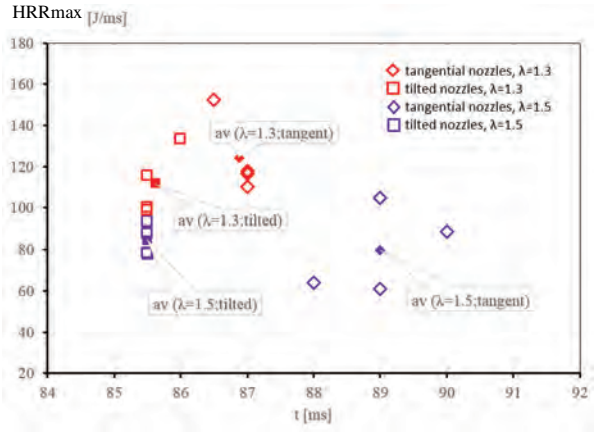

Fig. 7. HRRmax for tangential and tilted nozzles

Based on the cylinder pressure signal, the HRR values over their occurrence time at λ = 1.3 and λ = 1.5 (red and violet color respectively) for tangential (rotated squares) and tilted (squares) nozzles have been indicated for the single combustion cycles (Fig. 7). At high load points (λ = = 1.3), tangential nozzles provided approximately 9% bigger average value of HRRmax, which has been however retarded for 1.2 ms. At low load points (λ = 1.5), the tilted nozzles caused 4% bigger HRRmax. However, for both investigated λ, the occurrence of HRRmax indicates much smaller spread, when the tilted nozzles have been used. The better mixing characteristic with use of tilted nozzles results in smaller cyclic variability of Pmax and HRRmax.

5. Summary and conclusions

The combined optical and indicating RCM measurement approaches have been employed into the comparative investigation on ignition type and nozzles angularity modification of advanced ignition. The TJI has been related to the SI regarding the flame development in lean conditions – at λ = 1.5. Based on the recorded images, when the centralized ignition energy source applied, the flame develops from the source to the auxiliary chamber regions tangentially, while the igniting jets generated from TJI achieved the walls of combustion chamber within 2 ms and intensively develop perpendicularly to the flow. The maximal flame luminescence intensity and almost complete cover of combustion chamber with flame in 4 ms after SOI using the TJI. The flame of combustion initiated with SI reaches the optical access area in 22 ms. The cylinder pressure measurements indicated faster increase, despite SOI retarded for 8 ms and Pmax bigger for 15 bars. The calculated HRR indicates rapid and earlier heat release with HRRmax bigger for 50 J/ms. The combustion initiated with TJI is advanced in phase, intensified and faster.

The pre-chamber consisting 7 tangential nozzles has been compared to the pre-chamber with 7 tilted nozzles. It has been noted, that combustion cycles performed at λ = 1.5 indicate bigger cyclic variation of Pmax, regarding both their values and the occurrence time instance. The tangential nozzles achieved worse results in these points. For bigger mixture dilution, the nozzles rotation influencing the mixing inside pre-chamber and generating additional charge motion in the main combustion chamber. In contrast to the high load point (λ = 1.3), prechamber with tangential nozzles provided slightly bigger Pmax and HRRmax. However, the application of tilted nozzles resulted in earlier occurrence of HRRmax, confirming therefore improved prechamber mixing and positive results from introduced charge movement inside main combustion chamber.

Acknowledgements

This work was supported by the EU – Horizon 2020 [grant number 652816].

Nomenclature

A	area
av	average point
CNG	compressed natural gas
CR	compression ratio
D	diameter
e	energy
g	thickness
HRR	heat release rate
IMEP	indicated mean effective pressure
MC	main chamber
m	mass
n	engine speed
NO_x	nitrogen oxides
p	pressure
PC	pre-chamber
q_o	fuel dose
RCM	rapid compression machine
SI	spark ignition
SOI	start of ignition
TJI	turbulent jet ignition
V	volume
λ	air fuel equivalence ratio
Ø	fuel air equivalence ratio

Indexes

d	driving (start)
DIS	discharge
MC	main chamber
o	overall
OA	optical access
PC	pre-chamber
t	thermal
tot	total
V	volume

Bibliography

[1] ATTARD, W.P., BLAXILL, H., ANDERSON, E., LITKE, P. Knock limit extension with a gasoline fuelled pre-chamber jet igniter in a modern vehicle powertrain. *SAE Technical Paper* 2012-01-1143. 2012. DOI:10.4271/2012-01-1143.

[2] ATTARD, W.P., FRASER, N., PARSONS, P., TOULSON, E. A turbulent jet ignition pre-chamber combustion system for large fuel economy improvements in a modern vehicle powertrain. *SAE Technical Paper* 2010-01-1457. 2010. DOI: 10.4271/2010-01-1457.

[3] BISWAS, S., TANVIR, S., WANG, H., QIAO, L. On ignition mechanisms of premixed CH_4/air and H_2/air using a hot turbulent jet generated by pre-combustion. *Applied Thermal Engineering*. 2016, **106**.

[4] BUESCHKE, W. Identification of an engine lean burn gas air combustion system with turbulent jet ignition. Dissertation. *Poznan University of Technology*. 2017.

[5] BUESCHKE, W., SKOWRON, M., SZWAJCA, F., WISŁOCKI, K. Flame propagation velocity in 2-stage gas combustion system applied in SI engine. *IOP Conference Series: Materials Science and Engineering*. 2018, **421**. DOI: 10.1088/1757-899x/421/4/042009.

[6] BUESCHKE, W., SKOWRON, M., WISŁOCKI, K. Investigations on gas-air mixture formation in the ignition chamber of two-stage combustion system using high-speed Schlieren imaging. *MATEC Web of Conferences*. 2017, **118**, 00012. DOI: 10.1051/matecconf/201711800012.

[7] BUNCE, M., BLAXILL, H., KULATILAKA, W., JIANG, N. The effects of turbulent jet characteristics on engine performance using a pre-chamber combustor. *SAE Technical Paper* 2014-01-1195. 2014. DOI: 10.4271/2014-01-1195.

[8] CHEN, S., BECK, N. Gas engine combustion principles and applications. *SAE Technical Paper* 2001-01-2489. 2001, DOI:10.4271/2001-01-2489.

[9] DUAN, X., LI, Y., LIU, J. et al. Experimental study the effects of various compression ratios and spark timing on performance and emission of a lean-burn heavy-duty spark ignition engine fueled with methane gas and hydrogen blends. *Energy*. 2018.

[10] DUAN, X., LIU, J., YAO, J. et al. Performance, combustion and knock assessment of a high compression ratio and lean-burn heavy-duty spark-ignition engine fuelled with n-butane and liquefied methane gas blend. *Energy*. 2018, **158**.

[11] ECKHOFF, R.K. Explosion hazards in the process industries: why explosions occur and how to prevent them? *Oxford: Gulf Professional Publishing*. 2016, **2**.

[12] EHSAN, M.D. Effect of spark advance on a gas run automotive spark ignition engine. *Journal of Chemical Engineering*. 2006, **24**(1).

[13] FU, J., SHU, J., ZHOU, F. et al. Experimental investigation on effects of compression ratio on in-cylinder combustion process and performance improvement of liquefied methane engine. *Applied Thermal Engineering*. 2017, **113**.

[14] GHOLAMISHEERI, M., THELEN, B.C., GENTZ, G.R. et al. Rapid compression machine study of a premixed, variable inlet density and flow rate, confined turbulent jet. *Combustion and Flame*. 2016, **169**. DOI: 10.1016/j.combustflame.2016.05.001.

[15] HUANG, Q., LI, W., LIN, Q. et al. Catalytic performance of Pd-$NiCo_2O_4$/SiO_2 in lean methane combustion at low temperature. *Journal of the Energy Institute*. 2018, **91**. DOI: 10.1016/j.joei.2017.05.008.

[16] KAWABATA, Y., MORI, D. Combustion diagnostics & improvement of a prechamber lean-burn natural gas engine. *SAE Technical Paper* 2004-01-0979. 2004. DOI: 10.4271/2004-01-0979.

[17] KOTZAGIANNI, M., KYRTATOS, P., BOULOUCHOS, K. Optical investigations of prechamber combustion in an RCEM. *Combustion Engines*. 2019, **176**(1), 12-17. DOI: 10.19206/CE-2019-102.

[18] LEE, S., PARK., S., KIM, C. et al. Comparative study on EGR and lean burn strategies employed in SI engine fueled by low calorific gas. *Applied Energy*. 2014, **129**.

[19] Magazine Modern Power Systems – webpage. Available online: www.modernpowersystems.com.

[20] PARK, C., LEE, S., KIM, C., CHOI, Y. A comparative study of lean burn and exhaust gas recirculation in an HCNG-fueled heavy duty engine. *International Journal of Hydrogen Energy*. 2017, **42**.

[21] PIELECHA, I., BUESCHKE, W., CIEŚLIK, W., SKOWRON, M. Turbulent spark-jet ignition in SI gas fueled engine. *MATEC Web of Conferences*. 2017, **118**, 00010. DOI: 10.1051/matecconf/201711800010.

[22] RAPP, V., KILLINGSWORTH, N., THERKELSEN, P., EVANS, R. Lean Combustion. Technology and control. *Academic Press*. 2016.

[23] ROETHLISBERGER, R.P., FAVRAT, D. Comparison between direct and indirect (prechamber) spark ignition in the case of a cogeneration natural gas engine, part I: engine geometrical parameters. *Applied thermal Engineering*. 2002, **22**.

[24] ROETHLISBERGER, R.P., FAVRAT, D. Investigation of the prechamber geometrical configuration of a natural gas spark ignition engine for cogeneration: part II. Experimentation. *International Journal of Thermal Sciences*. 2003, **42**. DOI: 10.1016/S1290-0729(02)00024-8.

[25] TANOUE, K., KIMURA, T., JIMOTO, T. et al.Study of prechamber characteristics in a rapid compression machine. *Applied Thermal Engineering*. 2017, **115**. DOI: 10.1016/j.applthermaleng.2016.12.079.

[26] UYEHARA, O.A. Prechamber for lean burn for low NO_x. *SAE Technical Paper 950612*. 1995. DOI: 10.4271/950612.

[27] WISŁOCKI, K., PIELECHA, I., MASLENNIKOV, D., CZAJKA, J. Thermodynamic aspects of combustion in gasoline engines fitted with a multiple fuel injection. *Journal of KONES Powertrain and Transport*. 2011, **18**(4).

Wojciech Bueschke, DEng. – Faculty of Transport Engineering, Poznan University of Technology.
e-mail: *Wojciech.Bueschke@put.poznan.pl*

Maciej Skowron, MEng. – Faculty of Transport Engineering, Poznan University of Technology.
e-mail: *Maciej. Skowron@put.poznan.pl*

Prof. Krzysztof Wislocki, DSc. DEng. – Faculty of Transport Engineering, Poznan University of Technology.
e-mail: *Krzysztof.Wislocki@put.poznan.pl*

Filip Szwajca, MEng. – Faculty of Transport Engineering, Poznan University of Technology.
e-mail: *Filip.Szwajca@put.poznan.pl*

Article citation info:
HÄNGGI, S., HILFIKER, T., SOLTIC, P. et al. Control-oriented analysis of a lean-burn light-duty natural gas research engine with scavenged pre-chamber ignition. *Combustion Engines*. 2019, **176(1)**, 42-53. DOI: 10.19206/CE-2019-106

Severin HÄNGGI
Thomas HILFIKER
Patrik SOLTIC
Richard HUTTER
Christopher ONDER

CE-2019-106

Control-oriented analysis of a lean-burn light-duty natural gas research engine with scavenged pre-chamber ignition

Natural gas is well-suited as a fuel in the transport sector. Due to its excellent combustion characteristics, engines operating with compressed natural gas (CNG) reach high efficiency, especially if operated at lean conditions. However, CNG engine research mainly focusses on stoichiometric conditions in order to use a three-way catalytic converter for the exhaust gas after treatment system.

With the objective to explore the potential of CNG engines operated at lean conditions, a turbo-charged CNG engine with high compression ratio is developed and optimized for lean operation. In order to increase the ignition energy, the CNG engine is equipped with scavenged pre-chambers. A specific control structure is developed, which allows to operate the engine at a pre-defined (lean) air-to-fuel ratio. Further functionalities such as the combustion placement control and algorithms to estimate the conditions inside of the pre-chamber are implemented.

The first part of this paper describes this engine control structure, which is specifically developed for the lean-burn CNG engine. In the second part, the effects of pre-chamber scavenging on engine performance criteria such as the combustion stability, engine efficiency or engine emissions are analyzed. With the objective to use pre-chamber scavenging to improve engine performance, a scavenging feedback control strategy is proposed. In order to control the ignition delay, this strategy adapts the amount of CNG injected into the pre-chamber with a linear controller or an extremum seeking algorithm depending on the air-to-fuel ratio of the main chamber.

Key words: *gas engine control, pre-chamber ignition, ignition delay control, extremum seeking*

1. Introduction

Natural gas as a fuel for passenger cars is a promising alternative to Diesel or gasoline [8]. Due to its chemical composition, it has lower CO_2 emissions and it can be blended or substituted with renewable alternatives like biogas or synthetic methane. It is highly knock resistant and can be used in engines with high compression ratio, which promotes the engine efficiency [7].

Operated at stoichiometric conditions with a three-way catalytic converter, natural gas engines reach very low emissions [2]. However, efficiency could be increased if the engine is operated under lean conditions due to reduced wall heating and pumping losses [4]. Within a research project with the objective to investigate the efficiency potential and emission characteristics at lean operation, a natural gas engine is set up on a test bench. In order to ignite lean mixtures, the engine is equipped with scavenged pre-chambers, as described in [10].

For the operation of this research engine, a custom engine control strategy is developed and implemented. It offers extended functionalities such as the combustion placement feedback control and the precise control of lean air-to-fuel ratios. Further it allows to set a specific CNG mass to be injected into the pre-chambers in order to increase the ignition energy for lean mixtures. The implemented engine control strategy, which is described in section 2, is then used to investigate lean CNG combustion with scavenged pre-chambers. Results of this analysis are presented in [10]. Further, a control-oriented analysis of the effect of pre-chamber scavenging on engine efficiency and emissions is conducted and used to propose a pre-chamber scavenging control. This analysis is described in section 3 and the control proposal is presented in section 4.

Pre-chamber combustion for lean gas engine operation is well known in literature [1, 9]. However, to the authors knowledge, there is no literature about pre-chamber scavenging feedback control.

2. Research engine setup and control structure

2.1. Engine schematics with sensors & actuators

There are two gas engine configurations to be controlled, one standard version (engine 1) and one extended version with scavenged pre-chambers (engine 2). Except for the ignition system, both engines are identical. They are based on a four cylinder passenger car Diesel engine, which was adapted to run with compressed natural gas (CNG). A characterization of these engines can be found in [10].

Figure 1 shows a schematic of the research gas engine 2. Seven actuators are used to control the engine, as they are labeled in the schematic. The air mass flow through the engine is controlled by the waste gate valve (u_{WG}) and the throttle (u_{Thr}) in front of the intake. The amount of CNG, which is pre-mixed with the air can be controlled with the energizing duration of the mixer injectors in front of the throttle (DOE_{Mix}) and the mixer rail pressure regulator ($u_{PR,Mix}$). The timing and the amount of CNG injected into the pre-chambers can be controlled by the pre-chamber injector control signals (SOE_{PC}, DOE_{PC}) as well as the pre-chamber rail pressure regulator ($u_{PR,PC}$). The combustion placement[1] is controlled by the spark timing (CA_{Ign}). The ignition coil dwell time is set to a constant value of 2 ms.

Hence, a total of four main engine operation parameters are controlled by these seven actuators. However, these parameters are not intuitive to use as reference signals. In

[1] Here, the combustion placement refers to the crank angle at which 50% of fuel is burned (CA50).

a quantitative control approach as is chosen here, the reference signals of interest are the engine torque and the air-to-fuel ratio of the air-CNG gas mixture in the combustion chamber. For a constant air-to-fuel ratio, the engine torque is approximately proportional to the air mass flow. Therefore, instead of controlling the air mass flow, the throttle and the waste gate are used to control the engine torque directly, and instead of the amount of CNG, the mixer injectors and the mixer rail pressure are used to control the air-to-fuel ratio. However, torque and air-to-fuel ratio are strongly coupled variables. A change in one of them will act as a disturbance for the other one. These cross-coupling effects need to be considered in the control structure.

Figure 2 shows a signal flow chart of the engine in its test bench environment. The four reference signals can be set by the test bench operator via the test bench operating system. These parameters are transmitted to the engine control unit (ECU) via a controller area network (CAN) bus connection. As illustrated in the signal flow chart, the implemented feedback algorithms on the ECU use a number of sensor signals and combustion characteristics to derive all the control signals. These control signals are then transmitted to a power stage (dSpace RapidPro), which translates them to analog signals, able to actuate the corresponding actuators.

For each of the four reference signals, the ECU has a control structure implemented. These control loops are described in the next subsections. The first three control structures (load, air-to-fuel ratio and combustion placement) are identical for both engines. They are based on control approaches presented in [6] and are adapted to fit the engine setup. The additional control tasks allowing to manually set the pre-chamber scavenging of engine 2 are explained in section 2.5.

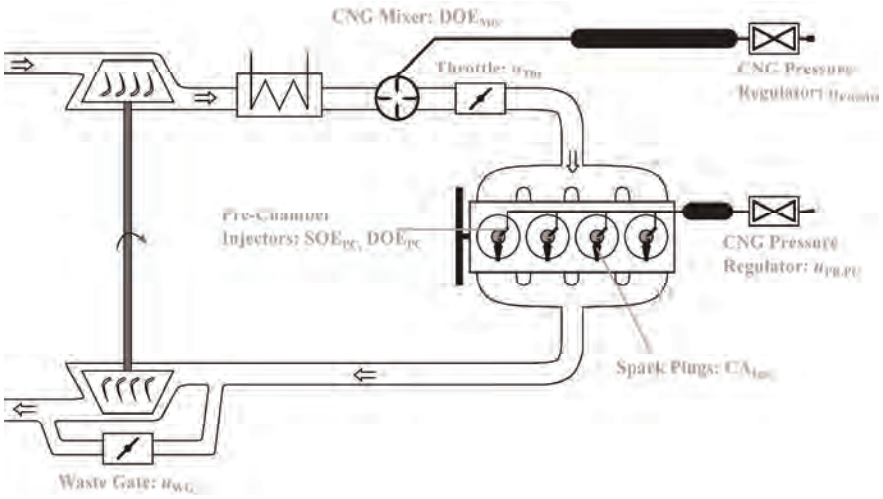

Fig. 1. Schematic of the research gas engine with scavenged pre-chambers (engine 2). Engine actuators and their corresponding control variables (referred to as actuator signals) are labeled

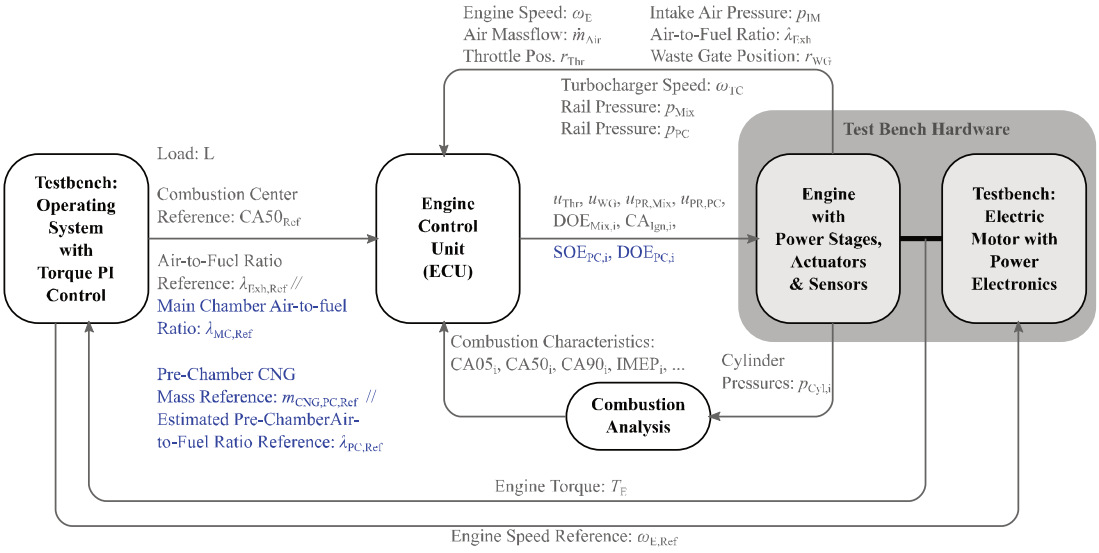

Fig. 2. Test bench setup of the research engines with the main signal flows used for the engine control. The test bench operating system sets four reference signals and the ECU uses feedback control to operate the engine accordingly. The blue reference and actuator signals are needed additionally for engine 2 with scavenged pre-chambers only

2.2. Load control

As depicted in Fig. 2, the test bench operating system controls the torque of the engine with a PI controller. The PI control output L is transferred to the ECU and represents the gas pedal signal of a car.

With this signal, the throttle and the waste gate position are controlled. Since we have two control outputs and one control input, we have one degree of freedom which can be used to achieve a desired engine performance. If we would want to optimize the dynamic behavior of the engine, we would have to close the waste gate at all times (except if the turbo charger speed increases above its limit and mechanical damage could occur) and control the engine with the throttle only. However, this strategy would lead to substantial pumping losses. The most fuel efficient strategy is to reduce pumping losses by operating the engine with completely open waste gate unless the throttle is completely open [5]. This strategy, illustrated in Fig. 3, was implemented on the ECU. With the assumption that the engine reaches a maximum intake manifold pressure of 2 bar, we reach a maximum load of approximately 50% without charging. Therefore, below 50%, the engine load is controlled by the throttle with open waste gate, and above 50%, it is controlled by the waste gate valve with open throttle.

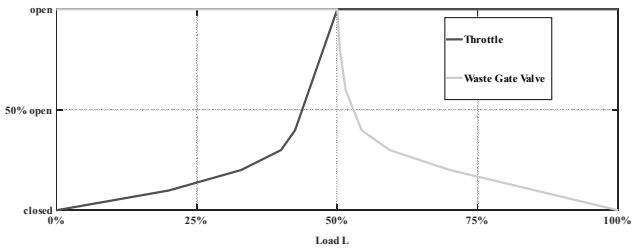

Fig. 3. Load control strategy, which is implemented on the ECU

In Figure 4 the complete load control structure is illustrated. The load reference signal L from the test bench operating system is limited if the cylinder averaged indicated mean effective pressure ($IMEP_{Mean}$) exceeds a predefined maximum level. This is necessary in order to protect the engine against mechanical damage. The limitation algorithm consists of an integral controller, which is limited to negative values and added to the unlimited load signal. A simplified version of the algorithm transfer function is stated in eq. (1). The algorithm implemented on the ECU additionally uses an anti-reset windup scheme to prevent integrator windup.

$$L_{Lim} = L + \min\left(0, (IMEP_{Max} - IMEP_{Mean}) \cdot \frac{k_i}{s}\right) \quad (1)$$

The limited load signal L_{Lim} is used to derive a reference throttle and waste gate position according to the strategy presented in Fig. 3. The derived reference value for the throttle position is directly fed to a proportional-integral-derivative (PID) controller, which adapts the duty cycle of the throttle u_{Thr} accordingly. For the waste gate, a further control algorithm is needed in order to limit the turbo charger speed n_{TC}.

$$r_{WG,Ref,Lim} = r_{WG,Ref} - \left(\min\left(0, (n_{TC,Max} - n_{TC}) \cdot \frac{k_{i,Max}}{s}\right) + \max\left(0, (n_{TC,Min} - n_{TC}) \cdot \frac{k_{i,Min}}{s}\right)\right) \quad (2)$$

Similar to the IMEP limitation, this algorithm sets lower and upper bounds to the turbocharger speed in order to protect it from physical damage. A simplified version of the algorithm transfer function neglecting the anti-reset windup scheme is stated in eq. (2). The limited waste gate position reference signal $r_{WG,Ref,Lim}$ is fed into a PID controller, which controls the duty cycle u_{WG} of the waste gate actuator.

2.3. Air-to-fuel ratio control

The air-to-fuel ratio in the exhaust manifold λ_{Exh} is controlled by the CNG mass injected into the fresh air in front of the throttle by the CNG mixer. This mixer consists of 4 injectors, where each of them opens once in an engine cycle of 720°CA. Over a cycle, all the injectors have the same opening duration.

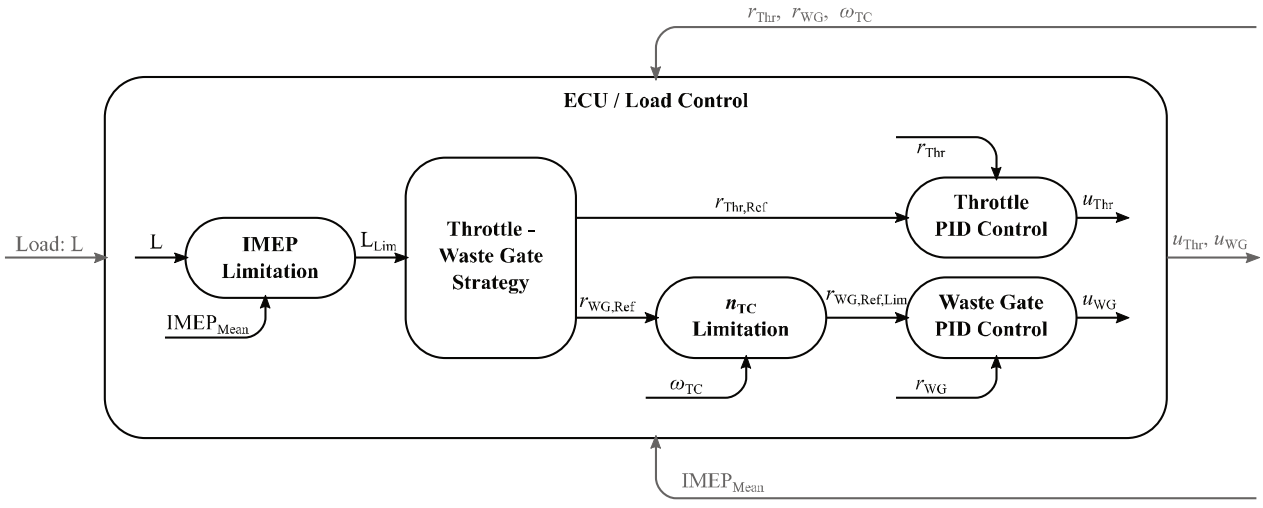

Fig. 4. Complete load control structure, implemented on the ECU

The mass injected by one injector is influenced by the CNG rail pressure (p_{Mix}) and the energizing duration of the injector (DOE_{Mix}). Two actuators control one reference signal, which means that we have one degree of freedom, which we can use for optimization. Here, the chosen strategy is to have a continuous CNG stream into the air stream in order to guarantee a good mixing. Therefore, each injector should be opened for $DOE_{Mix,Ref}$ = 180°CA per cycle[1].

The resulting control structure is illustrated in Fig. 5. It consists of a cascade control, with a fast and a slow control loop.

The fast loop controls the air-to-fuel ratio with the opening duration of the injectors. First, the CNG mass, which has to be injected in order to reach a desired reference air-to-fuel ratio is calculated ($m_{CNG,Cyl,Ref}$). This mass is corrected by a correction factor, derived by a PI feedback controller, which controls the air-to-fuel ratio to its reference. Together with the measured rail pressure p_{Mix} and an injector model, the corresponding duration of energizing (DOE_{Mix}) is calculated and applied.

The slow cascade loop controls the rail pressure such that the injection duration takes values of approximately 180°CA, depending on the precision of the CNG mass estimation. To reach that, an inverted injector model is used to calculate the mixer reference rail pressure, at which the opening duration reaches 180°CA for the given estimated CNG mass flow. A PID controller adapts the duty cycle ($u_{PR,Mix}$) of the pressure regulator in order to reach the corresponding reference rail pressure.

2.4. Combustion placement (CA50 control)

A common combustion control approach is to place the combustion such that the crank angle, at which 50% of the combustion energy is released (CA50), appears shortly after the top dead center. This can be done via a PI controller. Over several cycles, this controller places the spark advance such that the measured value CA50 corresponds to the reference value $CA50_{Ref}$. This is done for each cylinder individually.

2.5. Algorithms to manually set the pre-chamber scavenging

For lean operation with $\lambda_{Exh} > 1.7$, ignition of the charge becomes difficult, resulting in high cyclic variations and misfire. A possible solution to increase the provided ignition energy is using a scavenged pre-chamber, as introduced in engine 2. Figure 6 shows a schematic of its working principle. Instead of directly igniting the lean main-chamber, the spark plug ignites a richer mixture, created in a scavenged pre-chamber. This combustion increases the pressure in the pre-chamber, which causes the burning gas mixture to exit the pre-chamber through nozzles into the main chamber. These high-energy flame jets ignite the main chamber gas mixture and introduce additional turbulence, which increases the main-chamber combustion speed.

For engine operation with scavenged pre-chambers, the engine control unit is extended with additional functionalities.

To directly set the mass to be injected into each pre-chamber instead of the opening duration of the injectors, cylinder-individual injector maps are derived.

Further, an estimation algorithm of the air-to-fuel ratio inside of the pre-chamber at the time of ignition λ_{PC} is implemented on the engine control unit[2]. This estimation helps to choose the reference CNG mass to be injected in order to reach acceptable combustion conditions inside of the pre-chamber. Once the pre-chamber air-to-fuel ratio is known, the maximum energy Q_{PC} can be calculated, which would be released by an instantaneous combustion inside of the pre-chamber at the time of ignition.

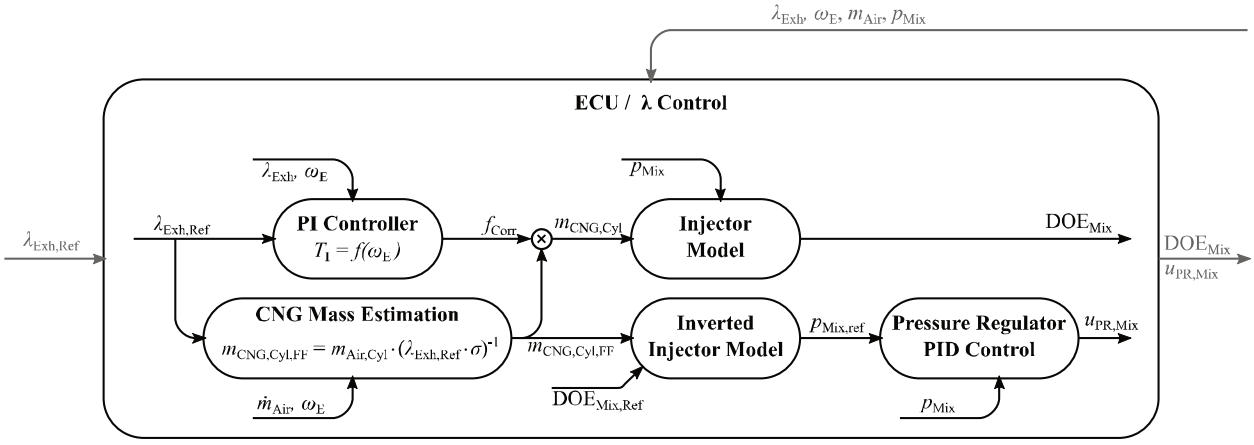

Fig. 5. Air-to-fuel control structure, implemented on the ECU with the according signals

[1] Here we assume that the energizing time corresponds to the opening duration of the injector. The error introduced due to this simplification is negligible.

[2] This approach has similarities with the pre-chamber air-to-fuel estimation presented in [9].

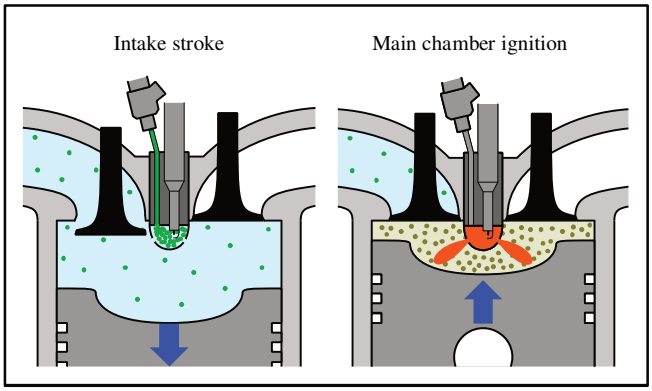

Fig. 6. Schematic of engine 2 operated with scavenged pre-chambers (graphics are taken from [13] and adapted)

The estimation algorithm uses the following simplifications:

- All gases are ideal, i.e. heat capacity ratios and isentropic coefficients are assumed to be independent of gas pressure and temperature.
- Prior to ignition, the pressure inside of the main chamber and the pre-chamber are equal.
- Isentropic compression is assumed during the compression stroke.

The algorithm is designed as follows:

- Using eq. (3), the air-to-fuel ratio of the main chamber before the CNG injection is calculated. The two CNG masses can either be measured, or calculated with injector maps. Also the cylinder (and pre-chamber) pressure at the end of the CNG injection into the pre-chamber is determined. It is equal to the intake pressure if the compression has not started yet, otherwise it is calculated assuming isentropic compression.
- The ideal gas law is used to calculate the volume which is filled by the injected CNG into the pre-chamber at the end of the pre-chamber injection. If this volume is larger than the pre-chamber volume, we assume that the whole pre-chamber is filled and any additional CNG is released into the main chamber through the nozzles of the pre-chamber. If the CNG volume is lower, the rest of the pre-chamber volume is assumed to be filled with the main-chamber air-CNG mixture.
- Assuming perfect mixing, the new air-to-fuel ratios of the main chamber and the pre-chamber after the CNG injection are calculated.
- Assuming an isentropic compression, the cylinder pressure and temperature of the gas mixture at the time of the ignition are calculated. At these conditions, the volume of the gas which originally filled the pre-chamber at the end of the CNG injection, is calculated. Subtracting this volume from the total pre-chamber volume equals the volume of the gas that had to enter the pre-chamber from the main chamber during the compression.
- Assuming perfect mixing, the air-to-fuel ratio of the pre-chamber at the time of ignition is calculated $\rightarrow \lambda_{PC}$
- We limit the derived pre-chamber air-to-fuel ratio to values larger or equal to 1[1] and use the definition of the air-to-fuel ratio to calculate the total CNG mass inside of the pre-chamber for which enough oxygen is available. Using this mass and the lower heating value of CNG, we derive the maximum possible combustion energy inside of the pre-chamber at the time of ignition $\rightarrow Q_{PC}$.

$$\lambda_{MC} = \lambda_{Exh} \cdot \frac{\dot{m}_{CNG,Mix} + \dot{m}_{CNG,PC}}{\dot{m}_{CNG,Mix}} \tag{3}$$

The described estimation algorithm is implemented on the engine control unit and allows to track the estimated pre-chamber conditions in real time. Further, the algorithm is inverted, in order to be able to set a desired pre-chamber air-to-fuel ratio $\lambda_{PC,Ref}$, which is translated to a CNG mass to be injected into the pre-chamber. This feed forward control strategy is illustrated in Fig. 7. Assuming that the estimation error is acceptable, this algorithm can be used to prepare an ignitable mixture inside of the pre-chamber at the time of ignition. However, having an ignitable gas mixture does not guarantee a sufficient ignition energy for the main chamber. The desired air-to-fuel mixture $\lambda_{PC,Ref}$ therefore still has to be adapted depending on the operating point and the air-to-fuel ratio inside of the main chamber.

[1] The limitation is only used for the calculation of Q_{PC}, the air-to-fuel ratio output λ_{PC} of the algorithm is unlimited.

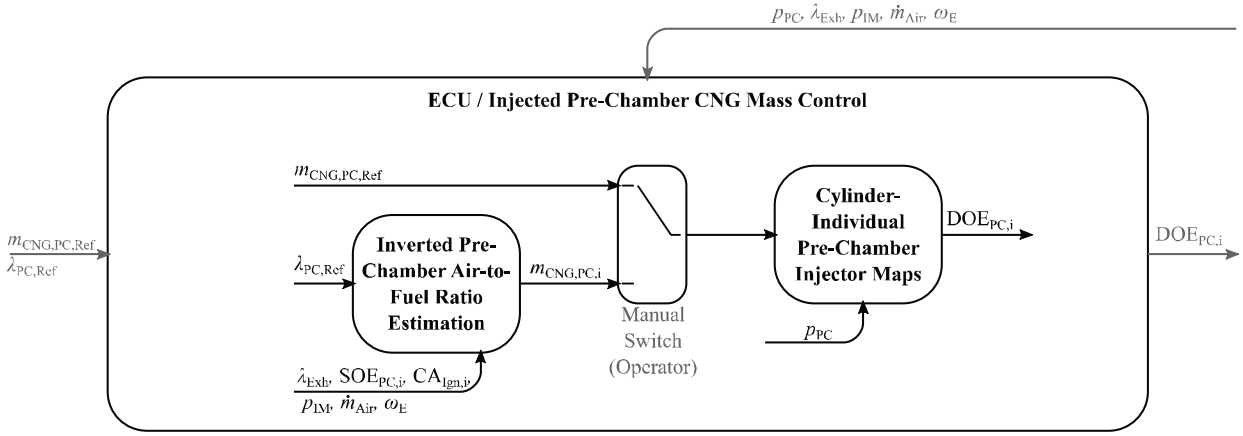

Fig. 7. Implemented feed forward functionalities for the pre-chamber scavenging. The operator can either set the desired air-to-fuel ratio inside of the pre-chambers at the time of ignition, or he can set the CNG mass to be injected directly

The injection timing ($SOE_{PC,i}$) is fixed at 300°BTDC just after the exhaust valve closes, in order to avoid methane slip and to ensure that the injection finishes before the compression stroke starts. With an early injection timing, the injected CNG has the longest possible time to mix with the gas inside of the pre-chamber and the gas entering the pre-chamber during the compression stroke. An initial variation of the injection timing has shown that this strategy has a positive effect on hydrocarbon emissions.

3. Pre-chamber scavenging analysis

With the control algorithms described in section 2, the engine is operated in steady-state-condition in order to investigate the influence of scavenging on performance parameters (engine efficiency, combustion stability and emissions).

The objective of the conducted analysis is to understand the effects of scavenging, in order to extend the basic pre-chamber injection functionalities derived in section 2.5 with a feedback control algorithm. In consideration of the main chamber air-to-fuel ratio, engine load and engine speed, this feedback approach would be able to set the amount of CNG injected into the pre-chamber such that combustion stability and engine efficiency as well as emissions are improved.

3.1. Analysis of an air-to-fuel ratio variation at a constant operating point

Figure 8 shows a comparison of the spark plug engine 1, the un-scavenged (passive) engine 2 and the scavenged (CNG injection enabled) engine 2. At constant engine speed and torque, the main chamber air-to-fuel ratio (λ_{MC}) is varied (The main chamber air-to-fuel ratio is calculated according to equation (3)). For the scavenged case (green), the amount of CNG injected into the pre-chambers is adapted manually in order to derive a stable combustion, indicated by a low IMEP covariance.

For air to fuel ratios $\lambda_{MC} < 1.6$, engine 2 has a lower efficiency with similar emission characteristics compared to the spark plug engine 1. Scavenging decreases efficiency even more while maintaining emission levels. For engine 1, the energy of the spark-plug is sufficient to reliably ignite the CNG-air mixture, and the combustion in the main chamber is fast already without the turbulence introduced by the flame jets of the pre-chamber nozzles. For engine 2, the pre-chamber increases the ignition energy and speeds up the combustion. However, the increased main-chamber combustion speed does not improve emissions or efficiency. Also the amount of CNG-air mixture burning inside of the pre-chamber does not contribute to the torque generation, because a main part of its energy is lost in turbulence and wall heat losses. Additional CNG injected into the pre-chambers (scavenging) further increases the energy loss in the pre-chambers without any positive effect on the main chamber combustion. We conclude that for air-to-fuel ratios $\lambda_{MC} < 1.6$, engine 2 with pre-chambers is outperformed by engine 1 with spark-plugs only. Also we see that for engine 2, scavenging has a negative effect on engine efficiency.

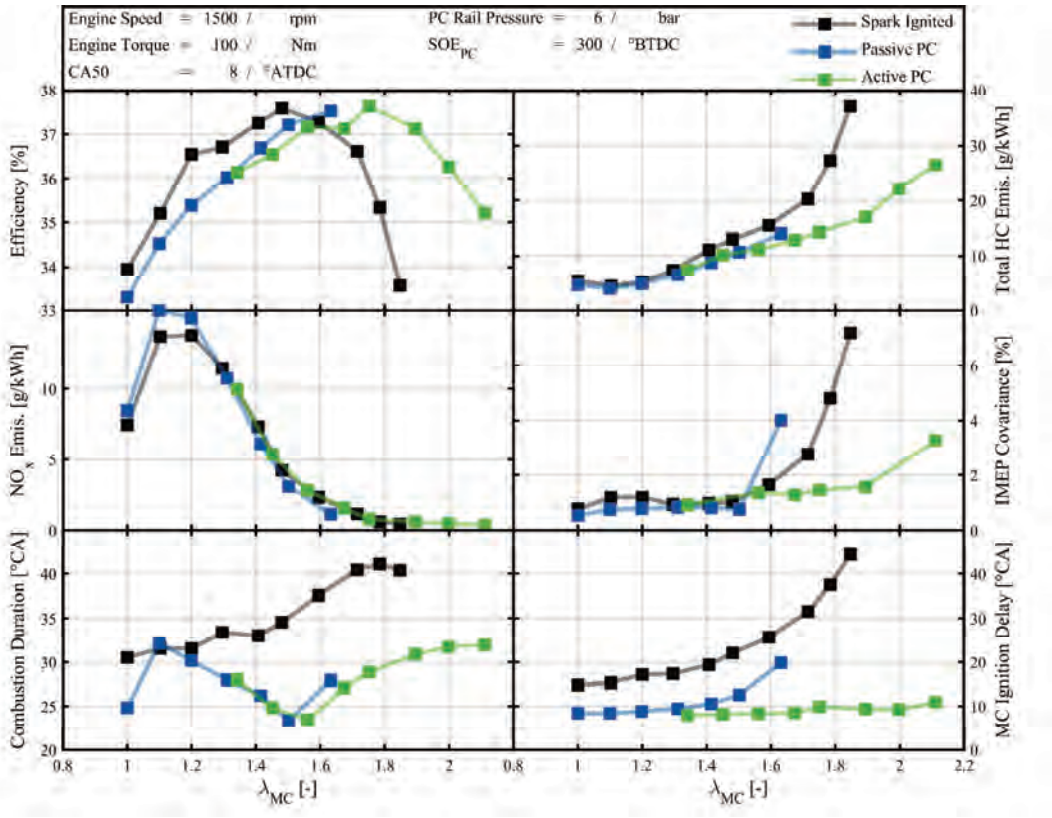

Fig. 8. Air to-fuel ratio variation at a medium load operating point with the spark-ignited engine 1, the pre-chamber engine 2 without scavenging (passive PC) and engine 2 with scavenging (active PC)[1].

[1] Efficiency and emission values presented in this figure are measured with a different piston shape and pre-chamber shape compared to other results stated within this paper. Absolute values are not comparable to other graphics.

For air-to-fuel ratios $\lambda_{MC} > 1.6$, engine 2 needs pre-chamber scavenging in order to ensure a stable combustion without misfire. In this region, it clearly outperforms engine 1 regarding efficiency, combustion stability and hydrocarbon emissions. We conclude that for very lean operation, the increased ignition energy and the additional turbulence introduced into the main chamber have a positive effect on engine efficiency and emissions. The spark ignition of engine 1 does not provide enough energy for a fast combustion anymore.

So far we have established that for $\lambda_{MC} < 1.6$ engine 1 performs better and scavenging has a negative effect, while for $\lambda_{MC} > 1.6$ engine 2 performs better and scavenging is necessary in order to reach acceptable combustion stability. Now we want to compare engine 1 with engine 2 for any choice of the air-to-fuel ratio with the efficiency as performance criterion. As we can see in Fig. 8 with spark-ignition only, we reach highest efficiency at $\lambda_{MC} = 1.5$ while the pre-chamber engine 2 reaches its efficiency maximum at $\lambda_{MC} = 1.7$. With this air-to-fuel ratio shift, we are able to drastically reduce NO_x emissions without any penalty in hydrocarbon emissions or efficiency when switching from engine 1 to engine 2. This fact clearly shows the advantages of scavenged pre-chambers for lean CNG engine operation and motivates further analysis of pre-chamber scavenging.

3.2. Analysis of a pre-chamber CNG injection variation at a constant operating point

For very lean operation around $\lambda = 1.8$, a variation of the CNG mass injected into the pre-chambers is analyzed. Measurement results including the estimated parameters described in section 2.5 are illustrated in Fig. 9. With the objective to study the influence of the pre-chamber combustion on the main chamber combustion and the resulting engine efficiency and emission characteristics, two measurement sets are compared. For a first measurement set (black), the air-to-fuel ratio in the exhaust is controlled to a constant value $\lambda_{Exh} = 1.8$, as described in section 2.3. However, by increasing the amount of CNG injected into the pre-chamber, the amount of CNG in the main chamber has to be reduced in order to keep a constant overall air-to-fuel ratio. Therefore, with increased CNG injection into the pre-chamber the mixture in the main chamber gets leaner, which influences the combustion characteristics. In order to study the effect of the pre-chamber combustion on the main-chamber combustion only, the main chamber gas composition has to be held constant. Hence, in a second (blue) measurement series, the air-to-fuel control algorithm described in section 2.3 is slightly adapted. An estimated air-to-fuel ratio of the main chamber air-to-fuel ratio λ_{MC} replaces the air-to-fuel ratio feedback signal λ_{Exh} of the controller. The main chamber ratio is calculated according to eq. (3).

For a constant main chamber air-to-fuel ratio (blue) we find that the highest efficiency occurs at the fastest combustion with the lowest ignition delay and IMEP covariance. Also the hydrocarbon emissions are close to their minimum. Hence, for such lean mixtures and constant main chamber air-to-fuel ratio, we have to adjust the amount of CNG injected into the pre-chambers such that we reach the fastest possible combustion in the main chamber, which is the case for the lowest ignition delay. For the operation point chosen in Fig. 9, this is the case for an injected gas mass of 1 mg/inj. Looking at the estimated signals described in section 2.5, we see that for this amount of injected CNG, the pre-chamber has its highest combustion energy. Since the estimated pre-chamber air-to-fuel ratio is clearly below 1 at this injection rate, the pre-chamber energy depends on the amount of air inside of the pre-chamber only. The amount of air inside of the pre-chamber increases with increasing cylinder pressure. Hence for a constant combustion center, a shorter ignition delay leads to a later ignition at a higher cylinder pressure, which leads to a higher amount of air and therefore to a higher energy content Q_{PC} in the pre-chamber.

We conclude that for a strategy where the main chamber air-to-fuel ratio is controlled to a constant value of $\lambda_{MC} = 1.8$ (or higher) and the combustion center is controlled to a constant value, there exists an optimal amount of CNG to be injected into the pre-chamber, which leads to the shortest ignition delay and to the highest ignition energy for the main chamber. Injecting a higher amount of CNG would produce too rich conditions and injecting a lower amount would lead to a weaker pre-chamber combustion with a lower ignition energy for the main chamber. With highest ignition energy, we reach fastest main chamber combustion, which leads to highest efficiency, best combustion stability and low hydrocarbon emissions compared to other injection rates.

For a constant λ_{Exh}, (black) we find that the efficiency maximum and the hydrocarbon emission minimum do not occur at the fastest combustion anymore. Due to the fact that the main chamber gas mixture gets leaner with a higher amount of injected CNG into the pre-chambers, these two maxima occur at lower injection rates already. We conclude that if we control the exhaust manifold air-to-fuel ratio λ_{Exh} to a constant value, we cannot find the optimum efficiency by controlling the ignition delay (or the combustion duration) to its minimum anymore.

In Fig. 10, the variation depicted in Fig. 9 with $\lambda_{MC} = 1.8$ is compared with variations measured at main chamber air to fuel ratios of $\lambda_{MC} = 1.5$ (green) and $\lambda_{MC} = 1.7$ (yellow). For all variations, the highest pre-chamber energy leads to the lowest ignition delay and to the fastest main chamber combustion. However, the strategy to control towards fastest combustion duration or shortest ignition delay is not the favorable strategy for $\lambda_{MC} = 1.5$ or $\lambda_{MC} = 1.7$ anymore.

The engine efficiency maximum as well as lowest NO_x emissions are derived with the lowest possible CNG injection[1] for $\lambda_{MC} = 1.5$. If we would inject an amount of 0.8 mg/inj in order to reach a minimum combustion speed, we would increase the NOx emissions by approximately 1.2 g/kWh and decrease the efficiency by approximately 0.75% compared to the lowest possible CNG pre-chamber injection. Figure 8 in section 3.1.shows that for a main-chamber air-to-fuel ratio of $\lambda_{MC} = 1.5$, no scavenging leads to a better performance than scavenging. Therefore, we assume here that no scavenging would further improve engine perfor-

[1] The minimum amount to inject is dependent on injector characteristics and the rail pressure.

mance compared to the lowest possible CNG injection into the pre-chamber. We conclude that the combustion is already fast enough without any further CNG injection into the pre-chamber. A further increase of the combustion speed would lead to increased wall heat losses inside of the pre-chamber and the main chamber and therefore negatively influence the engine efficiency as well as the NO_x emissions.

At a main chamber air-to-fuel ratio $\lambda_{MC} = 1.7$ we have to inject a minimum amount of CNG in order to guarantee a stable combustion without misfiring. This minimum amount also leads to best efficiency and lowest NO_x emissions. However, compared to $\lambda_{MC} = 1.5$, hydrocarbon emissions and combustion stability can be slightly improved without substantial efficiency reduction by a small increase from the minimum injected amount to about 0.3 mg/inj. Using an amount of 1.2 mg/inj in order to reach fastest combustion and lowest ignition delay would decrease the efficiency by 0.75% and increase NO_x emissions by 0.75 g/kWh. However, hydrocarbon emissions would be decreased by 0.6 g/kWh.

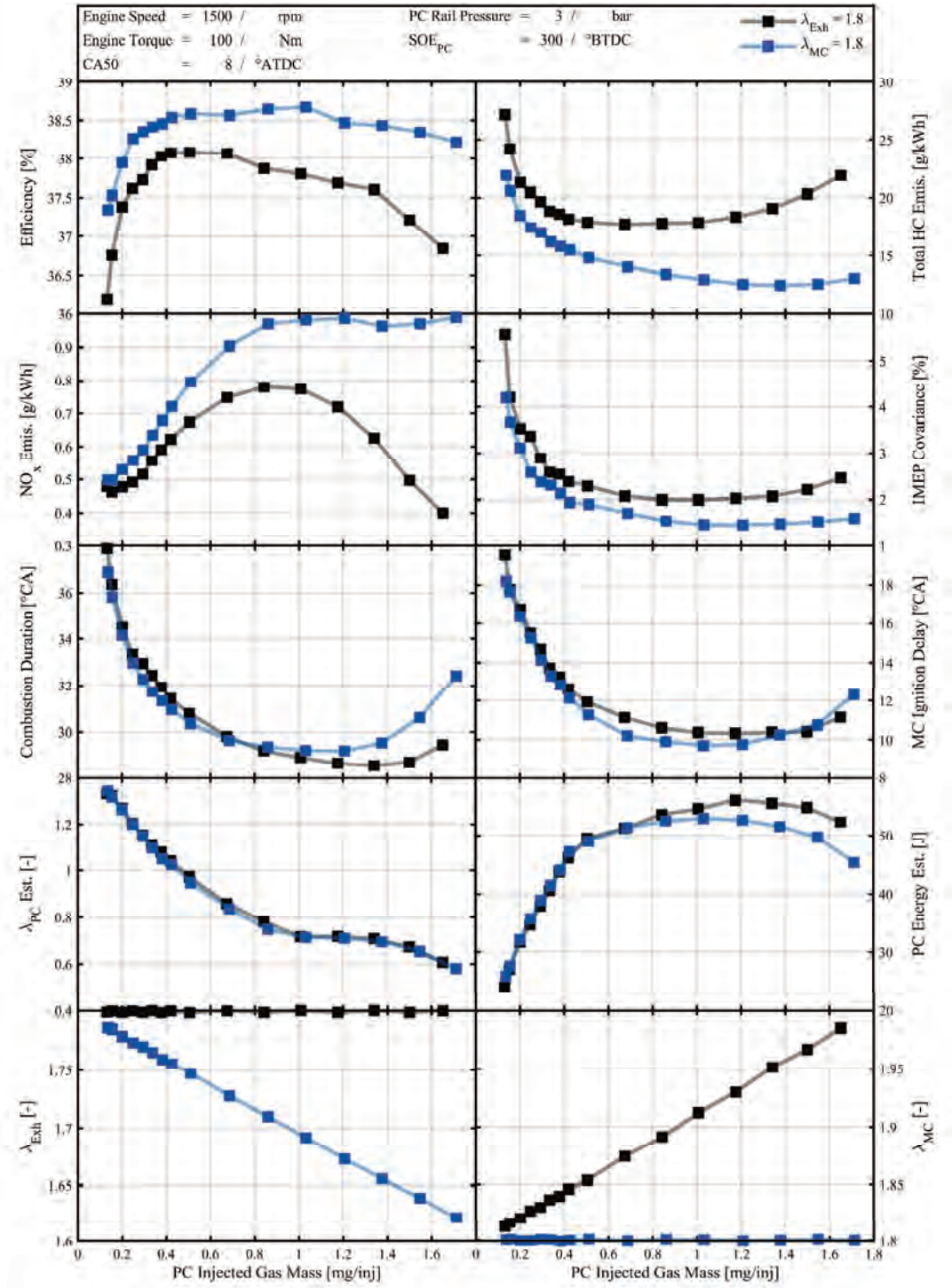

Fig. 9. Variation of the CNG mass injected into the pre-chambers. For the first (black) measurement series, the exhaust gas air-to-fuel ratio was controlled to $\lambda_{Exh} = 1.8$ and for the second (blue) measurement series, the main-chamber air-to-fuel ratio was controlled to $\lambda_{MC} = 1.8$

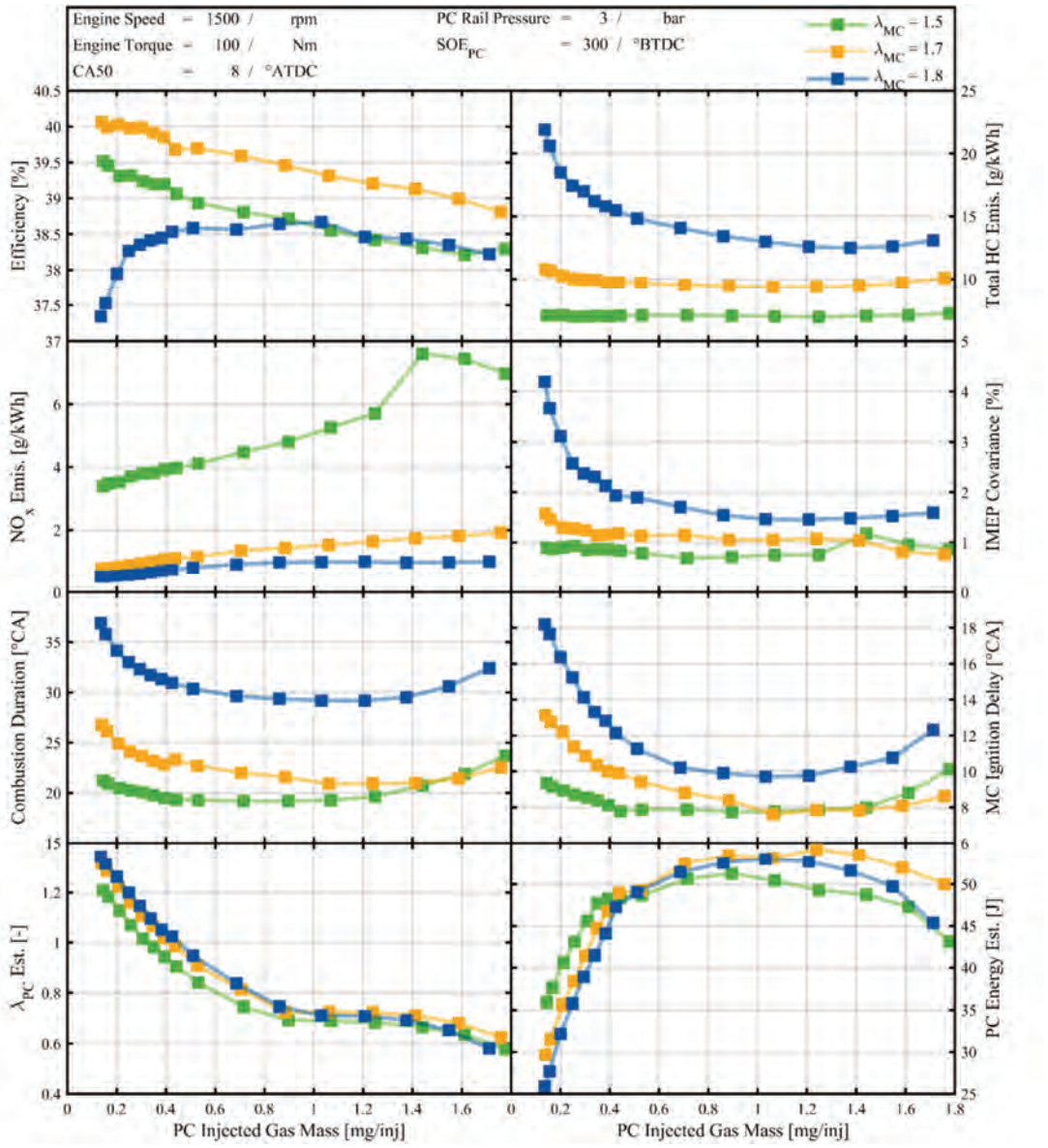

Fig. 10. Comparison of the pre-chamber injection variation depicted in Fig. 9 measured at λ_{MC} = 1.8 with injection variations measured at λ_{MC} = 1.5 and λ_{MC} = 1.7

A possible control strategy to compensate for changes in the main chamber air-to fuel ratio at a given engine speed and torque is to control the ignition delay to a reference value. Looking at Fig. 10, a PID controller with a reference ignition delay of 11°CA would control the injected CNG amount to [0.0, 0.3, 0.5] mg/inj for the main chamber air-to-fuel ratios [1.5, 1.7, 1.8]. these injection rates would lead to optimal results for λ_{MC} = 1.5 and λ_{MC} = 1.7, and acceptable results for λ_{MC} = 1.8. For air-to-fuel ratios higher than approximately λ_{MC} = 1.75, we assume to reach better results by controlling the ignition delay to its minimum.

3.3. Speed and torque variation at a constant air-to-fuel ratio

As derived in [10], the engine has its maximum efficiency close to an air-to-fuel ratio of λ_{Exh} = 1.7. At this ratio, an operation point variation is conducted in order to investigate the effects of engine speed and load on pre-chamber scavenging. For this variation, the amount of CNG injected into the pre-chamber was manually adjusted to an optimal value, which leads to best efficiency as well as high combustion stability and low emissions. Results of this variation are illustrated in Fig. 11. We see that the amount of injected CNG, optimized for best efficiency, is kept rather small for all operation points, however, it seems to be dependent on engine speed and load, and not straight forward to derive.

While engine efficiency and emissions are mainly dependent on engine torque, the combustion duration and the ignition delay are dependent on the engine speed only. Further we know from scavenging variations that the ignition delay reacts sensitive to low amounts of injected CNG. Both these facts can be used for the development of a high-level scavenging control. Concluding, an ignition delay control to a reference value depending on the engine speed only, could be a well working strategy to control the engine while operating around λ_{MC} = 1.7, where best engine efficiency is found.

4. Proposal for an extended pre-chamber scavenging control

Using the knowledge gathered in section 3, we propose a high-level feedback control strategy for the operation of engine 2 with scavenged pre-chambers. This strategy derives the reference values for the injected pre-chamber CNG mass and the pre-chamber rail pressure and therefore extends the functionalities presented in section 2.5. With this extension, the test-bench operator does not have to adapt these two set-values manually anymore. This extended control strategy proposal is depicted in Fig. 12. Further subsections explain its aspects in detail.

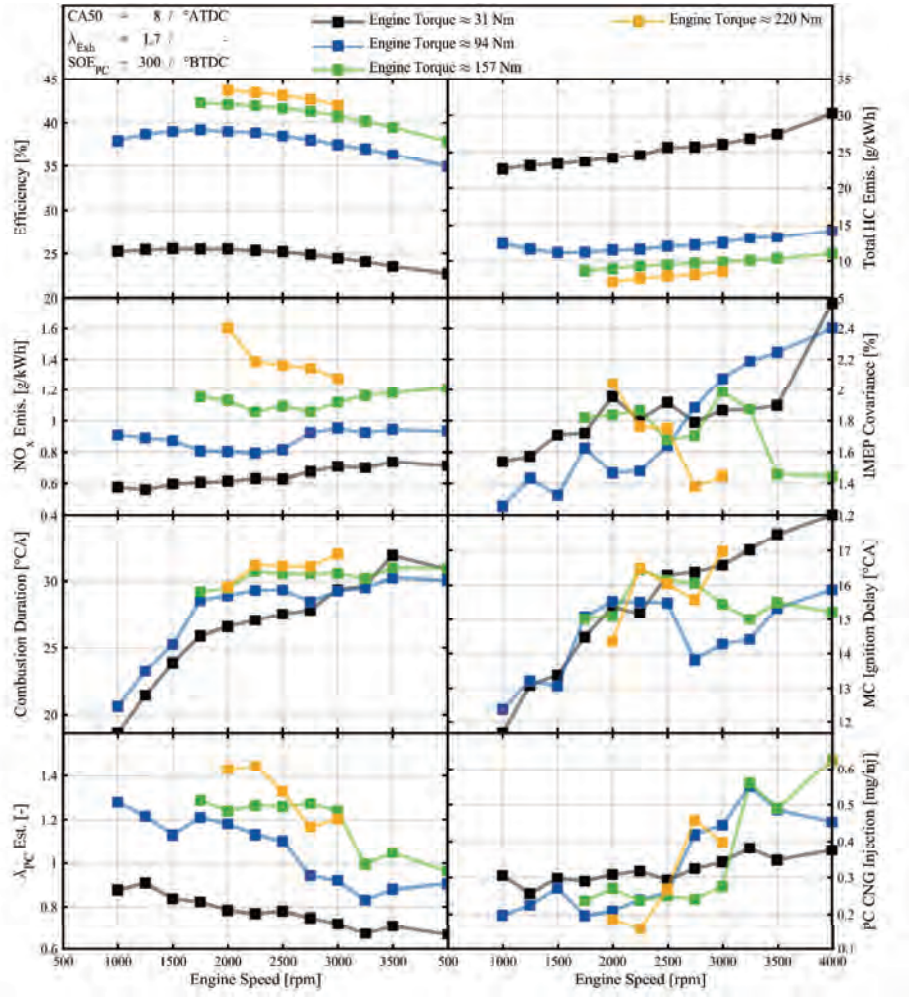

Fig. 11. Engine speed and load variation at an air-to-fuel ratio of λ_{Exh} = 1.7. The amount of CNG injected into the pre-chambers is adapted manually with the objective to increase engine efficiency and emissions for each operating point

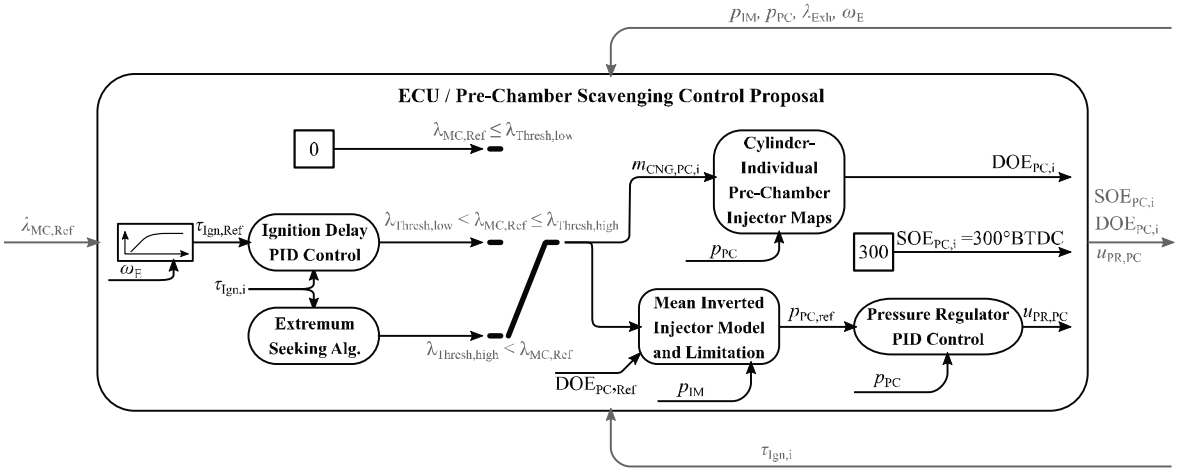

Fig. 12. Extended pre-chamber scavenging control suggestion. Depending on the main chamber air-to-fuel ratio, the strategy is to either control the ignition delay with the amount of CNG injected into the pre-chamber, or to minimize the ignition delay with an extremum seeking algorithm. For lower $\lambda_{MC,Ref}$ values, no injection is needed. Acceptable values for the strategy switching thresholds are $\lambda_{Thresh,low}$ = 1.6 and $\lambda_{Thresh,high}$ = 1.75

4.1. Main chamber air-to-fuel control

For scavenged operation, we propose to control the main-chamber air-to-fuel ratio instead of the exhaust gas air-to-fuel ratio, using the estimation depicted in equation (3). This approach allows to keep main chamber conditions constant, independent of the CNG amount directly injected into the pre-chamber. It decouples direct injection and mixer injection control, and it allows to control the ignition delay to its minimum in order to reach the efficiency maximum, as depicted in Fig. 9. This main chamber air-to-fuel feedback control approach was successfully implemented on the ECU.

4.2. Pre-chamber rail pressure control suggestion

Similar to the rail pressure control presented in section 2.3 and illustrated in Fig. 5, we propose to control the rail pressure such that the injection ends before the compression stroke starts. With an injection start at 300°BTDC, the reference duration of injection $DOE_{PC,Ref}$ has to be set to 120°CA. An inverted pre-chamber injector map, then uses this reference injection duration and the amount of injected CNG to calculate the reference pre-chamber rail pressure. A further aspect to consider is that the pressure difference between rail and pre-chamber has to be at least 2 bar, in order to open a back pressure valve in front of the pre-chamber (see [10]). Therefore, the intake pressure plus 2 bar acts as a lower bound on the pre-chamber rail pressure reference value.

This control strategy therefore sets the lowest possible pre-chamber rail pressure, which is still able to open the back pressure valve and ensures that the CNG pre-chamber injection finishes before the compression stroke starts. A low rail pressure is desired because it allows to inject a lower minimum amounts of CNG into the pre-chamber and it increases the control sensitivity.

4.3. Pre-chamber injection duration control suggestion

As depicted in Fig. 12, the control strategy for the CNG injection depends on the main chamber air-to-fuel ratio.

For values lower than a threshold $\lambda_{Thresh,low}$, there is no need of injecting any additional CNG into the pre-chamber. The mass entering from the main chamber during the compression stroke is sufficient to cause a pre-chamber combustion able to reliably ignite the main chamber and introduce enough turbulence for a fast combustion.

For air-to-fuel ratios between $\lambda_{Thresh,low}$ and $\lambda_{Thresh,high}$ we would like to guarantee a stable combustion without misfire, which only needs a small amount of injected CNG mass, lower than the mass which leads to the fastest combustion. The proposed strategy is to adjust the injected CNG mass in order to control the ignition delay to a reference value, depending on the engine speed. This control compensates for changes in the air-to-fuel ratio to a certain extent. Also, as depicted in Fig. 11, the ignition delay seems to be independent of the engine torque. Therefore, the reference value is a function of the engine speed only. However, this control approach can only be applied for a limited range of injected CNG mass. Due to the quadratic shape of the ignition delay, a linear controller is only stable as long as the gradient of the ignition does not change its sign.

At main chamber air-to-fuel ratios higher than an upper threshold $\lambda_{Thresh,high}$, we want to control the ignition delay to its minimum in order to minimize the combustion duration, which improves efficiency and hydrocarbon emissions as well as the combustion stability. Classic adaptive algorithms capable of that are generally referred to as extremum seeking [11]. Applied to the control problem described here, an extremum seeking algorithm would use an excitation signal to vary the CNG mass injected into the pre-chamber in every cycle. By comparing the ignition delays of these injection masses, the algorithm derives the ignition delay gradient. This gradient is then controlled to zero by an I-controller. Algorithms of higher complexity would estimate the quadratic shape of the ignition delay depending on the injected CNG mass [3]. Using these shape parameters, they would calculate the position of the shape minimum and set the CNG mass accordingly.

The minimization of the ignition delay suggested here has similarities to the Diesel minimal control algorithm proposed in [12], which is used to control the combustion placement of a Diesel ignited CNG engine. For this engine, the start of Diesel injection is set such that the amount of Diesel needed to derive a desired combustion center is minimized. For a constant operating point, this control increases the CNG-Diesel ratio, which reduces CO_2 emissions due to the higher hydrogen-carbon ratio of CNG. However, while for the Diesel ignited CNG engine the ignition energy (injected Diesel) is minimized, the extremum seeking algorithm proposed here for engine 2 maximizes the ignition energy in order to derive the fastest possible combustion.

5. Conclusions

A detailed analysis of pre-chamber scavenging at lean engine operation revealed that early pre-chamber injection leads to an increased homogeneity of the CNG-air mixture inside of the pre-chamber, which leads to lower hydrocarbon emissions. The amount of CNG injected into the pre-chamber affects combustion stability, engine efficiency and engine emissions. For air-to-fuel ratios below 1.6, scavenging has a negative effect. For higher air-to-fuel ratios, a small amount of CNG is needed in order to guarantee robust combustion without misfiring. For air-to-fuel ratios above 1.8, there exists an optimal amount of CNG to be injected, which minimizes ignition delay and combustion duration, and optimizes efficiency and hydrocarbon emissions, as well as combustion stability. An extremum seeking algorithm which minimizes the ignition delay is proposed to control the pre-chamber scavenging.

Best engine efficiency is derived with a main-chamber air-to-fuel ratio of 1.7. For this ratio an engine speed and torque variation indicates that a small amount of CNG injected into the pre-chamber leads to best engine performance. This amount is dependent on speed and load, however, the ignition delay is sensitive to changes of the injected CNG mass and is only dependent on engine speed. Hence it is a suitable parameter for the pre-chamber scavenging feedback control.

Acknowledgements

The work presented is part of the Horzon2020 project "GasOn". The authors would like to thank the project partners VW for their hardware support and the laboratory for aerothermochemistry and combustion (LAV) at ETH Zurich for fruitful discussions and the exchange of 0D models.

The Swiss partners have been supported by the Swiss State Secretariat for Education, Research and Innovation (SERI) under contract number 15.0145-1.

Funding

This project has received funding from the European Union's Horizon 2020 research and innovation programme under grant agreement No 652816.

The Swiss partners have been supported by the Swiss State Secretariat for Education, Research and Innovation (SERI) under contract number 15.0145-1. The opinions expressed and arguments employed herein do not necessarily reflect the official views of the Swiss Government.

Further, the authors have been supported and supervised by researchers of the Research Unit (FOR) 2401, which is funded by the German Research Association (Deutsche Forschungsgemeinschaft, DFG).

Bibliography

[1] ATTARD, W.P., TOULSON, E., HUISJEN, A. et al. Spark ignition and pre-chamber turbulent jet ignition combustion visualization. *SAE 2014 World Congress Exhibition*, 823-2012.

[2] BACH, C., LÄMMLE, C., BILL, R. et al. Clean engine vehicle a natural gas driven Euro-4/SULEV with 30% reduced CO_2-emissions. *SAE Technical Paper* 2004-01-0645. 2004. DOI:10.4271/2004-01-0645.

[3] BERTSEKAS, D.P., P.D. Dynamic programming and optimal control. *Athena Scientific*, 1995.

[4] CATON, J.A. A comparison of lean operation and exhaust gas recirculation: thermodynamic reasons for the increases of efficiency. *SAE Technical Paper* 2013-01-0266. 2013. DOI:10.4271/2013-01-0266.

[5] ERIKSSON, L., FREI, S., ONDER, C. et al. Control and optimization of turbocharged spark ignited engines. *IFAC Proceedings Volumes*. 2002, **35**. DOI:10.3182/20020721-6-ES-1901.01515.

[6] GUZZELLA, L., ONDER, C.H. Introduction to modeling and control of internal combustion engine systems. Berlin, Heidelberg: *Springer Berlin Heidelberg*, 2010.

[7] KHAN, M.I., YASMIN, T., SHAKOOR, A. Technical overview of compressed natural gas (CNG) as a transportation fuel. *Renewable & Sustainable Energy Reviews*. 2015, **51**, 785-797. DOI:10.1016/J.RSER.2015.06.053.

[8] KÜNG, L., BÜTLER, T., GEORGES, G. et al. Decarbonizing passenger cars using different powertrain technologies: Optimal fleet composition under evolving electricity supply. *Transportation Research Part C: Emerging Technologies*. 2018, **95**, 785-801. DOI:10.1016/J.TRC.2018.09.003.

[9] SHAH, A. Improving the efficiency of gas engines using pre-chamber ignition. *University of Lund*, 2015.

[10] SOLTIC, P., HILFIKER, T., HUTTER, R., HÄNGGI, S. Experimental comparison of efficiency and emission levels of four-cylinder lean-burn passenger car-sized CNG engines with different ignition concepts. *Combustion Engines*. 2018, **176**(1), 29-37. DOI: 10.19206/CE-2019-104.

[11] TAN, Y., MOASE, W.H., MANZIE, C. et al. Extremum seeking from 1922 to 2010. *Control Conf* (CCC), 2010, 29th Chinese 2010, 14-26.

[12] ZURBRIGGEN, F., HUTTER, R., ONDER, C. Diesel-minimal combustion control of a natural gas-diesel engine. *Energies*. 2016, **9**, 58. DOI:10.3390/en9010058.

[13] ZURBRIGGEN, F.J. Combustion control of a natural gas-diesel engine – feedback control and adaptation. *ETH Dissertation* 2016.

Severin Hänggi, MEng. – Swiss Federal Institute of Technology, Zürich (Switzerland).
e-mail: *SHaenggi@idsc.mavt.ethz.ch*

Thomas Hilfiker, Eng. – Empa, Swiss Federal Laboratories for Materials Science and Technology, Dübendorf, Switzerland.
e-mail: *Thomas.Hilfiker@empa.ch*

Patrik Soltic, DEng. – ETH, Empa, Swiss Federal Laboratories for Materials Science and Technology, Dübendorf, Switzerland.
e-mail: *Patrik.Soltic@empa.ch*

Richard Hutter, MEng. – ETH, Swiss Federal Institute of Technology, Zürich (Switzerland).
e-mail: *RiHutter@idsc.mavt.ethz.ch*

Prof. Christopher Onder, DEng. – ETH, Swiss Federal Institute of Technology, Zürich, Switzerland.
e-mail: *Onder@idsc.mavt.ethz.ch*

Article citation info:
HEINRICH, S., HIEN, M., KNITTEL, T., MUGGLI, J. Novel thermal method for determining properties of compressed natural gas. *Combustion Engines*. 2019, **176(1)**, 54-60. DOI: 10.19206/CE-2019-107

Stephan HEINRICH
Markus HIEN
Thorsten KNITTEL
Josef MUGGLI

CE-2019-107

Novel thermal method for determining properties of compressed natural gas

The article describes a new method for obtaining fuel properties, derived from the thermal properties of natural gas fuel mixtures. By measuring the thermal conductivity and the dynamic response with the help of a heated Micro Electro Mechanical System (MEMS), input values for a mathematical correlation are obtained which predict the calorific value of the gas. In this paper the fundamentals of the theoretical gas properties, the sensor operation and the first results on a gas test bench are presented.

Key words: *calorific value, methane number, heat capacitance, temperature conductance, natural gas quality*

1. Introduction

The composition of compressed natural gas (CNG) varies strongly worldwide. Even across Europe the gas blends differ according to the gas source location. Additional to the impacts of its origin, the manufacturing process plays a role in the content of the hydrocarbons methane, ethane, propane and butane as well as the inert gases carbon monoxide and nitrogen, which are the main fractions of hydrocarbons in CNG. New fuel trends like bio-methane, power to gas (PtG) methane and hythane (blends of hydrogen and natural gas) can lead to a further diversification of the gaseous combustion media.

According to the big variances the quality of the natural gas variation, which can be classified with the calorific value (CV) and the methane number (MN). This issue is specific to natural gas and has a strong influence on the engine control optimization capability. For a diagnostic and anticipatory engine operation the methane number and calorific value can be relevant optimization parameter. If an automotive sensor which delivers CV and MN can be developed, then ignition timing can be adjusted to operate the engine close to the knock line. With the calorific value it is possible to optimize ignition angle and/or boost pressure. In addition, the calorific value can play an important role for achieving gas-only, mono-fuel-engines. A sensor signal, provided to the engine management system in the time frame of one second before engine on, would avoid rich mixture combustion and potential critical engine crank-up conditions, especially just after the gas refilling operation.

Existing ways of measuring the quality of the natural gas like calorimetry can´t be used, are too complex or do not work in the relevant temperature and pressure range. A novel method with a simple microsystem chip is the starting point for a concept study to get information from natural gas blends by measuring thermal properties. The so-derived thermal properties are the inputs for a mathematical correlation model which should predict the calorific value and methane number.

2. Natural gas variety

Defining the quality of fuels, oils and other complex fluid mixtures is a difficult topic. The presence and variation of single compounds affect the properties of the fuel in many ways. Compressed natural gas blends can contain hydrocarbons, inert gases, sulfur components, hydrogen, water and odour gases. Of course, methane is the dominant fraction. The hydrocarbons ethane, propane and butane play a role in the percentage range. The inert gases carbon dioxide and nitrogen with a possible content of several percent have also a significant impact. An example how the content of the main components can vary over different locations is given in [7].

Table 1. Main components of natural gas blends at different locations [7]

Gas	Natural Gasoline H [mol%]			Natural Gasoline L [mol%]	
	Russia	North Sea	Denmark	Holland	Germany
CH_4	96.96	88.71	90.07	84.64	86.46
C_2H_6	1.37	6.93	5.68	3.56	1.06
C_3H_6	0.45	1.25	2.19	0.61	0.11
C_4H_{10}	0.015	0.28	0.90	0.19	0.03
larger HCs	0.03	0.07	0.28	0.13	0.01
N_2	0.86	0.82	0.28	10.21	10.24
CO_2	0.18	1.94	0.60	1.68	2.08

Some other gases like hydrogen, oxygen and long chained hydrocarbons are in a typical range of a few percent or less than 1% in concentration. For the generic study of a thermal quality sensor this small fractions are neglected so far.

Table 2. Selected gas species and relevant measurement ranges

Gas compound	Minimum range [vol%]	Maximum range [vol%]
Methane CH_4	70	100
Ethane C_2H_6	0	20
Propane C_3H_8	0	15
Butane C_4H_{10}	0	10
Nitrogen N_2	0	30
Carbondioxid CO_2	0	20

To cover the worldwide variations of CNG, detecting the variability at fuel refilling, providing an instantaneous measurement before engine start, adjusting the efficiency of

combustion and controlling knock resistance the calorific value and the methane number are the desired values for characterization. The target for the sensor concept proof is to measure MN and CV as accurate as possible.

In the quality sensor evaluation of work package 5 the investigations are restricted to gases which are in the percentage range. The physical properties used for the sensing of the gas mixture are dominated by the main fractions. A limitation on six CNG gas fractions with methane, ethane, propane, pentane, carbon dioxide and nitrogen seem to reflect the nature of the gas in an appropriate way. They allow adjusting a continuous composition for detailed investigations.

3. Lower calorific value and methane number

The lower calorific value (LCV) describes the whole redundant energy when a volume of gaseous fuels is completely burnt and water vapor leaves with the combustion products without being condensed. Because many gas burning applications cannot make use of the heat content of the water vapor, the lower calorific value is the more interesting one. It is essential for driving range estimation based on the calculated tank filling level [2].

$$\mathrm{LCV_m} = \sum_{n} \mathrm{x_n} \cdot \mathrm{LCV_{m,n}} \tag{1}$$

The methane number (MN) is an indicator for the knocking resistance of gaseous fuels, similar to the octane number of gasoline vehicles. The MN of a gaseous mixture is defined as the methane volume percentage of a pure combination of only methane and hydrogen, which has the same knocking resistance. The methane number was determined experimentally on test engines at AVL in the seventies and now standardized in DIN51624 [1].

4. Thermal properties as basis for gas quality prediction

It is difficult to get e.g. the calorific value without combusting the gas and simultaniously measureing the heat release. A direct measurement is not possible in a simple way. The novel approach is now to measure the thermal conductivity and specific heat capacity with a micromachined and miniaturized sensor. The typical specific thermal properties of each single gas in a CNG blend allow to destinguish concentrations in mixtures by measuring and tracking the thermal properties. In combination with a mathematic correlation model the prediction of gas quality properties is possible. As signal for the calculation input the thermal conductivity and the specific heat capacity is used.

Both physical values are temperature dependent. With a dedicated operation strategy of the MEMS device this temprature dependency can be exploited by measuring at different test gas temperatures. As a consequence an additional input parameter for the correlation modeling can be adapted. This widening of the input parameter is the key for a more detailed and accurate modeling taking the temperature dependencies into consideration.

4.1. Thermal conductivity of a single gas

Thermal conduction is the transfer of heat from hotter to cooler parts of a medium resulting in temperature equilibrium. Taking gaseous fluids into consideration, the thermal conductivity is the energy transfer between gas molecules from higher to ones with lower energy. The basic law of thermal conductivity is the Fourier Law which states that the heat flux density is proportional to the temperature gradient T in an isotropic medium [3]:

$$\mathrm{q} = \frac{\mathrm{dQ}}{\mathrm{A} * \mathrm{dt}} = -\lambda \frac{\mathrm{dT}}{\mathrm{dz}} \tag{2}$$

The proportional factor λ is the thermal conductivity. The minus indicates that the temperature decreases in the direction of the heat transfer [7]. The absolute temperature has an impact on the lambda value. An approximation for the temperature dependency of the thermal conductivity is described in the VDI Wäremeatlas [8] with an 4th polynomial equation and the gas specific coefficient A, B, C, D and E.

$$\frac{\lambda}{\mathrm{W/K \cdot m}} = \mathrm{A} + \mathrm{B}\frac{\mathrm{T}}{\mathrm{K}} + \mathrm{C}\left(\frac{\mathrm{T}}{\mathrm{K}}\right)^2 + \mathrm{D}\left(\frac{\mathrm{T}}{\mathrm{K}}\right)^3 + \mathrm{E}\left(\frac{\mathrm{T}}{\mathrm{K}}\right)^4 \tag{3}$$

The characteristics over the application temperature range for the CNG relevant gases is displayed in Fig. 1.

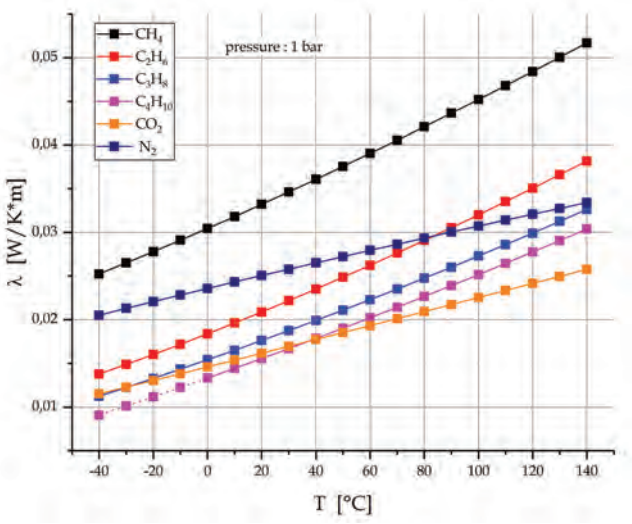

Fig. 1. Temperature dependency of the thermal conductivity λ for different pure gases

The overview shows the value of λ differs for each pure gas species at a dedicated temperature as well as the slope, taking the temperature influence into count.

4.2. Specific heat capacity at constant pressure for pure gases

The heat capacity of each medium tells us how much heat is required to raise a certain amount of it by one degree. For gases we can define a molar heat capacity, which is the heat required to increase the temperature of 1 mole of the gas by 1 K.

$$\mathrm{Q} = \mathrm{nC} \cdot \Delta\mathrm{T} \tag{4}$$

The value of the heat capacity depends on, wheater the heat is added at constant volume or constant pressure. Therefore, the specific heat capacity Cp at constant pressure is:

$$Cp = \frac{\Delta Q}{\Delta T} \tag{5}$$

Where accoding to the first law of thermodynamics some of the heat energy is doing work due to constant pressure [5]. The value for Cp is tempeature dependent. Like before described in the thermal conductivity section, the characteristics can be similar expressed by a interpolation equation with the coeffcients A, B, C, D and E [8].

$$\frac{c_p}{J/kg \cdot K} = A + B\frac{T}{K} + C\left(\frac{T}{K}\right)^2 + D\left(\frac{T}{K}\right)^3 + \frac{E}{(T/K)^2} \tag{6}$$

One can see in Fig. 2 the specific heat capacity of the inert gases carbon dioxide and nitrogen in comparsion to the main hydrocarbon fractions in the relevant temperature range.

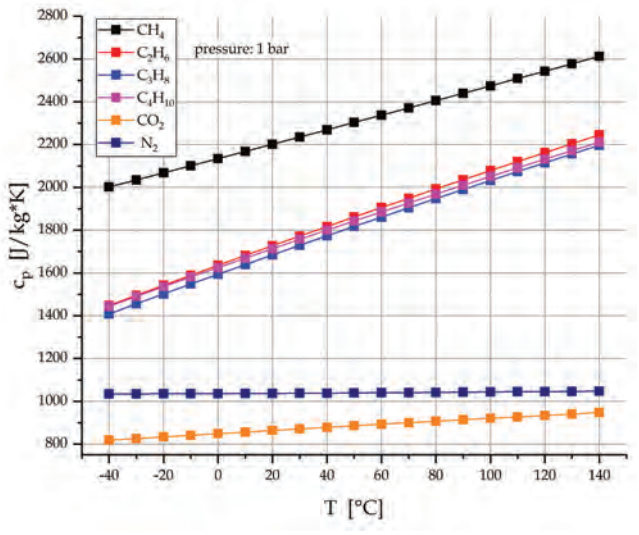

Fig. 2. Heat capacity at constant pressure for different gases and temperatures

The following content, can be derived from the data shown in Fig. 4. Methan has by far the highest heat capacity. The other hydrocarbons ethane, propane and butane are almost identical in value and slope. For the inert gases nitrogen and carbon dioxide the specific heat capacity values are much lower and the progression over temperatue, is almost constant, especially for nitrogen.

4.2. Time dependent temperature distribution

Another physical relation which discribes the time dependent temperature distribution is the so called thermal diffusivity. The thermal conductivity λ, the coefficient of heat capacity c and the density ρ of a substance can be summarized in absence of internal heat sources by the differential equation of thermal conductivity [6]:

$$\frac{\partial T}{\partial \tau} = \frac{\lambda}{\rho c} \cdot \nabla^2 \cdot T \tag{7}$$

$$\nabla^2 \cdot T = \frac{\partial^2 \cdot T}{\partial \cdot x^2} + \frac{\partial^2 \cdot T}{\partial \cdot y^2} + \frac{\partial^2 \cdot T}{\partial \cdot z^2} \tag{8}$$

With ∇ the Laplacian operator, τ the time, and x, y, z the cartesian coordinates. Wheras the group k = (λ/ρc) is known as thermal diffusivity. It characterizes the velocity of propagation of isothermal surfaces in a body.

In the study the specific heat capacity is taken as indicator or so to say deceicive propertie for the time dependent temperature change. The use of the thermal diffusivity would also be possible, but the operation of the sensor described later on is in contradiction to the absence of an internal heat source.

Although the pure specific heat capacity does not fully reflect the physical circumstances, the results achieved are sufficent.

4.2. Thermal properties of gas mixtures

The thermal properties of gas mixtures can be summarized by the properties of the single gases. The following two formulas are used for the theoretical calculations and the comparsion with the measurements achieved.

For the thermal conductivity the mixing equations of Wassiljeva, Ason and Saxena can be used. The indice i and j representing components according to the single gase. In the equation x stands for the quantity and F is an own gas specific summary, considering the viscosity gas and molare weight of the gas [4].

$$\lambda^{Gem} = \sum_i \frac{x_i \cdot \lambda_i}{\sum_j x_j \cdot F_{ij}} \tag{9}$$

For the calculation of the specfic heat capacity of an ideal gas only the massfraction of the heat capcity are summed up [8].

$$c_{p,Gem} = \sum_i x_i \cdot c_{p,i} \tag{10}$$

For the calculation of the specfic heat capacity of an ideal gas only the mass fraction of the heat capacity are summed up. These two mixing formulas are used for theoretical approximations.

5. Sensor properties

Typical sensor arrangenments for measuring the thermal properties of gases are micromachined membranes. They have the required sensitivity to destinguish small changes of e.g. the thermal conductivity. Typical for this membranes are silicon nitride processed layers, made in bulk micromachining technology to achieve the well thermally isolated measurement with a measurement spot on top of the membrane. An even more advanced setup shown in Fig. 3 is used for the CNG based measurement.

In the considered implemention the membane is not a fully closed one, etched from the backside. In the used device it is in fact a membrane layer processed in surface micromachined technology on top of the semiconducter which is opened due to an underetching process on two sides. A suspended bridge with heater structure on top remains as sensitive device. This allowes an even better

thermal isolation of the gas sensitive bridge from the solid state silicon substrate. The area which is responsible for the heat transfer is in the range of ~ 1 mm². A specific meander arrangement of the nickel-chrome heater provides a homogenous temperature distribution on the heated bridge. This tiny microstructure arrangement has a response of a few microseconds when heated up.

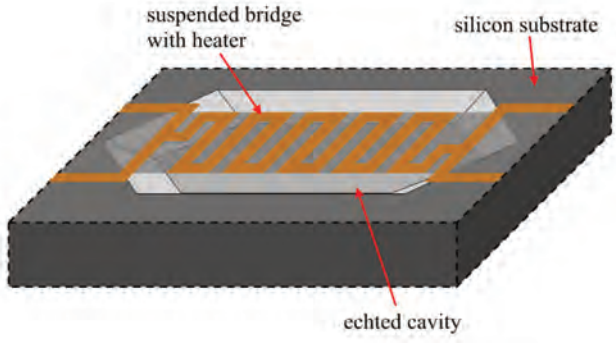

Fig. 3. Simplified setup of thermal MEMS

5.1. Sensor operation

The electrical heat source realized with nickel-chrome has a distinct temperature behavior of his electrical resistance. By heating up the structure with current in the submilliampere range, the corresponding temperature rise is several degrees in combination with a resistance change of several ~10%. A fast and highly accurate voltage measurement during an applied constant heating current pulse allows to derive the resistance at any time. The evaluation of the dynamic behavior when applying current pulses is used to get a feedback from the thermal properties of the gases tested.

In Figure 4a the heater current pulse applied is shown. A swichtable precision current source is used to operate the heater. With the current amplitude and the pulse time a fixed amount of energy is feeded into the microsystem. The reaction of the temperature deduced by the resistance measurement is visualized by Fig. 4b. Depending on the thermal conductance of the gas as well as the specific heat transfer, different end values for the temperature respective rise time can be seen. The temperature rise is represented by ΔT and the rise time by τ. 4c and 4d illustrate how this different transient reactions are reached. With the assumpten that in both test gas cases the same energy is processed, the gas with higher thermal conductivity reaches a lower level of maximum temperature due to the better conductance of the heat in the gas. Vice versa, the "isolating" gas is responsible that the heat is "blocked" and the temperature amplitude rises. Analog to the thermal conductivity the specific heat capacity has a similar effect. The amount of heat transfered with the pulse in the measurement structure per time unit is identical. For a gas with higher specific heat capacity the rise in temperature is slower than for a gas with lower one. Normalizing the rise time to the end evalue of the temperature plateau enables to conclude on Cp of the gas mixture.

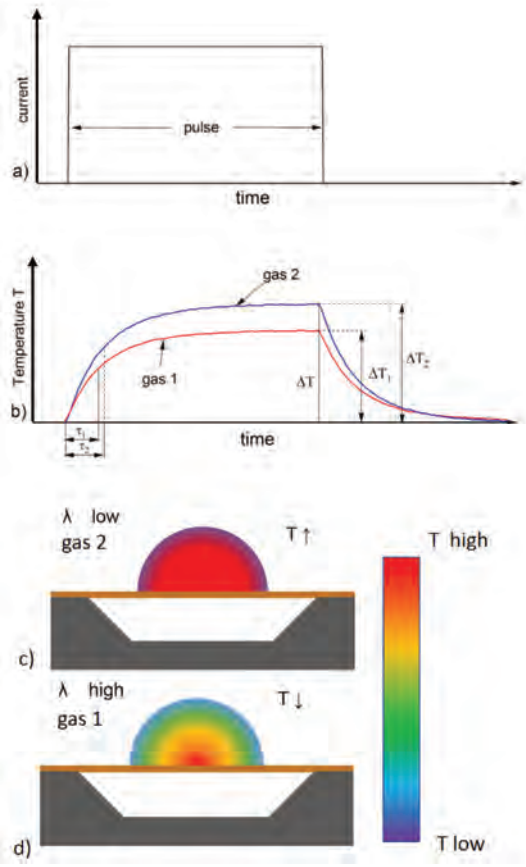

Fig. 4. a) current pulse for heating; b) temperature transient for two different gas species; temperature distribution on top of bridge structure for c) gas 1 and d) gas 2

The heat pulse is chosen to generate only a slight temperature reaction to determine the thermal properties at the tested gas temperature. A second sequence was developed to raise the bridge structure to a constant overtemperature. This overtemperature is heating up the surrounding gas molecules. When the applied heating pulse lasts enough, a small area with permanent higher gas temperature is created. With a third measurement pulse, similar to the first one, the thermal properties of the overheated gas can be derived with the difference that they represent the gas properties at overtemperature with sufficent accuracy. Thermal data for different gas temperatures can be collected with this methode.

5.2. Correlation model

Of course, the calorific values can be obtained with a caloric measurement device by gas combustion and measuring the heat release. This is not possible with a simple sensor device at automotive environmental conditions. Besides of optical spectroscopy, a multi-parameter correlation method may be expedient. By measuring other properties of the relevant gas and the use of statistical means a prediction of a target value can be obtained. In general, these properties don not necessarily have to be linked to the parameter of interest, like in our case the thermal properties to the calorific value. If the measurement value gives an adequate gas component distinction, a correlation algorithm

can achieve good results with sufficient accuracy. The optimization of the algorithm needs a defined set of gases.

Figure 5 shows an overview how the signal flow is handled to get a prediction of combustion relevant gas parameters. Out of the main fractions of the CNG the theoretical values for the thermal conductivity and the specific heat capacity are calculated over temperature. A set of four input parameters was taken for dedicated CNG gas blends and applied to numerous equation types. The input parameters were joined in a virtual value SCV (sensor correlated value) which is a function of λ(T1), λ(T2), cp(T1) and cp(T2), where T1 represents the gas temperature and T2 a fixed gas overtemperature. The mathematic correlation with the smallest average deviation for LCV prediction was taken for further steps. In analogy to the LCV the correlation can be done with the methane number or the stoichiometric required Air Fuel Ratio for combustion.

In the following Figure 5 the SCV as a function of λ(T1), λ(T2), cp(T1) and cp(T2) is shown. The good correlation result can be fitted with a quadratic equation. The error between the calculated values and the fit of the single gas is shown in the deviation chart. The deviation is normalized to the LCV of methane. For the investigated gases the theoretically achievable accuracy is better than ±2%.

Like described in the previous section the sensor measures a rise time and a temperature change, derived from the heater resistance, representing the values of λ and cp. The substitution of the values with the measured values of ΔT and τ and some small modifications in the equation parameters lead to the following result, when tested with the same gas blends.

With a slight modification of the equation and the inserted values of ΔT1, ΔT2, τ1 and τ2 the LCV prediction ends up in a similar good result, shown in Fig. 9. A linear regression of LCV based on SCV(ΔT, τ) is possible. The normalized deviation stayed in an error range of 2% for the tested gas blends.

6. Test bench results

After finding a promising correlation approach and static pre testing, the quality of the correlation result was validated with a dynamic blend testing. Hydrocarbon/inert gas blends, mixed by flow controllers were used at a the test bench. Successively, five identical sensor samples performed an automated test cycle over several minutes. After testing each of the nine test gases, a purge cycle with pure nitrogen and low flow was applied to get defined starting conditions. The result can be seen in Fig. 6.

It can be seen, that the gas variations caused the same reaction on the calibrated sensor devices with a small part to part variation. The single raw data value showed a noise level of ~ 1.5%. This value can be reduced significant by averaging the sensor output signals. The sensors also reacted in the same way when changing from gas to purge sequence. For example, gas blend no. 1 lead instantaneously to a steady state, while gas blend no. 7 has a delayed mixing, with a time constant of several ~10 seconds. The calculated deviation was in the range of ±4% without the averaging measure. This error is higher than the pure static measurement, but still in an acceptable range.

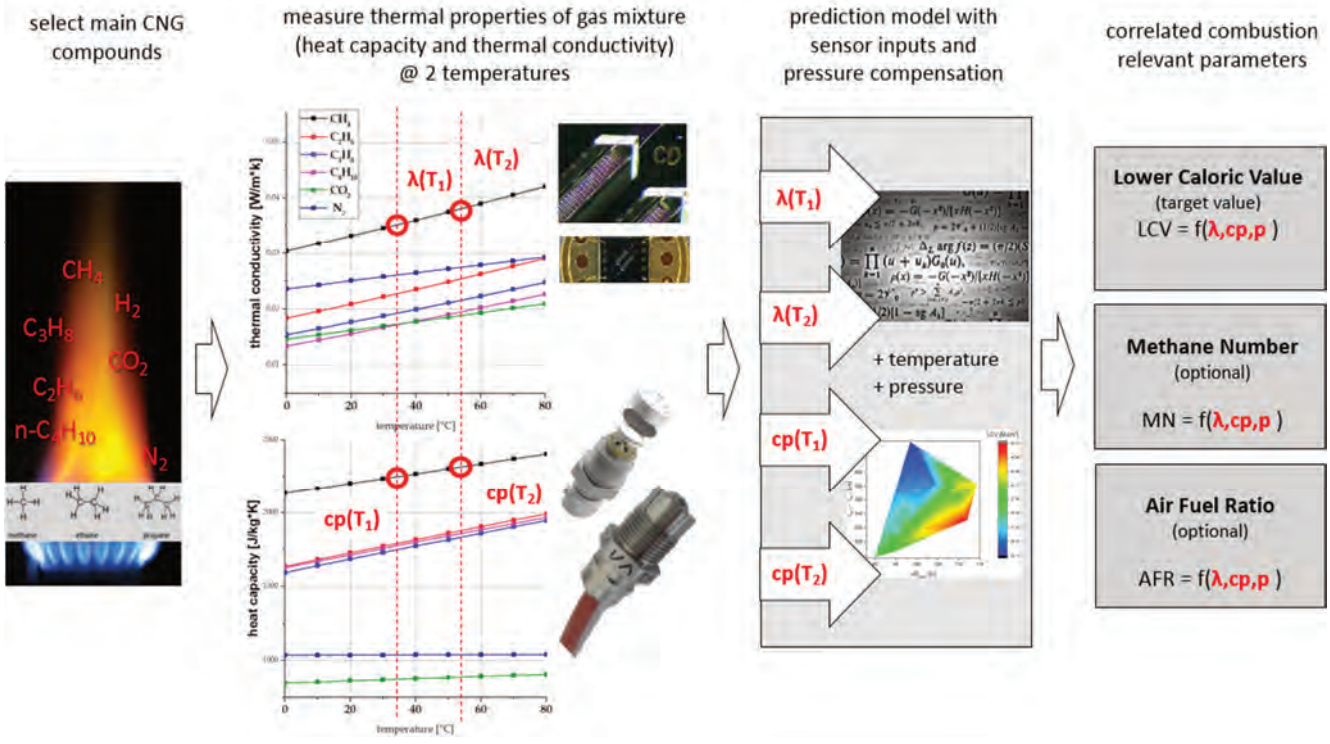

Fig. 4. Concept of the signal propagation of a multiple input correlation setup to predict quality values for CNG

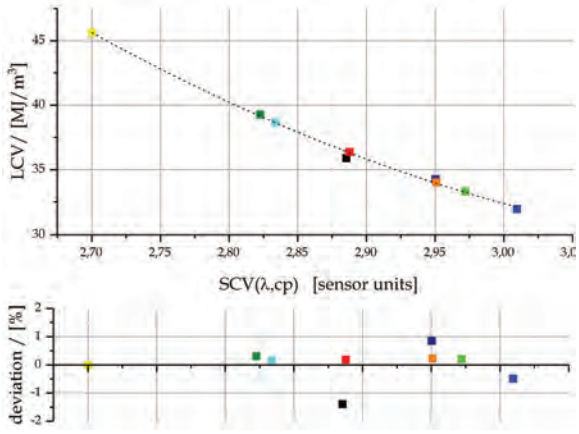

Gas No.	Gas compound [vol%]					
	CH_4	C_2H_6	C_3H_8	C_4H_{10}	CO_2	N_2
1	100	0	0	0	0	0
2	71	1	11	0	0	17
3	83	4	1	0	1	11
4	81	3	1	0	1	14
5	91	6	1	1	1	0
6	79	9	3	7	2	0
7	84	3	1	1	1	10
8	90	6	2	1	1	0
9	85	4	1	0	0	10

Fig. 5. Result of the theoretical correlation for the lower calorific value over a set of gas blends

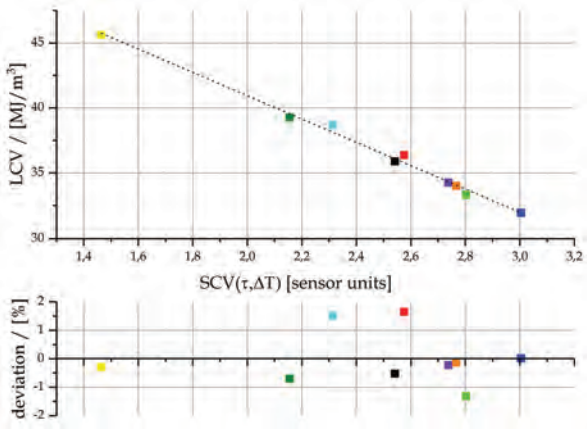

Gas No.	Gas compound [vol%]					
	CH_4	C_2H_6	C_3H_8	C_4H_{10}	CO_2	N_2
1	100	0	0	0	0	0
2	71	1	11	0	0	17
3	83	4	1	0	1	11
4	81	3	1	0	1	14
5	91	6	1	1	1	0
6	79	9	3	7	2	0
7	84	3	1	1	1	10
8	90	6	2	1	1	0
9	85	4	1	0	0	10

Fig. 6. Result of the theoretical correlation for the lower calorific value over a set of gas blends

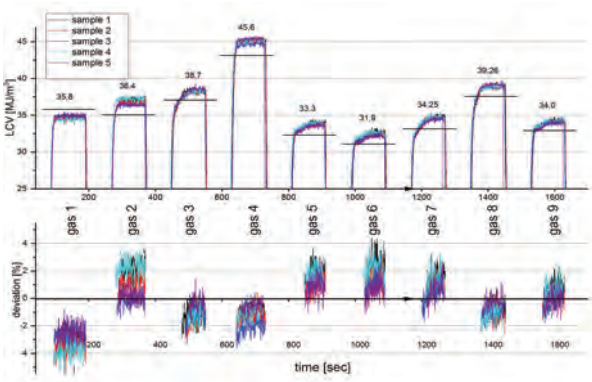

Gas	Gas blends [vol%]								
	1	2	3	4	5	6	7	8	9
CH_4	100	71	91	79	83	81	84	90	85
C_2H_6	0	1	6	9	4	3	3	6	4
C_3H_8	0	11	1	3	1	1	1	2	1
C_4H_{10}	0	0	1	7	0	0	1	1	0
CO_2	0	0	1	2	1	1	1	1	0
N_2	0	17	0	0	11	14	10	0	10
T = 23°C, P = 1 bar abs.									

Fig. 7. Testing of synthetic gas blends to predict the lower calorific value

7. Conclusion

Measuring the quality of CNG gas is a difficult topic. Direct measurements are not possible due to environmental limitations or are simply to complex and costly to be able entering the automotive market. Therefore a concept study was done with a correlative method based on the thermal properties of the typical single gas components of CNG. The statistical investigations were done with a novel MEMS chip based on a thermal isolated bridge structure. Before a dedicated test cycle was developed to measure the thermal conductance and the specific heat capacity a set of equations was tried and optimised. Parameter for the optimisation was the minimum error level on the lower calorific value for the entirety of defined test blend set.

After fixing a set of equations a comparison of the theoretical calculated accuracy levels was done with the corresponding test bench measurement. The basic investigation showed for the calculated as for the measured test blends similar accuracy levels of less than 2%.

To have a first overview about the principle robustness and the performance spread over different samples a test sequence with nine test blends at low flow was done. A fluctuation on the signal could be observed, which can be optimised by signal filtering and averaging. Without this optimisation the error was in the range of 4%.

For sure the measurement has some weaknesses compared to a colorimeter. However the low effort for electronic and the affordable miniaturized sensing element allow to get a solution which could fulfill the requirements of an automotive application. The first investigations have shown that a calorific value prediction with an accuracy level in the lower percentage range is possible. This information before engine start could be sufficient for a defined and save engine start in a monovalent CNG car.

Bibliography

[1] CARTELLIERI, W., PFEIFER, U. Forschungsberichte Verbrennungskraftmaschinen – Erweiterung der Energieerzeugung durch Kraftgase Teil 3 – Untersuchungen zur Übertragbarkeit der am CFR-Motor gefundenen Ergebnisse auf andere Motoren – Gültigkeitsbereich der Methanzahl, 1971.

[2] CERBE, G., LENDT, B. *Grundlagen der Gastechnik*, München: Hanser. 2017, **68**.

[3] CZICHOS, H. Die Grundlagen der Ingenieurwissenschaften, *Springer* Berlin Heidelberg. 2000, B83.

[4] MASON, E.A., SAXENA, S.C. Approximate Formula for the Thermal Conductivity of Gas Mixtures. *The Physics of Fluids*. 1958, 361-369.

[5] MESCHEDE, D., Gerthsen Physik, *Springer* Berlin Heidelberg, 2015.

[6] POLEZHAEV, Y.V, Thermal Conductivity in: A-Z Guide to Thermodynamics. *Heat and Mass Transfer and Fluids Engineering*. DOI:10.1615/AtoZ.t.thermal_conductivity.

[7] VAN BASSHUYSEN, R. Erdgas und erneuerbares Methan für den Fahrzeugantrieb. *Springer* Fachmedien Wiesbaden, 2015, **70**.

[8] Verein Deutscher Ingenieure VDI-Gesellschaft and Verfahrenstechnik und Chemieingenieurwesen (GVC), VDI-Wärmeatlas, *Springer* Berlin Heidelberg, 2006, Da16, Da17, Da25, DOI:10.1007/978-3-540-32218-4.

Stephan Heinrich, Dipl. Ing. (FH) – Electrical Engineering and Microsystem Technology, Continental Automotive GmbH.
e-mail: *Stephan.Heinrich@continental-corporation.com*

Marcus Hein, DEng. – Mechatronics, Continental Automotive GmbH.
e-mail: *Markus.Hien@continental-automotive.com*

Thorsten Knittel, Dr. Ing. Dipl. Phys. – Technology Souct, Continental Automotive GmbH.
e-mail: *Thorsten.Knittel@continental-automotive.com*

Josef Muggli, B.Sc. (FH) – Sensor and Analytics, Continental Automotive GmbH.
e-mail: *Josef.2.Muggli@continental-corporation.com*

Article citation info:
BOLLA, M., SHAPIRO, E., KOTZAGIANNI, M. et al. Numerical study of fuel and turbulence distributions in an automotive-sized scavenged pre-chamber. *Combustion Engines*. 2019, **176**(1), 61-67. DOI: 10.19206/CE-2019-108

Michele BOLLA
Evgeniy SHAPIRO
Maria KOTZAGIANNI
Panagiotis KYRTATOS
Nick TINEY
Konstantinos BOULOUCHOS

CE-2019-108

Numerical study of fuel and turbulence distributions in an automotive-sized scavenged pre-chamber

This article presents a numerical study of the fuel and turbulence distributions in a pre-chamber at spark-time. The study has been conducted in the framework of the H2020 Gas-On project, dealing with the development of a lean-burn concept for an automotive-sized gas engine equipped with a scavenged pre-chamber. The test case considered studies a 7-hole pre-chamber with circumferentially-tilted orifices mounted on the cylinder head of a rapid compression-expansion machine (RCEM), consistent with the experimental test rig installed at ETH Zurich. An accurate description of turbulence and fuel distributions are key quantities determining the early flame development within the pre-chamber. Both quantities have an influence on the overall combustion characteristics and therefore on the engine performance. For this purpose, computational fluid dynamics (CFD) is employed to complement experimental investigations in terms of data completeness. The performance of the Reynolds-averaged Navier-Stokes (RANS)-based turbulence model is compared with large-eddy simulation (LES) through ensemble averaging of multiple LES realizations, in which the fuel injection rate evolution into the pre-chamber has been perturbed. Overall, RANS results show that the distributions of the turbulent kinetic energy and fuel concentration at spark-time agree well with the LES ensemble-averaged counterparts. This constitutes a prerequisite in view of the combustion phase and the accuracy reported provides further confidence in this regard.

Key words: *scavenged pre-chamber, RANS, LES, mixture formation*

1. Introduction

Efforts to reduce CO_2 emissions from internal combustion engines have led to the use of natural gas as a fuel in lean-burn spark ignition engines. A widely used technology in lean-burn gas engines is pre-chamber ignition systems, in which the external ignition source is located in a separate small volume, connected to the main chamber via small orifices [6, 17]. This setup allows the design for favorable ignition conditions near the ignition source, which result in fast and repeatable early flame propagation. The use of pre-chamber systems in engines allows the combustion of very lean/diluted mixtures, resulting in higher efficiencies and lower NO_x emissions.

Research in the field of pre-chamber combustion has been extensive in the past years, aiming to increase our understanding and allow the practical application of such systems.

Computational fluid dynamics (CFD) of pre-chamber combustion system has been increasingly employed in the last decade to complement experimental testing. Most of the work has been focused on RANS models (e.g. [2, 5, 8, 10, 16, 21–23]) and some LES studies start to appear (e.g. [1, 4, 7, 18, 19]). A large variety of pre-chamber geometries have been considered, from stylized shapes with single-orifice nozzles up to close-to-production complex designs with multiple orifices. It is well known that the spatial distribution of the fuel concentration at the time of sparking plays a pivotal role on the flame development within the pre-chamber in gas engines equipped with a scavenged pre-chamber. The combustion within the pre-chamber is in turn a determining factor for the behaviour of the turbulent jets exiting the pre-chamber and therefore this influences the combustion of the premixed charge in the main chamber.

A detailed assessment of the turbulence and fuel distributions within the pre-chamber is a very challenging task; the main reason for this is twofold: First, spatial fuel distribution in real-geometry pre-chamber cannot be directly measured. Second, results of CFD simulation using a RANS approach for such a complex flow depend considerably on the choice of the turbulence model parameters, and results cannot be verified through experimental data. The approach employed in this paper is based on a so-called "numerical experiment", where simulation results from LES and RANS are compared in a consistent manner, in order to assess the RANS model performance.

The analysis is focused on the turbulence and fuel distributions at the time of ignition, in order to evaluate the RANS model performance in comparison to the LES, in view of the reactive phase.

The investigated pre-chamber shape was developed using CFD analysis with VECTIS CFD package within Horizon 2020 GasOn project. The project focusses on the reduction of emissions in natural gas passenger vehicle applications using scavenged pre-chamber technology to facilitate lean operation at high compression ratios.

Cold flow simulations have been selected as the focus of this publication in order to illustrate the approach to the verification of simulations based on a purely numerical study. Further development, application and validation of the computational methodology developed within the Horizon 2020 GasOn project to complex reacting flow simulations in pre-chamber and spark ignited engines is described in detail in [3, 9, 11, 13–15].

The remainder of the paper is structured as follows. The methodology section presents the rapid compression-expansion machine and pre-chamber characteristics, the LES and RANS setups, as well as the fuel injection strategy. In the results section, the results of the RANS turbulence model are compared to multi-cycle averaged LES in

terms of fuel and turbulence distribution within the pre-chamber. The paper closes with conclusions.

2. Methodology

2.1. Rapid Compression-Expansion Machine (RCEM)

The current study was performed in a Rapid Compression Expansion Machine (RCEM). The RCEM operates in a single cycle mode (compression-expansion) and combines excellent optical access with high flexibility in independently changing parameters, such as mixture composition, start of ignition, initial chamber conditions, etc. The RCEM employs a freely floating piston with an electrically controlled and pneumatically and hydraulically actuated driving system. A schematic of the RCEM, showing the most important components, is shown in Fig. 1. The most important technical characteristics are summarized in Table 1, while further details can be found in [14].

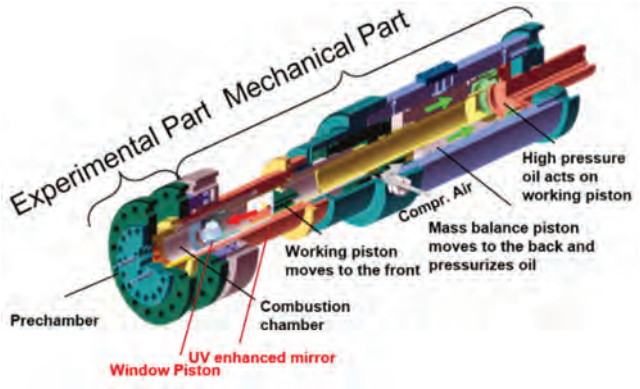

Fig. 1. Drawing of the RCEM, showing the most important components

The RCEM bore diameter is B = 84 mm and the quartz piston has a top hat bowl shape with diameter of 52 mm and depth of 2.2 mm. The piston stroke is adjustable (s = = 120–250 mm), and for this study was set at maximum. The temperature of the cylinder head and liner was set to 383 K using different heating elements and measured by 6 K-type thermocouples. Differently than in an engine, the filling process of the RCEM cylinder is occurring well before the compression and thus no turbulence exists in the main chamber at the beginning of the stroke.

The pre-chamber used is a prototype, and was positioned centrally and in a plane normal to the cylinder axis, similarly to its placement in an engine cylinder. The pre-chamber has 7 nozzles of 1.5 mm in diameter, which are placed at an angle to the cylinder axis in order to induce a swirling flow within the pre-chamber during compression.

Table 1. Technical characteristics of the Rapid Compression Expansion Machine

Parameter	Description
Bore (B)	84 mm
Stroke length (s)	Adjustable from 120–249 mm (here 249 mm)
Compression stroke (ε)	5–30
Loading pressure (P_{load})	1–3 bar (here 1.2 bar)
Max. cylinder pressure (P_{max})	up to 200 bar
Piston bowl	d_b = 52 mm, 2.2 mm depth (top hat)
Piston optical access	d_w = 52 mm, quartz window
Heating system	cylinder head and cylinder liner heating
Ignition	spark plug mounted inside the pre-chamber

2.2. LES model

OpenFOAM v4.x is adopted to solve the LES equations, which are implicitly filtered using the filter $\Delta = V_{LES}^{1/3}$. For turbulence the k-equation model [24] is used with OpenFOAM default constants. The measured piston position has been imposed in the simulation to ensure the correct compression stroke. Preliminary simulations of single realizations (with identical injection profile) have been performed with three different meshes with a homogeneous cell size within the pre-chamber of 0.125 mm, 0.100 mm and 0.080 mm, leading to approximately 1, 2 and 4 million cells within the pre-chamber. The choice of the LES minimum grid size has been assessed by comparing the temporal evolution of mean and rms of equivalence ratio and turbulence intensity within the pre-chamber for a single compression stroke (not shown here). Simulations with the finer mesh were observed to provide slightly more small flow structures, however the overall flow patterns were found to be very similar between the cases. For this reason, multiple realizations are conducted with a 0.125 mm cell size.

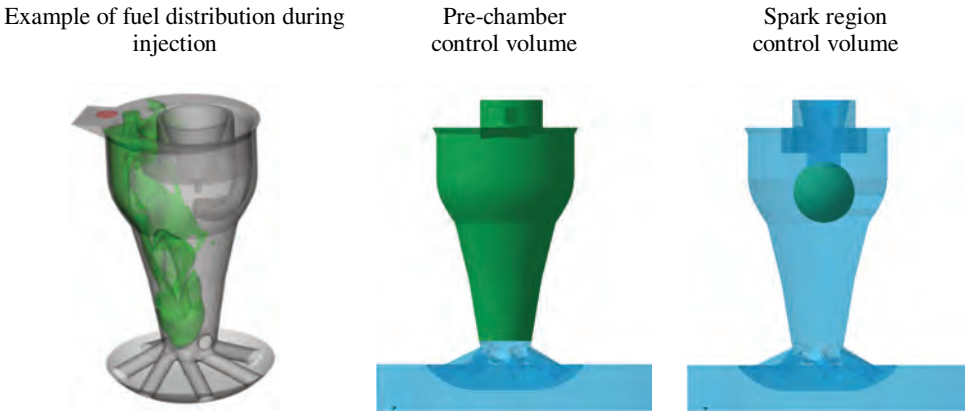

Fig. 2. Left: Example of fuel distribution from LES during the injection event. Centre: Definition of pre-chamber control volume drawn in green. Right: Definition of spark-plug region is a sphere with a 3 mm radius

2.3. RANS model

RANS simulations have been carried out with the commercial 3D-CFD solver Ricardo VECTIS [20]. RANS equations are solved using the finite volume method. The effects of turbulence are solved by means of Reynolds Averaged Navier-Stokes (RANS) methods, specifically the k-ε model time-scale bounded (TSB) model after [12]. As a baseline mesh, a homogeneous grid size of 0.18 mm has been used within the entire pre-chamber. The RANS grid size has been selected based on a convergence study with respect to the temporal evolution of fuel concentration and turbulence intensity within the pre-chamber. RANS simulations have been carried out with three meshes – referred as Coarse, Medium and Fine – with reference sizes of 0.180, 0.240 and 0.300 mm.

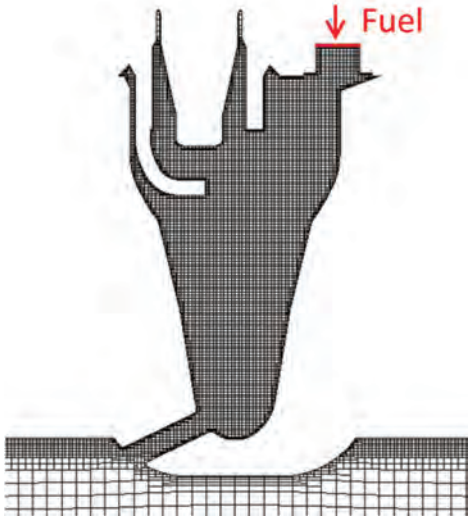

Fig. 3. RANS grid of 0.18 mm in the spark-plug symmetry plane

2.4. Fuel injection rate

Figure 4 shows the profiles of fuel injection rate into the pre-chamber employed for the RANS and LES simulations. In RANS a single profile is used whereas for LES 20 different injection rate profiles have been used to introduce a certain degree of perturbation, which as a result will slightly vary the turbulent flow field during the injection event. The total amount of fuel injected has been kept fixed at 1 mg, and the effective injection duration is 2.5 ms. The quantity of fuel injection corresponds to an on-average stoichiometric mixture within the pre-chamber at spark time for the test case considered and was found to provide a robust ignition source for the combustion in the main chamber during the experiments.

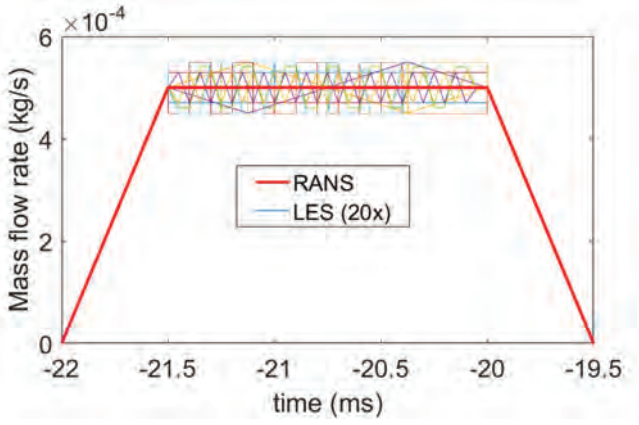

Fig. 4. Profile of fuel injection rate into the pre-chamber used in CFD. Total injected fuel is 1 mg. Single RANS profile in red and 20 different profiles for LES

3. Results

Figure 5 displays the temporal evolution of mean and variance of Lambda within the pre-chamber volume (top row) and within the 3 mm radius sphere around the spark-plug (lower row). The time is referred as time after top dead centre. The nominal spark time is –3 ms and is demarked with the red vertical line, whereas the blue vertical line at –22 ms represents the start of fuel injection into the pre-chamber. RANS results are shown for the three meshes (Coarse, Medium and Fine) and are compared with the LES mean (red line) arising from averaging the 20 LES realizations.

The mean value of lambda within the pre-chamber (Fig. 5 upper left) before the start of injection (–22 ms) into the pre-chamber is 2 and corresponds to the main chamber background lambda. During the injection the value of lambda is reduced drastically and shows a minimal value of around 0.3 at the end of injection. Later lambda shows an almost linear increase until top dead centre as a result of the piston motion that induces a flow of lean mixture from the main chamber into the pre-chamber. During the expansion stroke lambda is decreased again because of the fuel stratification in the pre-chamber, where the lean mixture present in the lower half of the pre-chamber leaves first the pre-chamber and this decreases the mean value of lambda. The comparison between RANS and LES is in good agreement and the same behaviour has been observed with all grid sizes.

The variance of lambda depicted in Fig. 5 upper right shows a different evolution. Before the start of injection, the variance is zero because lambda is homogeneous everywhere. During the injection there is a strong increase of the variance in accordance with the large fuel stratification. During the second half of the injection event the variance decreases because the injected fuel starts to be distributed in the entire pre-chamber. Later the variance increases again because the lean mixture entering through the orifices tends to remain the in lower part of the pre-chamber and it takes some time to mix with the richer mixture arising from the injection. The mixing rate and the lean mixture flow rate from the main chamber are counteracting effects influencing the degree of fuel stratification as quantified by the variance of lambda. At around –10 ms the variance of lambda shows a peak and at this point the effect of the two aforementioned phenomena are counterbalanced. During the second half of the compression (between –10 and 0 ms) the variance decreases prevalently due to mixing. The comparison between the models shows a reasonable agreement where all cases reproduce the same behaviour.

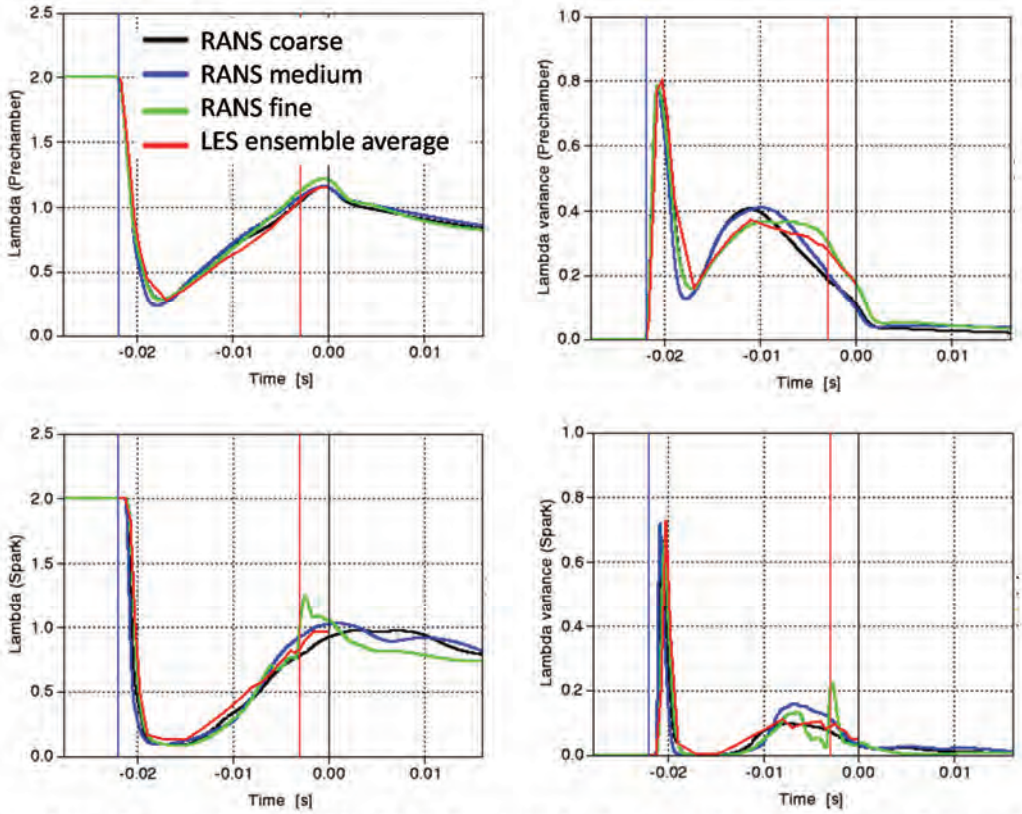

Fig. 5. Temporal evolution of mean and variance of Lambda in the pre-chamber (top row) and in the spark region (lower row). Coarse, Medium and Fine are the RANS grids and red is the LES ensemble average

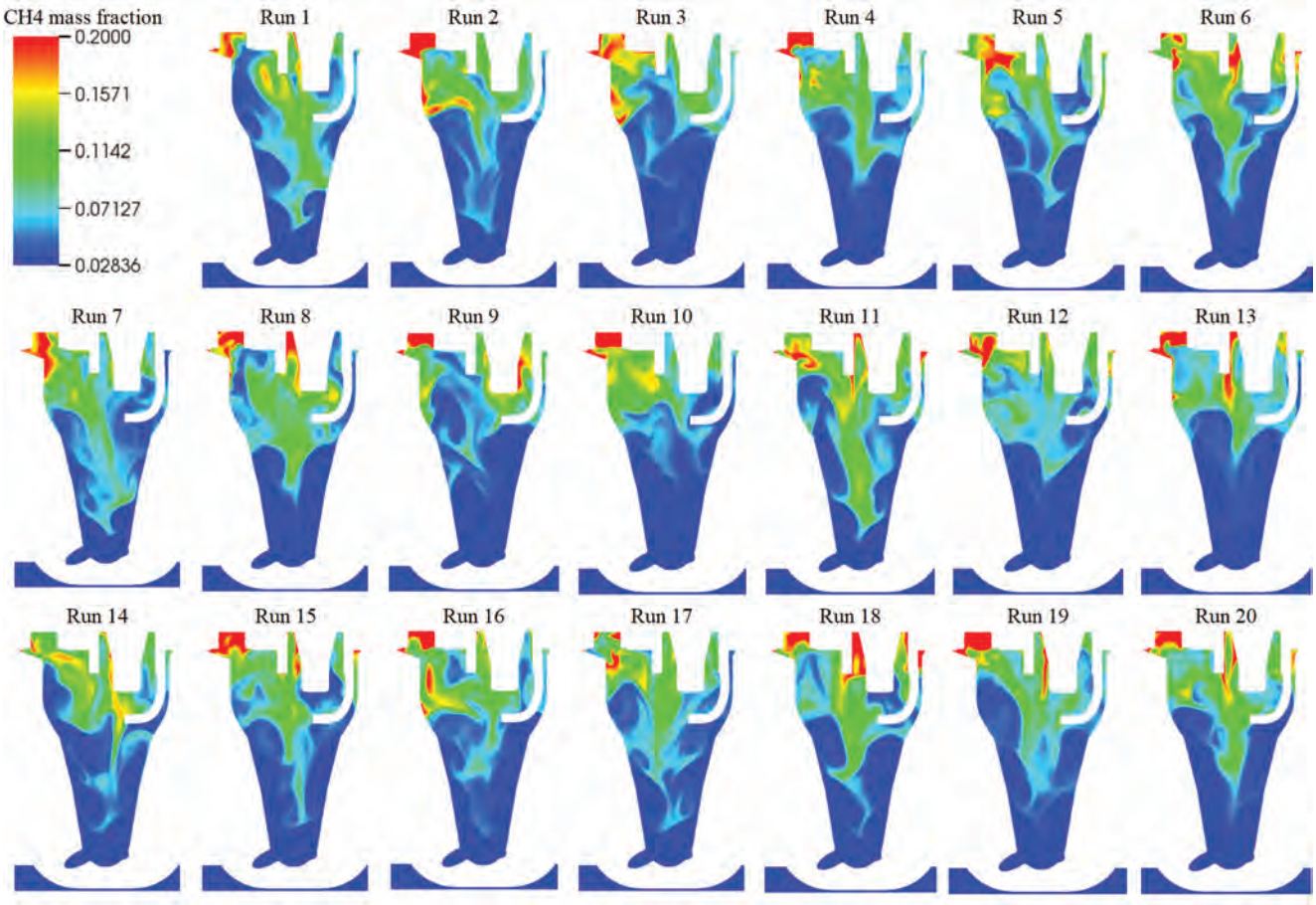

Fig. 6. Fuel mass fraction within the pre-chamber at spark time from 20 independent LES simulation realizations

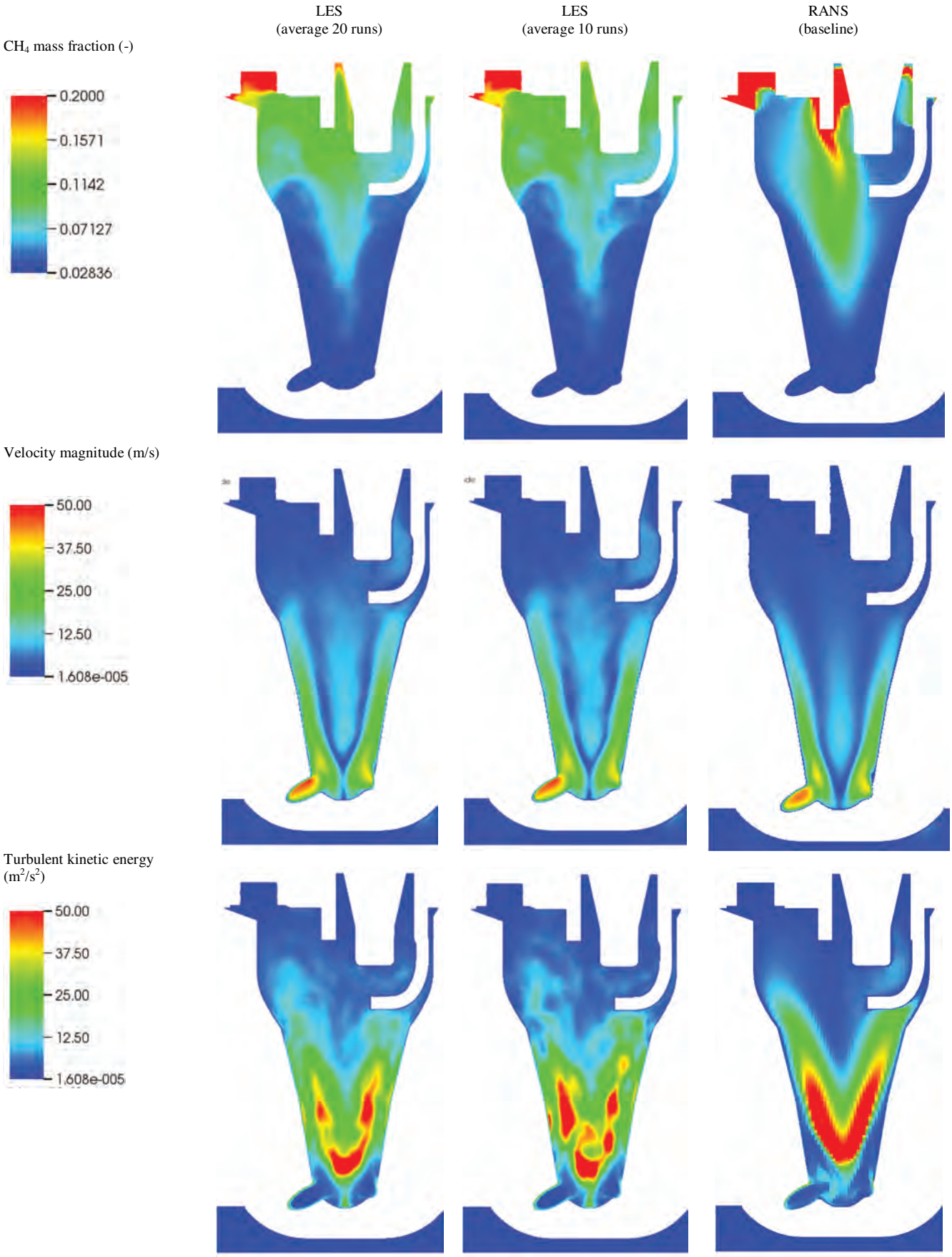

Fig. 7. Spatial distribution of fuel mass fraction (upper), velocity magnitude (middle) and turbulent kinetic energy (lower) at spark time (–3 ms). LES results have been averaged using 20 (left) and 10 (centre) runs and are compared with RANS (right)

The same analysis has been performed considering the region close to the spark-plug. This investigation was motivated by the fact that the early flame growth strongly depends on the local conditions around the spark-plug and this has an influence on the overall combustion behaviour and engine performance accordingly. It is important to note that the spark-plug control volume is much smaller than the one embedding the entire pre-chamber and therefore there it contains a considerably smaller number of cells. This is reflected in a noisier and spiky behaviour of the various lines since for some quantities the samples are not enough to guarantee a converged statistic. Nonetheless this doesn't prevent a qualitative assessment of the numerical methods employed. Overall, similar features as for the pre-chamber control volume are observed here, showing good performance of the RANS simulations.

Figure 6 portrays the fuel mass fraction distribution at spark time for the 20 single LES realizations, demonstrating the variability of the flow structures between runs. Note that the same colour scale has been applied for every subfigure. As expected, high fuel concentrations are encountered in the upper half of the pre-chamber because during the compression stroke the lean mixture from the main chamber enters the pre-chamber via the connecting orifices. The tangential orientation of these orifices generates a swirling flow and the fuel rich mixture is trapped in the centre of this helical vortex. Another observation is that there is a high fuel concentration at the deck of the pre-chamber that has not mixed completely. There are common features between the runs such as a vertical structure of fuel, but the location and concentration vary considerably between realizations. In the lower part of the pre-chamber the fuel concentration corresponds to the background lambda due to the filling process of the pre-chamber. Around the spark-plug there is some degree of variability and on average a richer mixture is present towards the radial centre of the pre-chamber. This means that the early flame generated from the spark is expected to propagate towards the centre and then downwards.

In order to perform a consistent comparison between LES and RANS, the solutions of the 20 LES simulations at spark time have been averaged as illustrated in Fig. 7. Three different quantities have been selected for this comparison, namely the fuel mass fraction (upper row), the velocity magnitude (middle row) and the turbulent kinetic energy (lower row). In order to understand how sensitive the statistical convergence of the LES results is, two different amounts of LES simulations have been employed to average the results (20 and 10 runs).

The number of runs taken to construct the average shows a weak dependence for the mean fuel mass fraction and velocity magnitude, whereas larger differences are observed for TKE because this is a quantity based on fluctuations of velocity and therefore needs more samples to achieve converged statistics. Nonetheless both with 10 and 20 samples the qualitative distribution of TKE is consistent, and with a larger number of realizations (e.g. 100) no major differences are expected, but rather a smoother shape as seen for the RANS solution.

The RANS results show a very good degree of agreement in terms of velocity and turbulence intensity as well as fuel concentration. This is a promising sign when applying the RANS model in the full engine setup because it builds some confidence on the appropriateness of the turbulence and fuel distribution within the pre-chamber. Based on this comparison the performance of the RANS model is considered as good.

4. Conclusions

This paper presents a numerical analysis of fuel concentration and turbulence distribution at spark time for an automotive-sized scavenged pre-chamber mounted at the head of a RCEM by means of RANS and LES turbulence models. The RANS model performance is assessed by a consistent comparison of RANS results with multi-cycle averaged LES results, for which a perturbation of the temporal injection profile of fuel into the pre-chamber has been introduced. Overall, RANS results show that the distributions of the turbulent kinetic energy and fuel concentration at spark-time agree well with the LES ensemble-averaged counterparts. This constitutes a prerequisite in view of the combustion phase and the accuracy reported provides further confidence in this regard.

Acknowledgements

This work has been supported by the Horizon 2020 GASON project, Grant agreement number 652816.

Bibliography

[1] ALLISON, P. et al. Pre-chamber ignition mechanism: experiments and simulations on turbulent jet flame structure. *Fuel*. 2018, **230**, 274-281.

[2] BISWAS, S., QIAO, L. A numerical investigation of ignition of ultra-lean premixed H_2/air mixtures by pre-chamber supersonic hot jet. *SAE International Journal of Engines*. 2017. 2017-01-9284, 2231-2247.

[3] BOLLA, M. et al. Numerical simulations of pre-chamber combustion in an optically accessible RCEM. *SAE Technical Paper* 2019-01-0224. 2019.

[4] BOLLA, M. et al. Numerical study of turbulence and fuel-air mixing within a scavenged pre-chamber using RANS and LES. *SAE Technical Paper* 2019-01-0198, 2019.

[5] CHINNATHAMBI, P., BUNCE, M., CRUFF, L. RANS based multidimensional modeling of an ultra-lean burn pre-chamber combustion system with auxiliary liquid gasoline injection. *SAE Technical Paper* 2015-01-0386. 2015.

[6] DALE, J.D., CHECKEL, M.D., SMY, P.R. Application of high energy ignition systems to engines. *Progress in Energy and Combustion Science*. 1997, **23**(5-6), 379-398.

[7] GHOLAMISHEERI, M., GIVLER, S., TOULSON, E. Large eddy simulation of a homogeneously charged turbulent jet ignition system. *International Journal of Engine Research*. 2017, 1468087417742834.

[8] GHOLAMISHEERI, M., WICHMAN, I.S., TOULSON, E. A study of the turbulent jet flow field in a methane fueled turbulent jet ignition (TJI) system. *Combustion and Flame*. 2017, **183**, 194-206.

[9] HERNÁNDEZ, I., et. al., Flame-wall interaction modelling for pre-chamber combustion in lean burn gas engines, *Pro-*

ceedings of 34th International CAE Conference and Exhibition. 2018, Vicenza, Italy.
[10] KOTZAGIANNI, M. et al. Experimental and computational investigations of prechamber jet ignition in a rapid compression expansion machine. *Tenth Mediterranean Combustion Symposium*. 2017.
[11] LUCAS, G., TALLU, G., WEIßNER, M., CFD-based development of an ignition chamber for a lean and highly efficient CNG combustion, *Proc. THIESEL 2018 Conference on Thermo- and Fluid Dynamic Processes in Direct Injection Engines*. 2018.
[12] PRZULJ, V. et al. The time scale bounded k-ε turbulence model and its assessment for automotive applications. In ICHMT digital library online. *Begel House Inc*. 2012.
[13] SHAPIRO, E. et al. Advanced ignition modelling for pre-chamber combustion in lean burn gas engines. *Proc. 4th International Conference on Ignition Systems for Gasoline Engines*. 2018, Berlin.
[14] SHAPIRO, E. et al. Experimental and numerical analysis of pre-chamber combustion systems for lean burn gas engines. *SAE Technical Paper* 2019-01-0260. 2019.
[15] TALLU, G. et al. 3D CFD modelling and simulation of spark ignition inclusive of turbulence effects and detailed chemical kinetics. *Proc. 3rd International Conference on Ignition Systems for Gasoline Engines*. 2016, Berlin.
[16] THELEN, B.C., TOULSON E. A computational study of the effects of spark location on the performance of a turbulent jet ignition system. *SAE Technical Paper*. 2016.
[17] TOULSON, E., SCHOCK, H.J., ATTARD, W.P. A review of pre-chamber initiated jet ignition combustion systems. 2010, *SAE International*.
[18] VALIDI, A., SCHOCK, H., JABERI, F. Turbulent jet ignition assisted combustion in a rapid compression machine. *Combustion and Flame*. 2017, **186**, 65-82.
[19] VAVRA, J. et al. Development of a pre-chamber ignition system for light duty truck engine. *SAE Technical Paper*. 2018.
[20] VECTIS CFD Release 2017.1 Theory Manual. December 2017.
[21] WANG, M. et al. A numerical study on the effects of the orifice geometry between pre-and main chamber for a natural gas engine. *SAE Technical Paper*. 2017.
[22] WANG, N. et al. The effect of in-cylinder temperature on the ignition initiation location of a pre-chamber generated hot turbulent jet. *SAE Technical Paper*. 2018.
[23] XU, G. et al. Characterization of combustion in a gas engine ignited using a small un-scavenged pre-chamber. *International Journal of Engine Research*. 2018, p. 1468087418798918.
[24] YOSHIZAWA, A. Statistical theory for compressible turbulent shear flows, with the application to subgrid modeling. *The Physics of Fluids*. 1986, **29**(7), 2152-2164.

Michele Bolla – ETH Zurich, Switzerland.
e-mail: *MBolla@lav.mavt.ethz.ch*

Evgeniy Shapiro – Ricardo, UK.
e-mail: *Evgeniy.Shapiro@ricardo.com*

Maria Kotzagianni – ETH Zurich, Switzerland.
e-mail: *Kotzagianni@lav.mavt.ethz.ch*

Panagiotis Kyrtatos – ETH Zurich & Vir2sense GmbH.
e-mail: *Kyrtatos@lav.mavt.ethz.ch*

Nick Tiney – Ricardo, Japan.
e-mail: *Nick.Tiney@ricardo.com*

Konstantinos Boulouchos – ETH Zurich, Switzerland.
e-mail: *Boulouchos@lav.mavt.ethz.ch*

The original letters by Rudolf Diesel

On December 7th 2018, during General Assembly of the Members of Polish Scientific Society of Combustion Engines held at the Faculty of Vehicles and Machines (SIMR) at Warsaw University of Technology, Professor Janusz Przastek D.Sc. Eng., donated to the Society two original letters by Rudolf Diesel from 1906 and 1907 written to the firm Brothers Sulzer in Winterthur-Switzerland.

Prof. J. Przastek received these incredibly interesting *cimelia* from the hands of one of the higher-ranking employees on the occasion of his stay in the Sulzer company. He was employed there as the specialist in the Four-Stroke engines Development Dept. in years 1990-1991.

Please, find the scans of both letters together with the translation of their content.

Letter 1
R. Diesel
Engineer

03056

Munich, the 15 September (19)06.
Maria Theresia Str(eet) 32
C. 6 *Phone 2811*
Telegramm: "Diesel Ingenieur München"

R 17 September

Mr.&Mr. Brothers Sulzer,
Winterthur

In the English translation our "Druckluftmachine" is more accurately named as in our German patent application, namely as Internal-Combustion-Compressed-Air Engine.

Also in the French translation upon suggestion of the Patent Attorney, I propose the following: Motours combines a Air Comprime et a combustion. I would like to allow myself the suggestion to make the input with the request of the possibility of replacement of the term "Druckluftmaschine" with the term "Druckluft-Verbrennungsmaschine".

It would not only sharpen the whole thing, but also bring consistency with our foreign patents. It would also be useful to make the same corrections in all foreign descriptions, and because the thing is new, you need to give it a new name.

Sincerely
Diesel

Letter 2
R. Diesel
Engineer

Munich, the 15 September (19)06.
Maria Theresia Str(eet) 32
C. 3 *Phone 2811*
Telegramm: "Diesel Ingenieur München"

Mr.&Mr. Brothers Sulzer,
Winterthur

Answer for (the letter) of the 1. March No. 12/2065/Rr.Alt.

Concerns Germany S. 19944

it would be useful if the other differences of opinion now patent litigations is also thrown into the negotiations.

I take great note of your messages in the above-mentioned matter.

As far as the display of the application is concerned, I would suggest to suspend the same until the pending affairs are done with Augsburg, which is likely to be the case in the next few weeks; it would be useful if the other differences of opinion in patent litigations are also now and again thrown into the negotiations.

Sincerely
Diesel

03056

P

R. Diesel
Ingenieur.

München, den 15. September 06.
Maria-Theresia-Str. 32
C. 6
Telefon 2811.
Telegramme: „Diesel Ingenieur München."

R 17. September

Herren Gebrüder Sulzer, wrl. Cc.
Winterthur

Betr. Deutsche Anmeldung S. 21616 "Arbeitsverfahren für Druckluftmaschinen".

In der englischen Uebersetzung ist unsere Druckluftmaschine präziser bezeichnet als in unserer deutschen Anmeldung, nämlich als Internal-Combustion- Compressed-Air Engine.

Auch in der französischen Uebersetzung schlage ich auf Anregung des Patentanwalts folgende Bezeichnung vor: Moteurs combinés à Air Comprimé et à combustion. Ich möchte mir den Vorschlag erlauben, beim deutschen Patentamt eine Eingabe zu machen mit dem Ersuchen, in der Beschreibung überall die Bezeichnung Druckluftmaschine durch die Bezeichnung "Druckluft-Verbrennungsmaschine" ersetzen zu dürfen.

Es würde hiedurch die ganze Sache nicht nur schärfer bezeichnet, sondern auch in Uebereinstimmung mit unseren Auslandspatenten gebracht. Zweckmässig wäre auch eine gleiche Korrektur in allen Auslandsbeschreibungen, denn da die Sache neu ist, so muss man ihr auch einen neuen Namen geben.

Hochachtungsvoll !

Diesel.

R. Diesel
Ingenieur.

München, den 4. März 1907.
Maria-Theresia-Str. 32
C. 3 Telefon 2811.
Telegramme: „Diesel Ingenieur München."

Herren Gebrüder Sulzer,

Winterthur

Antwort auf Geehrtes vom 1. März No. 12/2065/Rr.Alt.

Betr. Deutschland S. 19944

Ich nehme bestens Kenntnis von Ihren Mitteilungen in oben rubr. Angelegenheit.

Was die Auslage der Anmeldung betrifft, so möchte ich vorschlagen, dieselbe doch noch auszusetzen bis die schwebenden Angelegenheiten mit Augsburg erledigt sind, was ja doch voraussichtlich in den nächsten Wochen der Fall sein dürfte; es wäre doch misslich, wenn zu den sonstigen Meinungsdifferenzen jetzt auch noch Patentstreitereien mit in die Verhandlungen hereingeworfen würden.

Hochachtungsvoll !

Diesel.

VIII INTERNATIONAL
CONGRESS ON COMBUSTION ENGINES

POLISH SCIENTIFIC SOCIETY OF COMBUSTION ENGINES

17th-18th June 2019

TOPICS

The Congress will constitute an opportunity to discuss the latest achievements in such fields as design, manufacture, research and the ecological impact of internal combustion engines and fuels. The main topics of the Congress:

- Fuel injection systems and mixture formation
- Combustion processes control in SI and CI engines
- Engine thermal loading and utilization of heat released
- Alternative fuels
- Emission measurements and after treatment
- Alternative sources of power
- Engine testing, durability, reliability and diagnostics
- Modelling and optimization of engine processes
- Global trends in engine technology.

FOR PARTNERS FROM INDUSTRY AND SERVICES

Please accept our kind invitation to attend the VIII International PTNSS Congress. We would like to create an opportunity to present achievements of science and industry.

APPLICATION

If you wish to participate in the Congress, please register at www.congress.ptnss.pl

ABSTRACTS

Abstracts of papers (200-250 words), including the title, the author's name(s), affiliation and address, fax, phone numbers and e-mail should be sent with www.congress.ptnss.pl after logging. The paper authors should also fill in the application form.

ACCOMMODATION

Congress participants can choose accommodation in one of the hotels in Cracow. There are the following possibilities of accommodation in single or double room in the hotels:

Hotel Ibis Stare Miasto (170 m), www.accorhotels.com
Hotel Ibis Budget Kraków (170 m), www.accorhotels.com
Old Time Hotel (600 km), www.oldtimehotel.pl
Hotel Atrium (750 m), www.hotelatrium.pl
Hotel Delta (1.2 km), www.deltahotel.pl/pl

CONGRESS FEE (including VAT)

Participants*)	1100 PLN/250 €
Participants – the PTNSS member*)	950 PLN/220 €
Students, doctoral students*)	650 PLN/150 €
Accompanying person**)	650 PLN/150 €

*) **Congress fee includes:** admission to all the Congress sessions, the Congress proceedings, lunches and gala dinner.

) **Congress fee includes: lunches and gala dinner.

PAYMENT

Payment transfer to:
Bank: PEKAO S.A. O/Bielsko-Biała
BIC/SWIFT: PKOPPLPW
IBAN: PL 92 1240 6449 1111 0000 5290 4552

please add a note:
PTNSS CONGRESS 2019 – Name and Surname

CONGRESS LOCATION

VIII International Congress on Combustion Engines will be held at the Cracow University of Technology, which is located in a Campus at Warszawska Street in Cracow.

CONTACT

ORGANIZATION OFFICE:

Jerzy Merkisz – **Congress Chairman**
e-mail: jerzy.merkisz@put.poznan.pl

Marek Brzeżański – **Congress Vice-Chairman**
e-mail: mbrzez@pk.edu.pl

Magdalena Kalarus – Secretary for Organization
e-mail: mkalarus@pk.edu.pl
Tel/fax: +48 12 628 35 31/+48 12 648 13 44

Antoni Świątek
Congress Vice-Chairman for Industry Exhibition
e-mail: antoni.swiatek@bosmal.com.pl
Tel: +48 33 813 05 40

Piotr Bielaczyc
Congress Vice-Chairman for Foreign Participants
e-mail: piotr.bielaczyc@bosmal.com.pl
Tel: +48 33 813 05 98
GSM +48 698 637 991

SCIENCE OFFICE:

Zdzislaw Stelmasiak
Congress Vice-Chairman for Science
e-mail: zstelmasiak@ath.bielsko.pl
Tel/fax: +48 33 827 92 16

ADDRESS OF THE ORGANIZING COMMITTEE:

PTNSS Congress 2019
Cracow University of Technology
Institute of Automobiles and Combustion Engines
37 Jana Pawla II Street
31-864 Cracow, POLAND
www.congress.ptnss.pl
kongres_org@ptnss.pl

CRACOW University of Technology
31-155 CRACOW, Warszawska 24 Street, POLAND

SAE International Conference

Powertrains, Fuels & Lubricants Meeting
September 22-24, 2020, Krakow, Poland

ICE Krakow Congress Centre

Old-city Krakow

Information: Local Committee Chair
Dr. Piotr Bielaczyc
piotr.bielaczyc@bosmal.com.pl

NOTE: Website will be activated on: pfl20.org

Call for Papers Opens August 2019
Abstracts due February 18, 2020

Executive Leadership Provided by:

SAE INTERNATIONAL · PTNSS · BOSMAL

Collaboration:
Cracow University of Technology

Poznan University of Technology

Institute of Combustion Engines and Transport

POLAND, 60-965 Poznan, Piotrowo 3 str., tel. 48 61 6652207, fax. 48 61 6652204

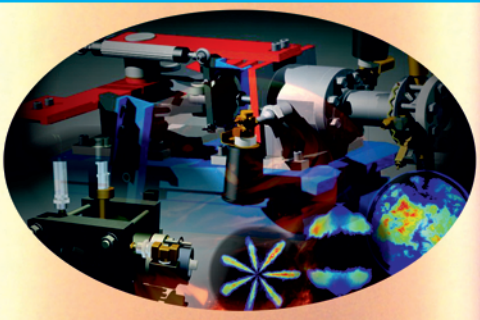

Optical research of engine processes

Rapid Compression Machine - fully controled single combustion cycle (Otto and Diesel cycle)
Constant Volume Chamber (air pressure up to 100 bar)
LaVision HighSpeedStar 5 camera up to 200 000 fps
Continuum YAG solid-state laser
Data image post processing with DaVis software

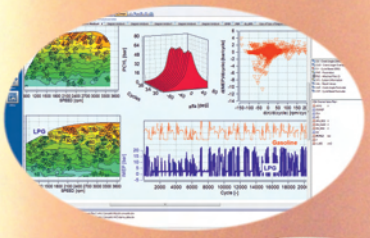

Cycle-by-cycle indicating processes

Powertrain combustion processes research on engine test bench, roller dynamometer and real drive conditions
AVL IndiSmart 621 (8 channel acquisition data system)
Data post processing with AVL Concerto software

Hybrid vehicles and Fuel Cells technology

Full-hybrid powertrain test bench, energy flow research
Real drive hybrid powertrain research

Engine and driveline load systems

Engine test bed for testing under dynamic conditions
AVL DynoRoad 120 kW

Combustion engines simulation

Gasoline and Diesel fuel injection simulation
Simulation of in-cylinder phenomena such as gas exchange mixture generation, combustion and emission formation

Simulation platforms

Passanger car simulator
AS1200-6 (AutoSim AS)
Flight simulator
MotionCor5 (CKAS Mechatronics Pty Ltd)

Research on RDE (PEMS)

Gaseous exhaust emissions (CO, HC, NO_x)
Semtech DS, Ecostar (Sensors), M.O.V.E. (AVL)
Particle mass (PM) & number (PN) emissions
Micro Soot Sensor, Particle Counter (AVL),
Ecostar PM, Ecostar PN (Sensors), EEPS (TSI)

www.cel.put.poznan.pl

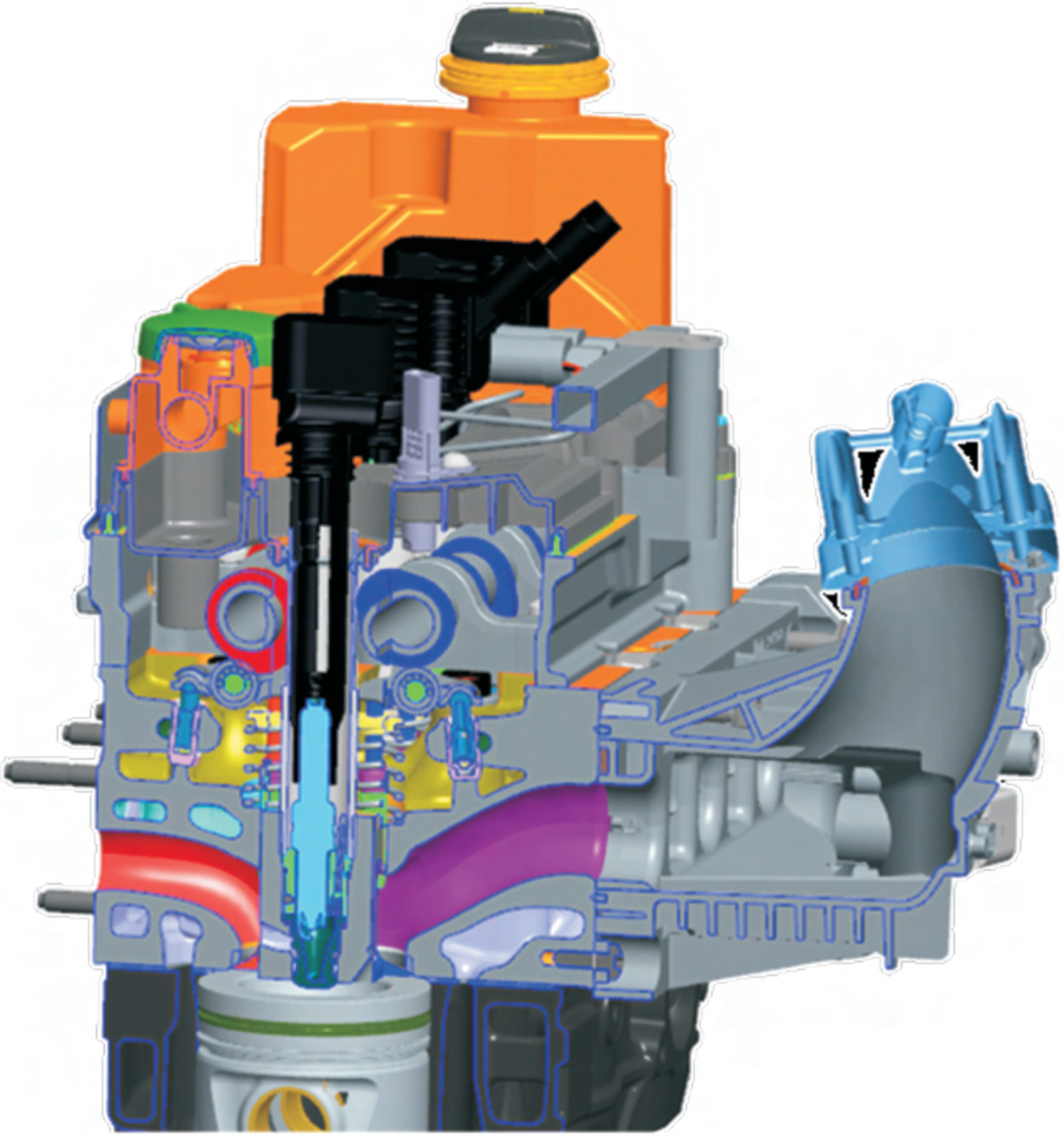

Publisher:

Polish Scientific Society of Combustion Engines

Combustion Engines

Polskie Towarzystwo Naukowe Silników Spalinowych

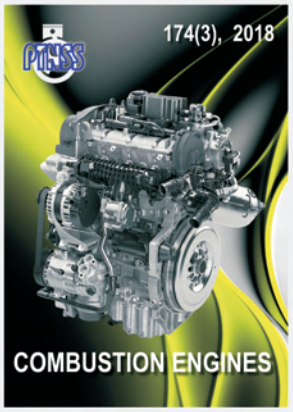

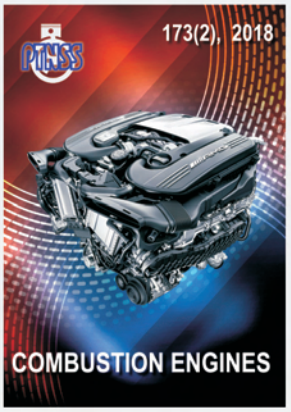

ISSN: 2300-9896

www.combustion-engines.eu